THE UNIVERSITY *of* LIVERPOOL

Frequency Supporting of Smart Grid with Wind Power via Demand Side Response

Thesis submitted in accordance with the
requirements of the University of Liverpool
for the degree of Doctor of Philosophy

in

Electrical Engineering and Electronics

by

Qi Zhu, B.Sc.(Eng.)

September 2016

Frequency Supporting of Smart Grid with Wind Power via Demand Side Response

by

Qi Zhu

Acknowledgements

I would like to express my special thanks of gratitude to my supervisor Dr. L. Jiang. He kindly helped and guided my research. My supervisor also taught me the how to research which will take benefits for me throughout my lift.

I also would like to thanks my second supervisor, Dr. X. Tu, for his kindly encouragement.

I offer my regards and blessings to all of the members of Smart Grid Control and Renewable Energy Subgroup, the University of Liverpool, especially to Dr. W. Yao and Dr. C.K. Zhang. I also thank my friends, Miss. L. Y. Li, Mr, S. J. Chen, Mr. Y. X. Ren, Miss. Y. F. Du, Mr. K. Shi, Mr. Y. Liu, Mr. C. Duan, Mr. Y. Y. Sang, Mr. W. Z. Deng and Mr. H. T. Xu, for their support and friendship. My thanks also go to the Department of Electrical Engineering and Electronics at the University of Liverpool, for providing the research facilities that made it possible for me to carry out this research.

Finally, I would thanks for my family for their loving and heartening me in these years.

Abstract

Renewable energy, especially wind power and solar power, has been rapidly and widely developed in this past decade, as a promised solution to meet the increased energy demand and the reduction of greenhouse emission. Due to the intermittent and time-varying characteristics, balancing the active power between the generation side and the demand side to maintain the grid frequency is one of the main challenge problems of integrating the increased intermittent wind power into the smart grid. Spinning generation reserve with enough capacity is usually used to compensate the fluctuations caused by intermittent wind power. However, this solution requires expensive auxiliary equipment, high installation and operation cost. Demand side response (DSR), which allows customers to reduce the peak load or reshape the load profile, has become a feasible solution to frequency regulation problem caused by intermittent wind power energy. The main objective of DSR is to reduce system peak load demand and operational cost.

Literature reviews of DSR approaches and their applications in the smart grid are carried out. Two types of DSR, indirect load control (ILC) and direct load control(DLC), are introduced. The ILC is controlled by consumers or autonomously operated to control the load consumption based on price signal. The DLC is controllable loads which are directly controlled by the control centre. Applications of DSR to balance active power between the generation side and the demand side in the power system has also been reviewed. Models of different types of controllable loads, such as plug-in electric vehicles (PEVs), air conditioners and heat pump water heaters (HPWHs) are investigated together with battery energy storage systems (BESS). Then BESS model, PEVs model, aggregated air conditioners model and HPWHs model are integrated into the load frequency control (LFC) model of

a power system. Communication networks are used in LFC for transmitting remote measurements and control commands, and in DSR for aggregating small-scale controllable loads. Finally, the general LFC model including DLC model which represents different types of controllable loads and considers time delay introduced by the communication channels is obtained.

Deregulation in the power industry is to restructure the electric industry and economic incentives so that the power production and distribution are competitive. Modelling and controller design for LFC together DSR in a deregulated environment is investigated, considering multiple time delays. The time delay model of the deregulated multi-area LFC with DSR based on air conditioners is obtained. A robust PID controller for LFC scheme is designed, through the H_∞ performance analysis and the particle swarm optimisation (PSO) searching algorithm, to deal with the load disturbances and multiple delays. Simulation results demonstrate the effectiveness of the proposed load frequency controller and the performance improvement from the DSR. Several delay stable regions are also revealed via simulation method.

Although the energy storage system, such as BESS, has potential to solve balance problem caused by intermittent wind power, the installation of the BESS with a large capacity is limited by its high cost. The frequency regulation of the smart grid working in the isolated mode with wind farms by introducing not only the BESS but also DSR via controlling air conditioners and PEVs is proposed. Firstly, the model of a single area LFC system is obtained, which includes the wind farms, the simplified BESS, air conditioners and PEVs. Then, state-space models of the closed-loop LFC scheme with communication delays in the control loops are derived and the stability of the closed-loop system with time delays is investigated via the Lyapunov functional based method. Thirdly, gains of PID-type controllers for LFC scheme are tuned based on the H_∞ performance analysis and the PSO searching algorithm. Both the theoretical analysis and the simulation studies demonstrate the contribution of DSR and BESS to frequency regulation, the robustness of the designed PID-type LFC and the delays arising in the control loops.

With the increasing penetration of wind power, wind turbines are required to participate in frequency regulation via augmented additional controllers, such as

inertial control (IC), rotor speed control (RSC) and pitch angle control (PAC) in different wind speed. Wind turbines and DSR participate in the frequency regulation to help the power system under intermittent wind power and demand load suddenly increase. This combination method can contribute to increase penetration of wind power and also reduce peak load.

Declaration

The author hereby declares that this thesis is a record of work carried out in the Department of Electrical Engineering and Electronics at the University of Liverpool during the period from October 2012 to September 2016. The thesis is original in content except where otherwise indicated.

Contents

List of Figures

List of Tables

List of Abbreviations and Notations

Abbreviations

AC	Air Conditioner
ACE	Area Control Error
AGC	Automatic Generation Control
AGPM	Augmented Generation Participation Matrix
AMI	Advanced Metering Infrastructure
BESS	Battery Energy Storage System
COP	Coefficient of Performance
CPP	Critical-Peak Pricing
CPSO	Cooperative Particle Swarm Optimization
CSP	Curtailment Service Provider
DDC	Dynamic Demand Control
DFIG	Doubly Fed Induction Generator
Discos	Distribution Companies
DLC	Direct Load Control
DSM	Demand Side Management
DSR	Demand Side Response
EER	Energy Efficient Ratio
EV	Electric Vehicle
EWH	Electric Water Heater
Gencos	Generation Companies
GRC	Generation Rate Constraint
HAN	Home Area Network
HPWH	Heat Pump Water Heater
HVAC	Heating, Ventilation, and Air-Conditioning
IC	Inertial Control

ICT	Information and Communication Technology
ILC	Indirect Load Control
ITAE	Integral of the Time multiplied Absolute value of the Error
ITSE	Integral of the Time multiplied Square of the Error
ISO	Independent System Operator
LFC	Load Frequency Control
LMI	Linear Matrix Inequality
MDMS	Meter Data Management System
PAC	Pitch Angle Control
PEV	Plug-in Electric Vehicle
PMSG	Permanent Magnet Synchronous Generator
PID	Proportional Integral Derivative
PSO	Particle Swarm Optimization
RMS	Root-Mean-Squared
RPI	Robust Performance Index
RSC	Rotor Speed Control
RTP	Real-Time Pricing
SOC	State of Charge
SGDS	Smart-Grid Dispatch System
TCA	Thermostatically Controlled Appliance
ToUP	Time-of-Use Pricing
Transcos	Transmission Companies
V2G	Vehicle-to-Grid
VSWT	Variable Speed Wind Turbine

Notations

Δf	frequency deviation
ΔP_m	mechanical power change
ΔP_L	load change
H	inertia constant
D	load damping coefficient
R	speed drop
∂	partial derivative
R	speed droop
β	bias factor
ΔP_{BESS}	power deviation from BESS
ΔP_{HPWH}	power deviation from HPWH
ΔP_{AC}	power deviation from DDC based on air conditioners
ΔP_{V2G}	power deviation from PEVs
ΔP_{wind}	active output power deviation from wind farm
D_{ac}	reheat coefficient of air conditioner
ΔP_{LC}	controllable change in power consumed
ΔP_{in}	per-unit response of the inertial controller
ΔP_0	initial operating power point
ΔP_{LC}	controllable change in power consumed
ΔP_{ref}	reference active power for the VSWT
ΔT_{st}	set point of a smart thermostat
m	mass of air flow
c_p	specific heat capacity of air
α_{AC}	reheat coefficient of air conditioner
K_{ddc}	combined integral gain for air conditioner model
M	total number of air conditioners in a control area
T^j_{heat}	expected heating period of the j^{th} HPWH
$E^j_{request}$	requested amount of hot water
P^j_{HP}	rated power consumption of each HPWH
$[h]$	time unit hour
T^k_{AVG}	average value of expected heating period of total HPWHs
T^k_{SD}	standard deviation of expected heating period in each group
N_{HP}	total number of controlled HPWHs in control area

E_{bt}	terminal voltage of the battery
α_{AC}	line to neutral RMS voltage
α_1^o	firing delay angle of converter 1
α_2^o	firing delay angle of converter 2
X_{co}	commutating reactance
I_{bes}	dc current flowing into battery
E_{boc}	terminal voltage of the battery
E_{boc}	battery open circuit voltage
r_{bt}	connecting resistance
r_{bs}	connecting resistance
K_{bes}	control loop gain
T_{bes}	measurement device time constant
$V_{boc,i}$	open circuit voltage of battery
$V_{dc,i}$	battery's DC current
$V_{b,i}$	battery overvoltage
$R_{bc,i}$	resistance of the battery's terminals and inter-cell connections
$I_{dc,i}$	battery's DC current
$C_{cp,i}$	battery capacitance reflecting the main storage capacity
$R_{bp,i}$	self-discharge resistance
$V_{dc,i}^o$	DC voltage of the battery at the initial time
$I_{dc,i}^o$	current of the battery at the initial time
$T_{b,i}$	time constant of battery power adjustment
$k_{b,i}^o$	battery gain of a PEV
$k_{ev,i}^o$	aggregated PEVs gain
T_r	generated torque on the rotor
ω_r	rotor speed
P_r	mechanical power absorbed from the wind
ρ	air density
R_{wind}	wind radius
υ	effective wind speed
C_p	power coefficient
θ	blade pitch angle
λ	tip speed ratio
θ_r	reference and the one control input for the wind turbine
J_r	inertia on the rotor side

J_g	inertia on the generator side
ω_r	rotational speed on the rotor side
ω_g	rotational speed on the generator side
T_r	rotor torque
T_g	generator torque
N_g	gear ratio
T_{sr}	torque at the rotor side of the transmission
T_{sg}	torque at the generator side of the transmission
D_s	damping
K_s	spring constant
δ	twist of the flexible shaft
P_e	generator power
T_{gr}	reference and one of the control inputs for the wind turbine
$P_{wind,desired}$	desired active power output of wind farm
$P_{e,j}$	active power output of the jth wind turbines
N_{wind}	total number of wind turbines in a wind farm

Chapter 1

Introduction

1.1 Introduction of Smart Grid Technology

The first power station and electrical power distribution system were established by Edison in 1880s, while some problems have appeared, such as disruption on the power grid and how to response to the demand quickly [1, 2]. This old equipment and infrastructures needed to discard and to replace. Meanwhile, electricity grids in most developed countries are used over 50 years. So these old power systems need to replace new systems. The new power system is required to reduce carbon footprint to mitigate the greenhouse effect, to increase the efficiency of electricity production and to make power network more reliable and secure [3, 4]. The new power system also needs to accommodate all types of generations and some new appliances, such as renewable energy and electric vehicle (EV). The smart grid is proposed and used in many countries. The smart grid is defined by the European Technology Platform as follows: "A smart grid is an electricity network that can intelligently integrate the actions of all users connected to it - generators, consumers and those that do both in order to efficiently deliver sustainable, economic and secure electricity supplies" [3]. Advantages of the smart grid are it improves reliability performance and encourages consumers to participate in the electric market to make efficiency decisions. The smart grid takes many benefits in both short and long-term. For consumers, it encourages consumers to take part in system and management

their demand and minimises costs bills via new technologies [5, 6]. For economic aspect, it creates jobs and improves energy security and reliability.

The smart grid also enables new reduced carbon technology developed to save carbon emissions. It allows much renewable energy, such as wind power and solar power, participated in the power system. Wind power energy is developing faster than other renewable energy. The wind energy is friendly to the environment and does not produce carbon. The disadvantage of wind power energy is it is time-varying and intermittent, so it will cause the imbalance problem when intermittent wind power increasing in the power system. In smart grid, it proposed using new technology, demand side response (DSR), to solve this problem.

The DSR is one of the essential requirements for the smart grid. The smart grid has advanced metering infrastructure (AMI), meter data management system (MDMS) and home area network (HAN). AMI can measures, collects and analyse energy usage of every consumer via advanced devices [7–9]. AMI and integration with HAN provide sufficient conditions for DSR developing. For example, the dynamic electricity price is sent to consumers and they can manage electric vehicles (EVs) and heat pump water heaters (HPWHs) to charge in low price time. The DSR is an economical and low cost method to balance the active power imbalance between the generation side and the demand side when intermittent wind power increases in the smart grid. Meanwhile, the DSR allows the consumers to manage their energy consumption time via the advanced devices and helps energy suppliers to reshape the load profile to reduce peak load demand.

1.1.1 Wind Power Energy in Smart Grid

Many countries concern the environment problems and the global warming problem. For example, UK Climate Change Programme aim to cut 80% of carbon emissions by 2050 (compared to 1990 levels) [3]. By this reason, the renewable energy, including wind power, hydropower, solar power and geothermal energy, is developing fast in many countries. Wind power is developing rapidly renewable energy in recent years because the wind power energy is sustainable and clean energy. In 2015, the increasing wind power generation capacity is 63 GW which means the

capacity of wind power generation grew by 16.9% and total capacity reached to 435 GW at the end of 2015 [10]. Wind power becomes a very important power in European countries. In 2015, Wind power provided 50% of power generation in Denmark and provided 15% of power generation in most of the European countries, such as Germany, Spain, Portugal, Ireland and Lithuania [10].

Due to the wind speed is intermittent, the wind power energy is intermittent and time-varying. With the wind power energy increasing in the power system, balancing the active power between the generation side and the demand side to maintain the frequency is one of the main challenging problems. Many methods can be used to solve the imbalance problem caused by intermittent wind power injection. The extra traditional generators with enough backup capacity are designed to provide the compensation to the gap between supply and demand. However, this treatment makes substantial backup idle for most hours within a year. It is harmful to generation companies (Gencos) to reduce operational cost and maximise the profit by operating generator with higher efficiency [11]. Then big capacity battery energy storage system (BESS) are used to solve this problem, but the installation cost is expensive. The DSR can be used to provide a contribution to frequency regulation. The DSR can shift demand load to match generation output. So DSR can be employed in the power system to solve the problem caused by high penetration of wind power energy.

There is another method to solve imbalance problem caused by intermittent wind power. Wind turbines can participate in frequency regulation via coordinate inertial control (IC), rotor speed control (RSC) and pitch angle control (PAC) under different wind speed. The RSC is used to control wind turbine in low wind speed and the PAC is used to control wind turbines at high wind speed. The IC combines with these two control approach to control wind turbines in different wind speed. In this thesis, the DSR also participate in frequency regulation to improve the stability of the power system. Combined method has serval advantages, including relatively fast response time and small fluctuation of frequency deviation.

1.1.2 Demand Side Response in Smart Grid

In the 1980s, DSR was proposed and had concentrated on the management of electricity demand. The technologies include load shifting, peak clipping, valley filling, strategic load growth and strategic conservation [13]. Historically, the DSR is interpreted as load management. With the smart grid developing and communication technology developing, customers are encouraged to modify their electricity consumption in response smart grid requirements. Based on these conditions, the DSR is developing very fast and it becomes a key role to balance electricity in the smart grid. DSR is defined as follows "change in electric usage by end-use customers from their normal consumption patterns in response to change in the price of electricity over time, or to incentive payments designed to induce lower electricity use at times of high wholesale market price or when system reliability is jeopardised" [14, 15]. DSR could rely on the smart grid to shift loads over time in order to match demand with produced output power by Gencos [16, 17]. The basic components of the DSR framework consist of local generators, smart devices, sensors, energy management unit and smart grid domains. Demand side management (DSM) is the utilisation of DSR for a purpose such as system security and system adequacy [18]. The main objective of DSR is to reduce system peak load and operational cost and to control load consumption [9, 19–21].

There are three characteristics of aggregated DSR [21, 30]: demand response speed, demand response reliability and demand incentive program. Demand side speed affects the efficiency of DSR in the power system. For power system stability, demand response in one hour ahead or minutes ahead is effective. Demand response speeds in different DSR methods are different, but they are in an acceptable range. Demand reliability is a major factor in DSR. When customers receive DSR requirements, some customers do not respond or can not achieve the DSR targets. So DSR needs a group reliable customers to respond to DSR requirement and reach DSR target value. In general, the reliable customer can receive high incentive price. Oppositely, uncertain customers receive low incentive price. Demand incentive program is a useful way to incent customers respond to DSR requirement quickly and effectively. The DSR need more consumers participate in programs, so many types

of incentive menu are defined. Incentive menus can be used in linear program or optimisation problem.

Based on the control method, DSR can be classified into two types: indirect load control (ILC) [22, 23] and direct load control (DLC) [25–27]. In ILC, consumers control the power consumption of loads by control signals, which include electric prices, system voltage, and grid frequency deviation [28]. The market-based price is one of ILC method that is widely used in many countries. In this approach, energy suppliers provide the flexible pricing to adjust the load. [22]. The price programs include critical-peak pricing, time-of-use pricing and real-time price. Customer will shift the demand load from peak time to valley time by the electricity price and sent the consumption information to Gencos. With the communication technology developing in smart grid, the reliable and real-time communication can transfer between the energy suppliers and the consumers. Customers can get the price in shorter intervals by advanced metering infrastructure or other advanced devices. The limitation of this method is communication technology. The energy suppliers should provide reliable and fast price information to consumers and get electricity consumption information from the consumers so that this approach can quickly help the power system in the steady stable when the demand load increases or decrease.

The DLC method can directly control controllable loads or remotely shut down some controllable load on demand side on short notice by a control signal to meet reliability requirement. The load consumption can be directly controlled and monitored by two-way communication technology and load aggregator to adjust the load consumption in order to maintain the power system stability. Therefore DLC is always used for load shifting and peak shaving. The controllable loads include thermostatically controlled appliances (TCAs) and energy storage systems which are installed on the demand side. TCAs loads include electric water heaters (EWH), refrigerators and air conditioners. Another kind of controllable load is energy storage system installed in the demand side, such as EVs.

The DSR is commercialised in Europe countries, U.S and Japan, such as Yokohama Smart City Project [29, 30]. DSR still has some challenges from technology and policy. As the most DSR requires a reliable and high bandwidth two-way com-

munication between consumers and Gencos to transmit information, such as price and bid data, the communication technology needs to be developed. Meanwhile, houses need to install some smart appliance to response on time with or without home interaction when consumers participate in the DSR. The DSR will take benefit to consumers and utilities and make the power system more secure, stable and social welfare. With technology developing, the DSR will widely used in many countries. In conclusion, DSR is a useful method to improve the power system stability and it takes benefits for both consumers and utilities. The DSR will be widely used in many countries.

1.1.3 Communication Networks and Time Delays in Power System

Some technologies of the smart grid, such as real-time pricing, DLC, and wide area monitoring, are required to consider communication service [31]. The information and communication technology (ICT) as a key technology is widely used in the smart grid. Communication devices or application are used in ICT to obtain, store, process and distribute information by telecommunication infrastructure [32]. The traditional technologies include television, radio, and video. The new technologies include the Internet and so on. The ICT can use these techniques to allow automation, to collect information and data and to solve problems for activities relating people [32]. The communication time delay happens when information or control commands transmit or receive among participators in the power system. As these time delays are very small, some researchers ignore them to analyse the performances of the power system. However, many types of research still analyse and calculate the time delay in the power system [33–35].

There are many applications can be used to transmit and receive information and control commands, such as smart meters and the conventional supervisory control and data acquisition (SCADA) systems. Smart meters is used in real-time pricing program, which sends the price signal to consumers and collects consumption information. The consumers can manage their load to reach the DSR requirement.

In SCADA systems, coherent and real-time data can be measured by advanced instrumentations [36]. Accurate time-stamping measurement can improve the system efficiency and stability. The technology of communication technology develops, but time delay still exists in the power system.

The load frequency control (LFC) scheme uses the communication channels to transmit the measurements and control commands, which will introduce time delays [33]. The aggregation of DSR uses two-way communication technology to transmit information, such as price, load consumption information, between customers and utilities, which will cause time delays [25, 37]. Time delays will deteriorate the dynamic performance or even cause instability of the closed-loop system [34, 35, 38–40]. The maximum time delay which allows an LFC scheme embedded with controllers to retain stable is denoted as delay margin for stability analysis [33, 41]. The delay margin of the LFC scheme has been calculated and applied in the design of LFC controller [35, 42]. The impact of the time delay on the DDC scheme has been investigated as well [37, 43]. In this thesis, time delay in the power system will be analysed and calculated.

1.2 Motivations and Objectives

With the global warming problem serious, the renewable energy is used widely in many countries, especially wind power energy. However, the intermittent and uncontrollable wind power energy causes imbalance the active power between the generation side and the demand side, which is one of the main challenges for integrating more wind power into the power system. The conventional spinning reserve such as thermal power plant, and energy storage system, such as BESS, can solve this problem, but with high installation and operation cost. DSR which is low investment method can control and shift controllable demand loads to balance the power in the power system. So DSR can be considered to replace some capacity of BESS to solve imbalance problem caused by the intermittent wind power energy.

Moreover, wind turbines themselves are also required to support grid frequency. However, sometimes the total produced power may be less than the demand load

because the demand load may suddenly increase or wind turbines can not produce enough output power. DSR can shift controllable loads to improve the stability of power system. Considering these two aspects, the DSR and wind turbines together participate in frequency regulation can be researched. This combined method may allow the power system with high penetration of wind power energy and improve the stability of power system.

The main objective of this project is to investigate the contribution of DSR to the frequency regulation of modern power system with high penetration of wind power, via

1) Building up the modelling of LFC system including DSR, BESS, wind turbine and communication system.

2) Stability analysis and robust control design of the LFC with DSR system in deregulated environment including multiple delays.

3) Coordinated control of DSR and wind turbines for frequency regulation in the smart grid.

1.3 Main Contributions

The main purpose is DSR participating in the frequency regulation to improve the power system stability and to solve the imbalance problem caused by intermittent wind power energy. At first, models of DDC based on air conditioners and HPWHs, BESS and plug-in electric vehicle (PEV) have been reviewed and prepared for the following chapters. Then, LFC with DDC based on air conditioners is modelled and controller design for LFC scheme is investigated in a deregulated environment, considering multiple time delays. The gains of PID controller is tuned based on H_∞ and the particle swarm optimisation searching algorithm. After that, DDC, BESS, and PEV have been investigated the frequency regulation of smart grid working in the isolated mode with wind farms. The stability of the closed-loop system with time delays is investigated via the Lyapunov functional based method. The PID-type controller for LFC scheme is also designed. Finally, wind turbines and DSR participate in frequency regulation to solve imbalance problem cause by

high penetration of wind power and demand load suddenly increase problem.

The publications produced from this research work are listed in this section as follows:

1. Qi Zhu, L. Jiang. Load Frequency Control with Dynamic Demand Control in Deregulated Environment. *Manchester Electrical Energy and Power System*, A workshop at the University of Manchester, 6th, November 2013.

2. Qi Zhu. Wei Yao, L. Jiang, Cheng Luo and Q. H.Wu. Load Frequency Control with Dynamic Demand Control for Deregulated Power System. In 2014 IEEE PES General Meeting, National Harbor, Washington DC, U.S., 27th-31st, July 2014.

3. Qi Zhu, L. Jiang, Wei Yao, Chuan-Ke Zhang and Cheng Luo. Robust Load Frequency Control with Dynamic Demand Response for Deregulated Power Systems with Communication Delays. *Accepted by Electric Power Components and Systems*, Sept. 2016.

4. Qi Zhu, Wei Yao, Chuan-Ke Zhang and L. Jiang. Chapter 8: Frequency Regulation of Smart Grid via Dynamic Demand Control and Battery Energy Storage System. *Smarter Energy: from Smart Metering to the smart Grid*, IET Press, 2016.

1.4 Outline of the Thesis

There are seven chapters in this thesis, details of every chapter are introduced as follows:

- Chapter 1 presents background and introduction of this whole project. The technology of smart grid, wind power and DSR are introduced.
- Chapter 2 is a survey of DSR approached and DSR applications for wind power system. The DSR approaches are introduced based on DLC and ILC methods in the power system. Then, applications of DSR in a wind

power system are presented. The DLC, ILC and forecasting of wind generation and demand method used to solve imbalance problem caused by intermittent wind power have been reviewed.

- Chapter 3 presents models of DSR based on different types of controllable loads, including PEVs, air conditioners and HPWHs and BESS. The input signal for PEVs and air conditioners is frequency deviation. The input signal to HPWHs is LFC signal and the area control error (ACE) is the input signal to BESS. Then the general DLC model which represents different types of controllable loads is described. This model considers the time delay using the $Padé$ approximation. The single area LFC model and time delay model of LFC with DSR model are also investigated, respectively.
- Chapter 4 investigates the model of LFC with DDC in a deregulated environment. The controller design for LFC scheme, considering multiple time delays introduced by the usage of communication channels. Time delay model of the deregulated multi-area LFC with DDC is obtained at first, in which aggregated air conditioners model is used for DDC. Then the H_∞ performance analysis and the PSO searching algorithm are used to design a robust PID load frequency controller, which considers the load disturbances and multiple delays in the LFC loop and the DDC loop. Case studies show the DDC can improve the power system stability and designed PID controller can perfectly control the power system with time delays. Several delays stable regions are revealed via simulation method.
- Chapter 5 proposed the frequency regulation of the smart power grid working in the isolated mode with wind farms by introducing not only the BESS but aggregated of air conditioners and the PEVs with vehicle-to-grid (V2G) service. The stability of the closed-loop models with time delays is investigated via the Lyapunov functional based method. A PID controller for LFC scheme is designed based on the H_∞ performance analysis and the PSO searching algorithm. The robustness of the de-

signed PID-type LFC against to the disturbances caused by the load changes and the intermittent wind power and time delays. Case studies show LFC with DDC, the BESS and PEVs can significantly alleviate the power imbalance caused by intermittent wind power. Delay margins in control loops via theoretical analysis and simulation method are very similar.

- Chapter 6 investigates wind turbines and DSR participated in frequency regulation in different wind speed. The RSC and PAC combined IC are controlled wind turbines in low and high wind speed, respectively. The DSR and wind turbines participating in frequency regulation is tested in the power system with low or high penetration of wind power. Case studies are simulated in single area LFC with a wind farm, the PEVs, and air conditioners. Combined RSC or PAC with DSR can help the power system with high penetration of wind power and demand load suddenly increase.
- Chapter 7 presents conclusions and possible future work.

Chapter 2

A Survey on Demand Side Response Approaches and Applications in Smart Grid

2.1 Introduction

The increasing intermittent renewable energy and fast growing demand load in recent years have brought out problems to balance active power between the generation side and the demand side. Although energy storage system and spinning generation reserve with enough capacity can solve this imbalance problem, those methods are not economic as they require high installation cost and also harm the advantages of renewable energy. DSR is a feasible and economical solution between to achieve the balance between the supply side and the demand side with less adding of the installed capacity of energy storage system or reducing the spinning generation capacity [43,44]. The technologies of DSR include peak clipping, valley filling, load shifting, strategic conservation, strategic load growth and flexible load shape as shown in Figure 2.1 [3]. With the developing of technology of smart grid and communication technology, smart meters and intelligent appliances will be increasingly equipped. Thus the consumers and electric power companies can monitor electricity consumption and actively control demand load at household level [16].

DSR can be classified based on control method, as ILC and DLC. The purposes of DSR in smart grid has two parts which are system stability and economic impact [45,46]. For system stability, the DLC based on TCA loads and energy storage system installed on the demand side can participate in frequency regulation and balance active power if disturbance happened in the system. In DLC, the load management agreement is protocolled between utility companies and customers. Based on this agreement, the utility or aggregator can remotely control these demand loads and energy consumption to reduce the spinning capacity and maintain power system in stable. The TCA loads include electric water heaters, refrigerators and air conditioners and energy storage systems include BESS installed on the demand side and EVs. The DLC is an effectively way to reduce the spinning generation capacity to improve the system stability. This thesis focuses on using DLC to support the grid frequency in the smart grid.

The ILC is investigated in the smart gird for economic impact. The ILC based on variable electricity price is widely used in many countries and encourages customers to manage their loads to change load pattern [47–51]. The popular methods in price programmes include critical-peak pricing (CPP), time-of-use pricing (ToUP) and real-time pricing (RTP) [45]. With the development of communication technology developing, energy suppliers can provide RTP to consumers and can get energy consumption information from consumers with two-way communication devices. Based on advanced metering infrastructure, the real-time price method can provide the consumers daily, hourly, or in even shorter intervals. The electricity price is high during peak time and is low in valley time. These approaches encourage consumers to shift loads from peak time to valley time via adjusting electricity price. For customers, participating in these methods can save their bills. For energy suppliers and utility companies, they do not require installing spinning generation reserve with enough capacity or big capacity BESS in the generation side to ensure the stability of the power system stable when the disturbance occurs in the power system.

With environment problem pressure increasing, the renewable energy is widely used in the power system, especially wind power energy. The wind power energy is intermittent and time-varying because of the intermittent wind speed. So the in-

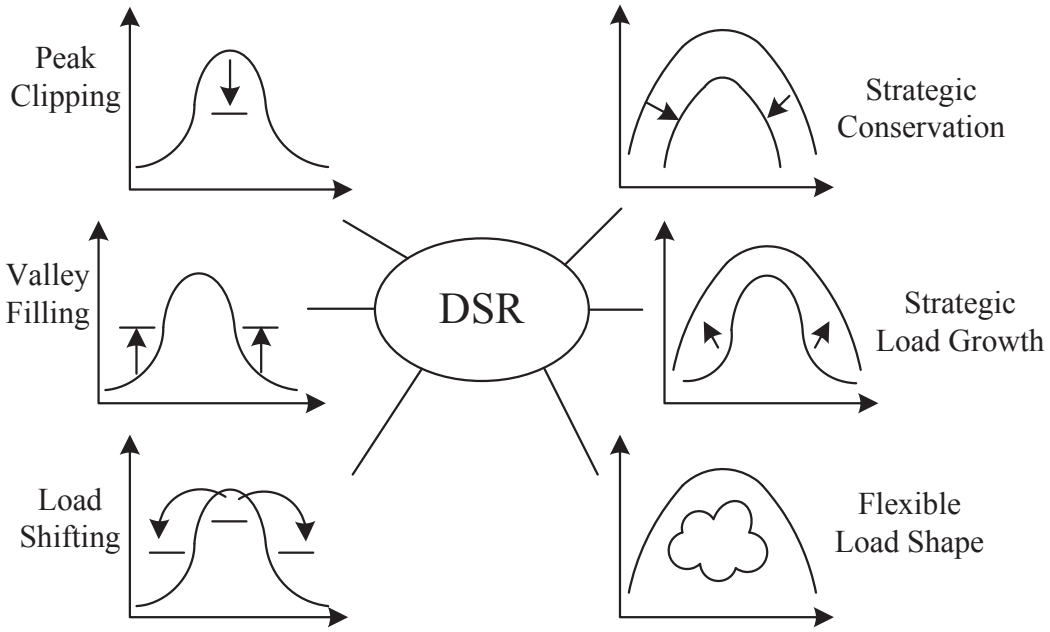

Figure 2.1: Basic technologies of DSR [3]

creasing penetration of wind power energy will cause the power system imbalance between the generation side and the demand side. Because the DLC can improve the power system stability, it can solve the imbalance problem caused by intermittent wind power energy increasing in the power system. In DLC method, utility companies making the contract with customers directly control or cut off controllable loads to maintain the power system in stable. In ILC method, utility companies send a price signal to consumers to encourage consumers shifting load from peak time to valley time to maintain the power system in balance and receive the power consumption information from consumers. DSR which is a low investing cost for generation company method can change or shift the load consumption to provide a valuable demand-side reserve capacity for solving imbalance problem caused by intermittent wind power energy. There is another type of method to solve this problem, which is wind generation output and demand forecasting method. After forecasting these two parts, the Gencos will formulate some scheme to maintain the power system in stable. However, there are many uncertainties of wind and demand forecasting method, such as weather variations and load fluctuation. DSR

can be seen as ancillary services to solve the imbalance problem caused by these uncertainties fluctuation. Compared with other methods, such as energy storage and spinning generation reserve, the DSR is a more effective and cheaper approach to solve this problem.

The rest of this chapter is organised as follows. The DLC methods in the smart grid are introduced in Section 2.2. Section 2.3 describes the ILC methods used in the smart grid. The optimisation DSR model is introduced in Section 2.4. In Section 2.5, DSR used in wind power system to solve imbalance problem caused by intermittent and time-varying wind power energy. Conclusions are drawn in Section 2.6.

2.2 Direct Load Control Supported Grid Frequency

The DLC is based on energy storage system in demand side and TCAs can participate in frequency regulation to improve the power system stability. When DLC based on energy storage system is used in the system, their charging/discharging dynamics can improve the system frequency stability. For DLC based on TCAs, the TCA loads are directly controlled to maintain the frequency staying in the suitable range.

2.2.1 DLC Based on Energy Storage System Approaches

As the demand load is growing fast and the difference between peak and valley is gradually widening, it is necessary to take measures to implement peak load shifting. The energy storage system depending on charging/discharging are suitable for the applications because it has high energy efficiency, fast response and low maintenance requirement [44]. The BESSs installed in the demand side and EVs used in DLC to maintain power system stability are introduced as follows. Because the BESS can install in the generation side and the demand side and it usually is installed in the generation side to balance the power system, in this situation, the BESS does not belong to DSR.

The BESS can cope with the frequency fluctuation in the power system due to

its fast response time [12,44,52,53]. Cheng et al. [70] present a new BESS based on dynamic available automatic generation control(DAA) and apply proportional automatic generation control (AGC) distribution strategies. The AGC based on ACE distribution can enhance the fast response capability of BESS. This approach tested in EI Salvador system, which indicates significantly improve the system AGC performance when BESS and the independent AGC control strategy use DAA concept. The new approach of BESS can improve the system stability. Kyoho et al. [11] introduce using DDC based on HPWHs and EVs as controllable loads to optimise battery storage capacity. The increasing competition in retail and power sector leads to power company reducing investment cost and maximising the benefit by a generator with high efficiency. The capacity of BESS should be reduced because the installation cost of BESS is expensive. The DDC and PEVs used in the power system can reduce the capacity of BESS, improve the system stability and satisfy the transmission constraints. Setlholo and Xia [54] combine residential TCAs loads and energy storage system for residential customers for five households in South Africa. Two parts have been studied. The first part presents an energy management system which utilises DSR to minimise the consumer's cost and to reduce the power consumption from the grid. Customers can realise cost savings and the power demanded from the grid is reduced by the optimal scheduling of power sources when the storage system based DSR and photovoltaic are used in the power system. The second part develops a model to investigate the joint influence of price and CO_2 emissions. Because it would enable co-optimization of electricity consumption costs and carbon emissions reductions, customers are stimulated to shift loads by an environment motivation during peak time. This study proposes model combines TCAs load and energy storage system to improve the stability of system frequency and reduce CO_2 emissions. Wang et al. [55] develops a novel method using energy storage devices for home area energy management as a key vehicle for DSR. The advantages of energy storage are giving lower wholesale energy and supporting low voltage distribution networks for reducing network investment. In this approach, the new operation strategies for domestic energy storage are developed. The contribution of energy storage is to maximise the overall savings in energy costs and

investment costs. The end customers and network operator manage the operation of the energy storage devices. The study is also carried out to investigate the impacts of different dispatch strategies on wholesale energy costs and network investment costs. Total benefits savings from energy costs and investment costs are evaluated by benefit quantification methods.

The disadvantages of the BESS, especially the one with large capacity, usually are their expensive auxiliary equipment and high installation price. To reduce the greenhouse gas emission and installation price, aggregating a number of small batteries of PEVs into an equivalent BESS instead of using a real BESS. The PEVs have drawn increasing attention in the transportation electrification in recent years [56–60, 62–64].

Dallinger et al. [61] present the V2G where a large number of small batteries of EVs are aggregated to improve the long-term dynamics of power system with a high penetration of wind power in Denmark. The V2G is investigated in the LFC scheme. The V2G is used to reduce the required spinning reserve of control power plants in the power system with high penetration of wind power. The V2G can charge/discharge the energy with quickly start, fast ramp up and down features. These characteristics are suitable for the integration of large penetration of intermittent wind power in the future Danish power system. This approach benefits the power system operation by minimising transmission congestions and deviations of electricity balancing. Yang et al. [65] propose a distributed acquisition method to control PEVs supporting grid frequency. Limited communication between neighbouring PEVs/distribution can obtain from frequency deviation for all PEVs. Based on battery charging/discharging, a dynamic PEVs model with feedback control is proposed and integrated with frequency regulation. This approach can provide accurate control signals for all PEVs, improve system stability and reduce device costs. Pham et al. [66] introduce a method uses EVs in LFC to help thermal turbine to maintain the system stability. Firstly, a closed-loop state-space model for the general power system is given. Then the four-area power system with a renewable discharged EVs is presented. Based on others' development on functional observers, novel distribution function observers are designed for each area and implemented

in given global state feedback controller. Compared with centralised observer based controller scheme, this approach is more robust in cope with accidental failures. Shimizu et al. [67] discuss a V2G model which consider the consumer's convenience used in power system with wind power to solve imbalance problem caused by the wind and solar power. The SOC control method enables the SOCs of all EVs to be synchronised. The proposed method is used in LFC scheme. Results show the V2G controller can help power system to suppress the frequency fluctuation. Lopez et al. [68] present an optimisation model to perform load shifting in the smart grid by EVs. In this model, the agents are responsible for load, generation and storage management. The EVs can provide load shifting and congestion alleviation services to the smart grid. In conclusion, the EVs used in the grid can flatten the load curve.

2.2.2 DLC Based on TCAs Approaches

The DDC method is also widely used in the power system in recent years. In DDC, the controllable load can be controlled by energy provider with short notice or automated response to frequency deviation. Conventionally, the DDC employs the TCAs, such as EWHs [71–75], refrigerators [43, 78] and heating, ventilation, and air conditioners (HVACs) [79–82].

Vrettos et al. [83] show a dynamic model of EWHs used in the LFC scheme. The water tank of the EWHs is the thermal stratification. This model describes the power consumption behaviour of a large number of water heaters and to assess customers comfort which loses of some external control actions. Four rule-based control approaches for aggregate power set-point tracking are introduced and compared in the simulations. The control strategies are assessed by the tracking quality, device operation and customer comfort when EWHs is operating. Heffner et al. [84] describe a low-cost statistical approach for a pilot effort to measure load reductions from EWH loads control program. In this experiment, the curtailment service provider (CSP) can collect hourly load data for two substations and hundreds of households of load control testing over six weeks. Substation level and premise level data from tests which verify some point estimates in the hourly diversified demand curves are analysed. Based on this experiment, the recommendation is provided for independent

system operator (ISO) and DSR managers to consider before choosing the conventional or costly program-wide load research approach developing.

Angeli and Kountouriotis [78] propose controlling the refrigerators to manage power consumption. The operating temperature of these refrigerators and energy consumption is modified dynamically in a safe range to response the fluctuation of frequency. The decentralised random controllers are designed to respond to sudden plant outages and to avoid the instability phenomena. A stochastic approach is used to achieve desynchronization of each refrigerator and to keep total power consumption regulated. Short et al. [43] investigate incorporating DDC based on refrigerators into certain consumer appliances to maintain frequency stability. Devices can monitor system frequency and switch appliances on or off to keep the system in balance. The simple power system model includes incorporating aggregate generator inertia and governor action of the DDC. The DDC controls 1000 individual refrigerators to participate in frequency regulation. This method shows that an aggregated controllable loads have the potential to provide significantly enhanced frequency stability to the power network, both at times of sudden increase in demand (or loss of generation) and during wind power fluctuation.

[82] and [28] introduce the DDC which controls the heating, ventilating and air-conditioner (HVAC) system. In [82], it investigates aggregated HVAC system used in smart grid to provide the potential intra-hour load balancing services. The simplified model of HVAC was developed and considers the thermal energy balance. Then the aggravated HVAC model is investigated. A temperature-priority-list approach is used to optimally control the HVAC systems to keep customer-desired indoor temperatures and system balance under different outdoor temperature profiles and indoor temperature setting. The intra-hour load balancing services based on aggregated HVAC can meet the performance requirements. In [28], it focuses on designing a centralised load controller to control HVAC system for continuous regulation reserves (CRRs). This paper uses measurement data to describe the controller logic for setting up baseline load, generate priority lists, issue dispatch commands and tune the simplified forecaster model. The centralised TCAs load controller can provide robust, good quality CRRs with reduced communication. Results show

controller can precisely control the aggregated HVAC model. So there are many controllable load services used for many other DSR programs, such as peak shaving and load shifting. Lu et al. [85] investigate the TCAs which include HVAC systems from a centralised controller as the energy storage services. The turn-on and turn-off time and duration of individual TCAs are arranged by dispatch algorithms for the controller. Each TCA operates within the customer-desired temperature range, maintains the TCA load diversity, and makes the aggregated TCA load at the target load level are the goals of the control method. There are 1000 units of HVACs modelled to demonstrate the control algorithms to provide load shifting and load balancing services for 24 hours in the power system. Offering customers' appliances for high value load balancing services can provide them revenue and this action can help integrate more renewable resources into the power grid.

Pourmousavi and Nehrir [25] introduce DSR loop in the traditional single-area LFC system. This formulation can be expanded to a type of controllable loads in different size with different characteristics. Power sharing between the supply side and the demand side optimised can achieve optimal operation in the LFC with DSR model. The PI controller design considers the communication delay of DSR via $Padé$ approximation. DSR control loop increases the stability margin of the system and DSR effectively improves the system dynamic performance. Pourmousavi and Nehrir [86] propose a general DSR algorithm for frequency regulation in the microgrid with/without wind power energy. An adaptive hill climbing (AHC) strategy is used in the DSR strategy designed to continuously balance generation and demand. After sudden disturbance happening in the system, the application of AHC controller decreases the frequency deviation with maximum effort. It also finds a minimal quantity of controllable loads to keep the frequency within the desired range and to maintain the system in stable.

With DSR technology developing, many papers focus on modelling and control of aggregated homogeneous or heterogeneous thermostatically controllable loads by DDC [26, 27, 87–91]. Zhang et al. [26] introduce a highly accurate aggregated model for a population of air conditioning loads. This method systematically deals with load heterogeneity, statistical information of the load population, and accounts for

second-order dynamics in the model to accurately capture the transient dynamics in the collective response. A novel aggregated control method which is fully responsive and achieving the control objective without sacrificing end-use performance for this model is designed under realistic conditions. This model is simulated by GridLAB-D software which is an open source distribution simulation tool. This proposed approach can manage aggravated air conditioning systems to regulate frequency and to reduce peak load. Kalsi et al. [92] develop aggregated control models for a large population of homogeneous TCAs based on EHWs and HVAVs in this paper. The effect of DSR and user over-ride on the load population dynamics are investigated. The proper controller is designed for this model and the system can be in stable from any initial state. So it is possible to control TCAs to match intermittent renewable energy with reducing the capacity of energy storage system. In the future, it would control other kinds of loads which are controlled by a timer and consumer behaviour, such as microwaves and clothes dryer.

Zhang et al. [89] develop an aggregated model for a heterogeneous population of TCAs, in which can accurately capture TCAs's collective behaviour in DSR. The aggregated model needs to capture the transient dynamics in the collective response. The model is simulated by GridLAB-D software. Results show the aggregated load model can accurately reduce the oscillations in the transient behaviour of the population of TCAs. Koch et al. [93] present a novel control approach for a large number of the aggregated of heterogeneous TCAs. Compared with traditional DSR methods, this approach can provide short-term ancillary services, such as balancing the power system and frequency control. A statistical modelling approach which uses Markov Chains describes the evolution of probability mass in a temperature state space. The bin transition modelling provides accurate enough the dynamic behaviour of the aggregated TCA loads. The approach uses a predictive controller. Results show this approach can be used in the realistic system.

2.3 Indirect Load Control Methods for Economic Influence in Smart Grid

The DLC can control controllable load to support grid frequency. However, DLC can not control some kinds of loads, such as lightings and washing machines. The ILC is another type of DSR to shift demand loads of the peak time. In ILC, consumers are encouraged to shift their loads by price signal and the load consumption information is sent to generation companies. Customers can shift some demand loads from peak time to valley time to reduce the load in peak time due to the electricity price is high in peak time and it is low in the valley time [22,23,94–97]. Table 2.1 introduces three main approaches of ILC, which are RTP, ToUP and CPP.

Table 2.1: Introduction of different ILC methods [21,45]

ILC Approaches	Description
Real-time pricing (RTP)	Customers can receive the RTP on day-ahead or hour-head basis. The price of electricity typically fluctuates hourly reflecting the wholesale electricity price changes.
Time-of-use pricing (ToUP)	ToUP is different unit electricity price for usage in different time and it is usually defined for 24 hour a day. ToUP reflects the average cost of generating and delivering power during those time.
Critical-peak pricing (CPP)	CPP is a hybrid of the RTP and ToUP design. CPP includes a pre-specified, extra-high rate and affects for serval hours.

Bae et al. [98] present a system architecture and an algorithm for DSR called user-friendly DSR which is based on time-varying price information. The electricity bill, usage pattern, and rebound peak load algorithms are three factors in the user-friendly DSR. At first, the objective function is formulated based on the electricity bill and the usage pattern, in which the electricity bill is minimised and the usage similarity is maximised. Then, a load balancing algorithm is applied to avoid

a blackout and to minimise rebound peak. The proposed ILC scheme shifts some loads from peak load time to valley time and leads to significant electricity bill saving and users satisfaction ratio. Safdarian et al. [95] incorporates ILC in distribution companies (Discos) short-term decision model in a real-time pricing environment. Consumers are charged based on hourly varying prices. Besides the hourly real-time prices, this model also accounts for other Disco's short-term activities, such as hourly purchases from the grid, invocation of load curtailments and commitment of distributed generation units. This model considers the stochastic nature of wholesale market prices and customers load. The model is a mixed integer linear programming problem solved by commercial software packages. The objective of this method is the Disco's expected maximum profit while its revenue is limited by regulating bodies. Ma et al. [22] propose price-based energy control method to shift peak load in the smart grid. The consumers can control their energy consumption to make a tradeoff between the electricity cost and the load curtailment cost. The real-time pricing is based on the total load consumption. The distributed energy control algorithm is proposed in this method and it provides a sufficient convergence condition to converge to the equilibrium. Results show this method can shift peak load and balance system between the generation side and the demand side. Kwac et al. [99] use advanced metering infrastructure (AMI) for household electricity segmentation. This method uses an encoding system which has a pre-processed load shape dictionary. Five samples program and policy relevant energy lifestyle segmentation strategies in the encoded data are driven by the structured method. This method describes the implication for utility policy, DSR and energy efficiency. Using customers' load shape can reach the objective that customers can have the highest potential for profit from ILC programs. DSR changing load shape can obtain significant benefits for the power system, such as energy savings and public relations benefits from successful engagement in utility programs.

In conclusion, the DSR can be classified to DLC and ILC. The DLC and ILC can improve the stability of power system and solve the imbalance problem caused by intermittent power system. These two types of DSR are compared and shown in Table 2.2.

Table 2.2: Comparison of DLC and ILC [9, 145]

Attributes	DLC	ILC
Why participate	Bill savings Environmental benefits	Bill savings Environmental benefits
Required equipment	Remote control switches Embedded controls Building energy management system Communication systems	Controllers and timers Smart meters Communication systems
Required actions	Limiting loads Peaking clipping Maintain grid frequency	Shifting loads Flexible loads
Who controls loads	Distribution utility ISO Aggregators Customers	Customers

2.4 Optimisation DSR Model

Optimisation models for DSR are using some technologies to improve efficiency for the power system, such as PSO and convex optimisation, etc.

DSR based on convex optimization method is researched in many papers [100–102]. Gatsis et al. [101] propose a formulation for load control between multiple residences and the electricity provider. The residential end user has two type of adjustable loads. One kind of load must consume a specified total energy over the scheduling horizon, but it can be changed to use in different time. Another kind of load cannot entail a total energy requirement, but operation away from a user-specified level results in user dissatisfaction. This method considers minimising the electricity provider cost and user dissatisfaction. The advanced metering infrastructure (AMI) is used to exchange information between utility companies and the end-users. The two-way communication network should converge to the optimal amount of electricity production and the optimal power consumption schedule. The

algorithm can find near optimal schedules ever when AMI messages are lost.

There are some other methods to optimise DSR models [77, 103–106]. Faria et al. [104] present a PSO to minimise of the operation costs of a virtual power player that manages the resources in a distribution network and itself. Resources include the distributed energy resource in the considered period and the energy brought from external energy suppliers. In this paper, the approach considers constraints of the network. The Gaussian mutation of the strategic parameters is used in this approach. Sepulveda et al. [106] propose binary PSO (BPSO) to find the optimal load demand schedule. This approach can make the peak demand load in minimum and keep customer conform level in maximum. This model based on EWHs is simulated by Matlab and used data is collected from 200 households by smart meters. The proposed method can keep the stability of the power system and save cost. Zhu et al. [105] use integer linear programming (ILP) technique to minimise the peak hourly load, so that it achieves an optimal daily load schedule for DSR in the smart grid. Both the optimal power and optimal operation for power- or time-shiftable appliances according to all the individual appliances are scheduled by proposed mechanism. This approach considers users preference and the power consumption patterns.

2.5 Applications of DSR in a Wind Power System

The wind power energy develops fast and is widely used in the power system. A challenging problem of integrating intermittent wind power into the modern smart grid is to balance the active power between the generation and the demand and to maintain the frequency at its desired value. The DSR, which includes DLC and ILC, solves this imbalance problem. The forecasting wind power and demand approach is also used to solve this problem, but there are some uncertainties in this method. The DSR as ancillary services is used in the power system to optimise this method. These methods can improve the power system stability and allow more wind power generator to participate in the power system.

2.5.1 DLC for Wind Power System

The DLC can handle some controllable loads to keep the balance between the generation side and the demand side when large scale wind power is integrated into the power system. The controllable loads consist of energy storage system and TCAs load. These two kinds of controllable loads used in DLC can be used in the power system to solve the problem caused by intermittent wind power energy.

Energy Storage System for Wind Power System

When intermittent wind power energy is integrated in the power system, the energy storage system is a conventional method to solve the imbalance problem caused by intermittent wind power energy and improve renewable energy penetration in power system [69, 107–109]. Yao et al. [109] present a new BESS approach which enables dispatch from power system with wind power energy in the short-term. There are two BESSs used in this scheme: one BESS is charged by wind power. Meanwhile, the second BESS discharges power into the grid. The role of these two BESS can be interchanged when the BESS reaches specified state of charging/discharging. This method forecasts charging wind power and monitors states of charge of these two BESS so that wind energy is maximised to harness. This method also achieves the minimum number of the BESS switch-over which prolongs the service life of the BESS.

With the development of technology, many people pay their attention to EVs because EVs do not produce greenhouse gas and the quantity of EVs installed increases quickly in recent years. The EVs can provide frequency support of smart grid via controlling the charging/discharging of these batteries [60, 67, 111]. Huang et al. [112] apply PEV charging strategies to help the system to handle the high penetration of wind power. The PEVs absorb intermittent output power from wind turbines. Customers will charge their PEVs parked at home at minimum cost time. Therefore PEVs absorb as much surplus wind as possible. Because the domestic EVs are parked for 95% of the time, the contribution of this paper is that EVs can be used to balance the power system. This approach utilises PEV charging to regulate surplus wind power by implementing an electricity price function. As PEVs are

charging at minimum cost, the cost function shift to the cheapest electricity time and use surplus wind power energy as much as possible. This method can also benefit the consumers when the EVs are charged in the cheapest way. Masuta et al. [111] propose using EVs, BESS and HPWHs as controllable loads in LFC method to some problems, such as frequency fluctuation, caused by wind power energy and solar power energy. The LFC signal is taken as the input signal to control these DSR models. This new method is effective to restrain frequency fluctuation in the LFC system with a large integration of wind power energy and solar power energy.

DDC Method for Wind Power System

While installation price of energy storage system is too high, DDC which controls the TCAs load is a better approach to reduce the scale energy storage system and to solve imbalance problem which caused by intermittent wind power energy [110, 113, 114]. Rijcke et al. [115] discuss using the DDC to balance demand and supply when the integration of wind power system increases. Traditional balancing methods are provided by generation units. DDC provides a new approach to balance the system and to reduce the generation margin. There are two groups of appliances: one group appliances operate daily during a period of one to three hours and another one is constantly in standby mode and operate with on and off periods. Controlling the second group loads is called DDC, in which load shifted depends on load characteristics and desired comfort. DDC can contribute significantly to resolve imbalances from wind power. Masuta et al. [73] present an efficient control of HPWHs equipped in the power system with a high penetration of wind power energy and solar power energy by using two-way communication networks. In this paper, a statistical HPWHs model is used by the central load dispatching centre. In this system, the BESS is also used to solve this problem. Oldewurtel et al. [12] provide different DSR to solve the problem caused by fluctuating renewable energy. There are four resources, which contain BESS, PEVs, DDC based on TCAs and commercial building. The main challenges associated with using DDC and energy storage system include ensuring availability of the resources, properly incenting participants, and coping with high installation costs. The new algorithms which

manage the resources better and new technologies of battery and communication which reduce investment cost are of potential to solve those challenges. The contribution of this paper is developing a framework for assessing DDC and energy storage resources, analysing these resources for proving power system service and comparing these four resources.

2.5.2 ILC Method for Wind Power System

The ILC can also be used to solve the imbalance problem caused by intermittent wind power energy in the power system [116–118]. Roscoe and Ault [116] use real-time electricity pricing to dispose of intermittent wind power energy. Many paper presents using DLC to maintain the system balance, but the limitation of DLC is that it is less acceptable for loads such as lighting and washing machines. So this paper uses real-time electricity pricing in the power system. This method allows customers to be flexible to retain overall control. Results show the demand can reduce between 8 and 11GW at the peak demand and low wind can be achieved in the UK. So the ILC method can shift load and keep systems with intermittent wind power energy in stable. Khomami and Javidi [117] propose using real-time pricing program for energy management of renewable energy in the smart grid. The wind and solar supply and gas turbine are equipped on the generation side and smart houses are capable of responding according to real-time prices. The day-ahead schedule is determined. Then mathematical optimisation model defined as the is the mixed integer non-linear problem is used to solve this problem. The purpose of this method is maximising the benefit to the operation with specific constraints.

2.5.3 Wind Generation and Demand Forecasting Method

The forecasting of wind power output and demand load is another kind of method to solve imbalance problem caused by intermittent wind power energy. While some uncertainties from forecasting method which reflected in the forecasting error, the DSR is used to increase flexibility and integration of wind power energy [119–121]. Pascual et al. [121] propose an energy management strategy for a residential micro-

grid including photovoltaic (PV) panels and a wind turbine. It allows for a controlled power exchange through a BESS and its control strategy. The proposed control strategy uses the battery SOC as input date. The SOC of BESS can correct the forecasting errors from the using forecasted data. Compared with other state-of-the-art strategies, the proposed energy management strategy results in a better grid power profile for a given storage system. Sahin et. al [122] use hourly scheduling of reserves stochastic method to solve the problem caused by the hourly forecasting errors of wind power and load. This method is based on security-constrained unit commitment (SCUC) model, the day-ahead scheduling of wind energy and conventional units with $N-1$ contingencies. The DSR is used to manage hourly violations and decrease the cost of supplying load. The hourly wind energy and system load forecasting errors are represented in the mixed-integer programming (MIP) model by applying the Mote Carlo method. The ISO or a vertically integrated utility can use this method to address the stochastic cost of security.

2.6 Conclusion

The objectives of DSR are improving system stability and influencing economic in the power system. The DSR can be classified into DLC and ILC based on control method. The DLC which handles controllable loads can participate in frequency regulation to improve power systems stability. The controllable loads include TCAs load and energy storage system. The ILC which encourages customers to shift load from peak load to valley time can produce benefits for customers, retailers and generation companies. From Gencos' point of view, the DSR can help system to reduce the peak demand load and reshape the load profile, so that they can reduce the installation of expensive equipment, such as enough backup capacity. Form consumers point of view, consumers can reduce their bills through the DSR.

The DSR can solve power system imbalance problem caused by high penetration of intermittent wind power energy. The DLC can participate in frequency regulation to solve the imbalance problem. The ILC depends on shifting demand load to solve this imbalance problem. Wind generation and demand forecasting method is also

capable of solving this problem. However, uncertainties will affect the forecasting results. The DSR as an ancillary service can regulate these errors to guarantee the system operating normally.

Chapter 3

LFC with Direct Load Control in Power System

3.1 Introduction

DSR is a very promising solution for improving power system resilience and stability [78, 129]. DSR can be classified as DLC and ILC, as introduced in Chapter 1. In the smart grid, the grid frequency is an indicator of the balance between the demand and the supply of the active power. In this thesis, the frequency response services from the generation side have been extensively investigated, providing the frequency response services from the demand side will be investigated, i.e., the DLC participated in frequency regulation in smart grid will be investigated. The DLC is investigated based on the controllable loads.

In recent years, research has been initiated on the possibility of using frequency responsive loads, which called dynamic demand control (DDC) [78]. As one promising DSR technology, dynamic demand control (DDC) can provide the following two benefits in frequency control markets: providing an additional control and reducing the spinning capacity [130, 131]. The TCAs use thermostat to keep the temperature of appliances near the desired setpoint, including EWHs, refrigerators and air conditioners (ACs). The HPWH is one kind of EWH, which uses a heat pump to heat water. A number of customers use air conditioners and HPWHs in the

home. Hence, aggregated air conditioners model and aggregated HPWHs model are investigated. The DDC based on air conditioners model is controlled via an integral controller using the frequency deviation of the power system. For HPWHs model, the input signal is LFC single and output is the total power consumption of total HPWHs.

Energy storage systems introduced in this thesis include BESS and PEVs. The BESS equipped with a controller based on area control error (ACE) has successfully achieved the frequency regulation [53]. The different capacity of BESS can be equipped on the generation side and the demand side. The BESS depends on its discharging/charging to participate in frequency regulation in the power system. The disadvantage is that the BESS, especially the one with large capacity, usually requires some expensive auxiliary equipment and high installation cost. The EVs which are parked at home or workplaces most time have drawn increasing attention in the transportation electrification in recent years because the EVs can reduce the greenhouse gas emission. An EV is propelled by an electric motor using batteries that are charged by an external power source [132]. The PEV is one type of EVs and EVs also include battery EVs, hybrid EVs and range extended EVs. The small capacity battery of PEVs can be used as distributed energy storage to provide support of the grid operation, called vehicle-to-grid (V2G) service [133]. V2G is required to aggregate a large number of small batteries of individual PEV as an equivalent grid-scale BESS and then provide frequency regulation of smart grid via controlling the charging/discharging of these batteries by the same controller [60, 65, 66]. Thus, the aggregated model of PEV should be investigated.

The model of LFC with general DLC which has communication time delay using $Padé$ approximation is introduced. This general DLC model is as general as possible for different kinds of controllable loads and considers the time delay in DLC loop [25]. In this model, it gives an opportunity to the system operator to choose the DSR or spinning/non-spinning reserve, or a combination of the two reserves.

As the LFC system and the aggregated DLC use the communication channels to transmit the measurements and control commands, multiple time delays exist in the LFC scheme and DLC scheme. Time delays will deteriorate the dynamic

performance or even cause instability of the closed-loop system [34, 35]. In this chapter, the time delay model of LFC with different DLCs is investigated.

The rest of this chapter is organised as follows. The LFC with DSR model is introduced in Section 3.2. Section 3.3 the DDC model based on the air conditioners or HPWHs is described, respectively. The details of BESS model and PEVs model is described in Section 3.4. After that, the general DLC model is presented in section 3.5. Conclusions are drawn in Section 3.6.

3.2 Load Frequency Control with DSR Model

This section describes single area LFC model and time delay model of LFC with BESS, DSR based on air conditioners, HPWHs and PEVs based on [25, 53, 65, 111, 124, 125]. The structure of frequency regulation and single area LFC model and time delay model of LFC with different DSR are introduced.

3.2.1 Single Area LFC Model

Three instabilities, which include rotor angle instability, voltage instability and frequency instability, are in the power system [127, 128]. Although power system is highly non-linear and time-varying nature, the frequency deviation after disturbance is small. So the linearized model is used for the frequency response of power system under load disturbances.

The simplified LFC model, is shown in Figure 3.1. The generators equipped in the power system are assumed to a non-reheat turbine. The relationship between the energy imbalance and the corresponding frequency deviation can be expressed as follows in time domain:

$$\Delta P_m(t) - \Delta P_L(t) = 2H\frac{d\Delta f(t)}{dt} + D\Delta f(t) \tag{3.2.1}$$

where ΔP_m, ΔP_L and Δf are mechanical power change, load change and frequency deviation, respectively. The H is the inertia constant and D is the load damping coefficient.

Using the Laplace transform, equation 3.2.1 can be represented in frequency domain as:

$$\Delta P_m(s) - \Delta P_L(s) = 2Hs\Delta f(s) + D\Delta f(s) \tag{3.2.2}$$

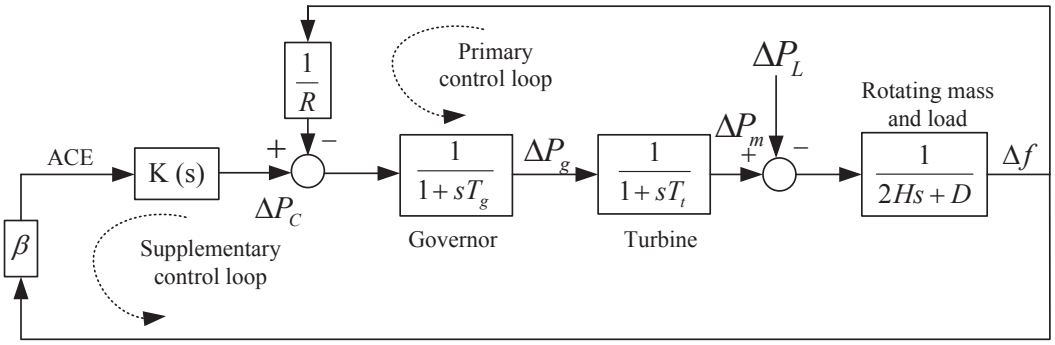

Figure 3.1: Single area LFC model [41]

In the LFC system, the primary control loop which operates at ten of seconds can stabilise the frequency but the frequency can not restore the nominal value. In primary control loop, the speed governor (with time constant, T_g) with the droop unit (speed droop, R) senses the frequency deviation and quickly decreases the deviation at stable [24]. The supplementary control loop (usually called LFC) is required to eliminate the steady state error of the frequency deviation [25]. In the supplementary control loop, the β is a bias factor. $K(s)$ is a controller, which commonly uses the PID type controller in practice.

Because there is no tie-line power exchange in the single area LFC system, the area control error (ACE) is defined as:

$$ACE = \beta\Delta f \tag{3.2.3}$$

Using ACE as the input of the LFC, a PID type controller is designed as

$$u_i(t) = -K_{Pi}ACE_i - K_{Ii}\int ACE_i dt - K_{Di}\frac{d}{dt}ACE_i \tag{3.2.4}$$

where $K_i = [K_{Pi}\ \ K_{Ii}\ \ K_{Di}]$ are proportional, integral and derivative gains, respectively.

3.2.2 Time Delay Model of LFC with DLC

The LFC scheme and the aggregation of DSR will use the communication channels to transmit the measurements and control commands. The model of LFC with the DSR is modified to include communication time delays into LFC loop and DSR loop shown in Figure 3.2 [33, 126]. DSR models consist of PEV model and DDC model based on air conditioners and HPWHs. The input signal for the BESS is the ACE signal and input signal of HPWH model is LFC signal. The grid frequency deviation is the input signal for PEV and air conditioner model.

Because the communication channels are used in the system, the multiple time delays exist in the LFC with DSR model. The τ_1, τ_2, τ_3, τ_4 and τ_5 are the communication delays in LFC control loop, BESS loop, PEV loop, DDC loop and HPWH loop, respectively. The communication time delay τ_i is represented by $e^{-s\tau_i}$ in Figure 3.2.

From Figure 3.2, the relationship between the energy imbalance and the corresponding frequency deviation can be given as follows:

$$\begin{aligned} & \Delta P_m(s) - \Delta P_{BESS}(s) - \Delta P_{HPWH}(S) - \Delta P_L(s) - \Delta P_{AC}(s) \\ - \quad & \Delta P_{V2G}(s) = 2Hs\Delta f(s) + D\Delta f(s) \end{aligned} \tag{3.2.5}$$

where $\Delta P_{BESS}(s)$, ΔP_{HPWH}, ΔP_{AC} and ΔP_{V2G} are the power deviation from BESS, HPWH, air conditioners and PEVs, respectively.

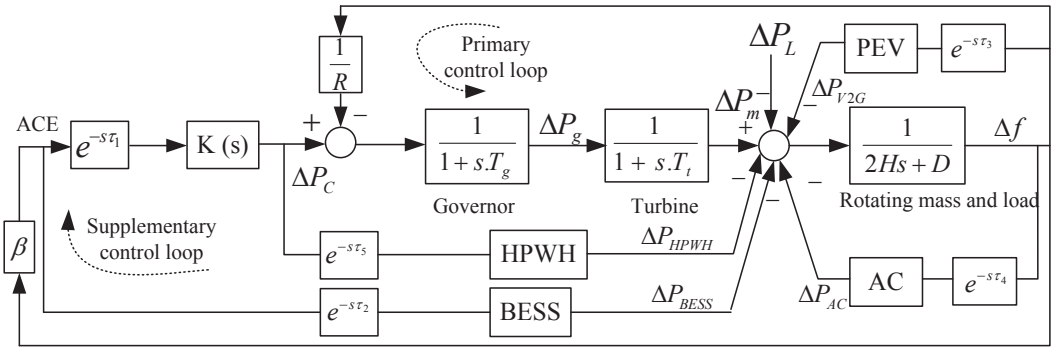

Figure 3.2: Single area time delay model of LFC with different kinds of DSR

3.3 DLC Method Based on TCAs Load

Besides the controlling of the power support through the generators or storage facilities, the management of the power demand is an alternative way to solve the power imbalance problem of the smart grid. Domestic electric appliances of the user side can be classified into five different groups based on their characteristics [96], in which the TCA loads (such as air conditioners, refrigerators and HPWH) and energy storage system (such as PEVs) can be used as controllable load for frequency regulation, since they are relevant directly to the frequency derivation. In this section, it will introduce the DDC model based on air condition or HPWH, respectively.

3.3.1 Model of Controllable Air-Conditioner

In this section, a typical thermostatically controlled load, air conditioner, is considered as the DDC loads, in which the controllable loads participate in the frequency regulation by adjusting their usage of electricity based on the frequency deviation [79, 80, 124].

The frequency dependent characteristic of thermostatically load can be expressed as:

$$\Delta P_{\mathrm{DDC}} = \Delta P_{LC} + D_{ac}\Delta\omega \tag{3.3.1}$$

where D_{ac} is the reheat coefficient of the air conditioner, $\Delta\omega = 2\pi\Delta f$ is the deviation of the speed, and ΔP_{LC} is the controllable change in power consumed, which depends on the characteristic of the air conditioner and the set point of a smart thermostat, ΔT_{st}, and can be represented as follows:

$$\Delta P_{LC} = \frac{mc_p}{EER}\Delta T_{st} \tag{3.3.2}$$

where m is the mass of air flow, c_p is the specific heat capacity of air, and EER is the energy efficient ratio (EER) defined as the ratio of the capacity output to electricity input of a air conditioner [87].

The smart thermostat is usually controlled via an integral controller using the frequency deviation (Δf) from the control area as the input and the temperature

set-point as the output, namely,

$$\Delta T_{st} = \frac{\bar{K}}{s}\alpha_{AC}\Delta f \tag{3.3.3}$$

where $\bar{K}$ is integral gain and α_{AC} is a coefficient (given as 0.5 Rs/Hz in this paper). The temperature set-point is bounded and varies based on the weather condition and different time interval in a day. In this paper, these variations are ignored and the thermostat set-point is simply bounded as $[24°C, 29°C]$.

From the aforementioned discussion, the load model with respect to frequency deviation of air conditioner is given as:

$$\Delta P_{\mathrm{AC,i}} = \left(\frac{0.5K_{ddc,i}}{s} + 2\pi D_{ac,i}\right)\Delta f \tag{3.3.4}$$

where $K_{ddc} = \frac{mc_p\bar{K}}{EER}$ is the combined integral gain.

Due to the small capacity of an individual air conditioner, it is necessary to aggregate a number of small domestic loads into a relatively large and lumped DDC load to participate the LFC scheme. Assume that there are M air conditioners in the smart homes of the grid and these M air conditioners have the same characteristic, then the aggregated power of the DDC can be presented as following:

$$\Delta P_{AC} = \sum_{i=1}^{M}\Delta P_{AC,i} = \left(\frac{0.5K_{DDC}}{s} + 2\pi D_{ac}\right)\Delta f \tag{3.3.5}$$

where $K_{DDC} = \sum_{i=1}^{M} K_{ddc,i}$, and $D_{ac} = \sum_{i=1}^{M} D_{ac,i}$.

3.3.2 Model of Heat Pump Water Heater

The HPWH which belongs to TCA load is a high efficient and energy saving appliance, which stores hot water in a tank and can be used in one day [111]. The HPWHs are widely used in many families and always operate to heat water as much as the requested for the next day use during the night. The power consumption of the HPWHs can be controlled without decrease in efficiency in the range of $90 \pm 10\%$ of the rated power consumption via LFC signal [111]. Then HPWHs are uncontrollable when the power consumption becomes stable which is (the HPWHs model in this chapter is after starting 0.25[h]) and the operation period can be controlled [73].

This section introduces the HPWH model based on [73, 111], in which the temperature of the heated rate for HPWHs based on customer choose temperature range. However, the aggregated HPWHs model will set a uniform temperature range for HPWHs which participate in frequency regulation.

A number of HPWHs are installed in the controllable area. These HPWHs have same characteristics. The power consumption of an HPWH is considered as 90 % of the rated power consumption because the power consumption of each HPWH is controlled in the range of 90 ± 10 % of the rated power consumption. The following equation shows the expected heating period of the jth HPWH (T^j_{heat}).

$$T^j_{heat} = \frac{E^j_{request}}{0.9P^j_{HP} \cdot COP^*_{estimated}} \tag{3.3.6}$$

where $E^j_{request}$ is the requested amount of hot water and P^j_{HP} is the rated power consumption of each HPWH. The $COP^*_{estimated}$ is the coefficient of performance, which is calculated based on weather forecast as the average value.

Assume the controllable area has a number of HPWHs which are controlled in the same time. However, those HPWHs are divided into several groups and each group operates in the different period. So the average values of expected heating period of total HPWHs (T^k_{AVG}) is calculated by equation (3.3.7) and sent back to each group:

$$T^k_{AVG} = \frac{\sum_{j=1}^{N_{HP}} T^j_{heat}}{N_{HP}} \tag{3.3.7}$$

where N_{HP} is the total number of controlled HPWHs in the controllable area.

Then the standard deviation of the expected heating period in each group is shown:

$$T^k_{SD} = \sqrt{\frac{\sum_{m=1}^{N_{HP}} (T^m_{heat} - T^k_{AVG})^2}{N_{HP}}} \tag{3.3.8}$$

Figure 3.3 shows the dynamic behavior of lumped HPWH model in one group. Based on the statistical information, T^k_{AVG} and T^k_{SD}, it estimates the change of the total power consumption of the HPWHs. It also determines the start-up time and the control period. Meanwhile, it dispatches the start command and LFC signal to each HPWH. The input of the model is LFC signal for HPWHs in one group and output

is the total power consumption of them. In Figure 3.3, the $P^k_{installed}$ is the total rated power consumption of installed HPWHs and T_{im} is delay of induction motor.

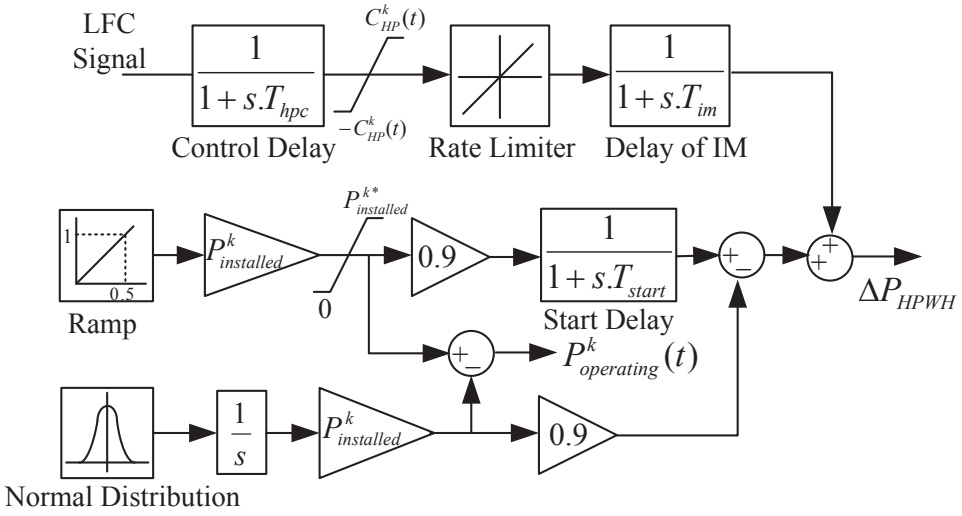

Figure 3.3: Lumped HPWH model [111]

The total controllable capacity of the HPWHs in the k^{th} group is shown as:

$$C^k_{HP}(t) = \begin{cases} 0, \quad if\ t < t^k_o + 0.25[h] \\ 0.1 \cdot P^k_{operating}(t - t^k_o - 0.25, \quad if\ t^k_o + 0.25 < t < t^k_o + 0.75[h] \\ 0.1 \cdot P^k_{operating}(t), \quad if\ t^k_o + 0.75 < t[h] \end{cases} \tag{3.3.9}$$

where $P^k_{operating}(t)$ is the total rated power consumption of the operating HPWHs which are shown in Figure 3.3.

When the first one of the HPWHs starts, the t is equal to t^k_0. The $t^k_0 + 0.25$ [h] is defined when the first starting HPWH's power consumption becomes stable [111]. The $t^k_0 + 0.75$ [h] is defined when the last starting HPWH's power consumption become stable [111]. The last starting HPWH in this introduced model starts at $t = t^k_0 + 0.5$ [h]. Assume that HPWHs do not start after $t = t^k_0 + 0.5$ [h] and no HPWHs stop operating from $t^k_0 + 0.5$ [h] to $t^k_0 + 0.75$ [h], the $P^k_{operating}$(t) is kept constant in this period. After $t = t^k_0 + 0.75$ [h], all the operating HPWHs are controllable and $C^k_{HP}(t)$ changes in proportion to $P^k_{operating}$(t).

3.4 DLC Method Based on Energy Storage System

The energy storage systems includes PEVs model and BESS model which installed in the demand side. The BESS usually installs in the generation side, in situation, the BESS can not be seem as regard as DSR. So this section introduces the aggregated PEVs model. Energy storage systems charge in valley time and discharge in the peak time. The energy storage systems participate in frequency regulation by their charging/discharging dynamics.

3.4.1 Model of Plug-In Electric Vehicles

The BESS with large capacity usually requires some expensive auxiliary equipment such that it is not a very economical way for frequency regulation. The PEVs have drawn increasing attention in recent years, and some the small batteries of those PEVs can be considered as an equivalent large scale BESS. Therefore, large scale PEVs have the potential to provide frequency support to the grid. The battery of the PEV comprising parallel/series connected battery cells is connected to the distribution grid through the dc/ac inverter, and its equivalent circuit is shown in Figure 3.4 [65, 125, 134].

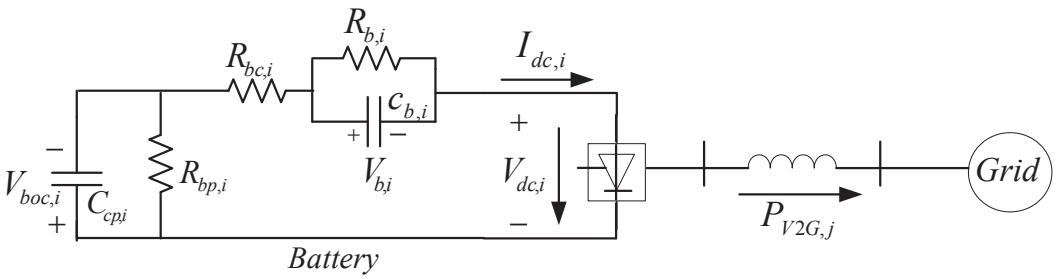

Figure 3.4: Equivalent circuit of grid-connected PEV

The equivalent circuit reflects the discharging/charging characteristics of the battery (self-discharge, battery capacity storage and over-voltage etc.) [65]. The dy-

namic equations of battery are given as below:

$$(3.4.1)$$

$$C_{cp,i}\frac{dV_{boc,i}}{dt} + \frac{V_{boc,i}}{R_{bp,i}} = I_{dc,i} \tag{3.4.2}$$

$$C_{b,i}\frac{dV_{b,i}}{dt} + \frac{V_{b,i}}{R_{b,i}} = I_{dc,i} \tag{3.4.3}$$

where $V_{boc,i}$ is the open circuit voltage of battery, $V_{dc,i}$ is the battery's DC voltage, $V_{b,i}$ is the battery overvoltage, $R_{bc,i}$ is the resistance of the battery's terminals and inter-cell connections, $I_{dc,i}$is the battery's DC current, $C_{cp,i}$ is the battery capacitance reflecting the main storage capacity, $R_{bp,i}$ is the self-discharge resistance, and $C_{b,i}$ and $R_{b,i}$ describe the transient overvoltage effects.

In this chapter, the active power losses in the inverter and the transformer are ignored, thus the active V2G power injected into the grid, P_{V2G}, can be given as

$$P_{V2G,i} = I_{dc,i}V_{dc,i} \tag{3.4.4}$$

Linearizing (3.4.4) yields the incremental active power as follows

$$\Delta P_{V2G,i} = V^o_{dc,i}\Delta I_{dc,i} + I^o_{dc,i}\Delta V_{dc,i}s \tag{3.4.5}$$

where $V^o_{dc,i}$ and $I^o_{dc,i}$ are the DC voltage and current of the battery at the initial time, respectively. Decomposing the DC voltage, $\Delta V_{dc,i}$, into two components, $\Delta V_{r,i}$,$\Delta V_{s,r}$, yields

$$\Delta P_{V2G,i} = V^o_{dc,i}\Delta I_{dc,i} + I^o_{dc,i}(\Delta V_{r,i} + \Delta V_{s,i}) \tag{3.4.6}$$

Similar to the BESS, the partial adjustment of battery voltage is used to compensate the power change resulting from current deviation [65]. That is, the $I^o_{dc,i}\Delta V_{r,i}$ in (3.4.6) is to compensate power deviation resulting from $\Delta I_{dc,i}$ and the $I^o_{dc,i}\Delta V_{s,i}$ is the adjustment of V2G power responding to frequency regulation. So ith PEV output power is given as:

$$\Delta P_{V2G,i} = I^o_{dc,i}\Delta V_{s,i} \tag{3.4.7}$$

During taking part in the frequency regulation, the DC voltage, $\Delta V_{s,i}$, of the PEV is adjusted with the acquired frequency deviation signal, namely,

$$\Delta \dot{V}_{s,i} = \frac{1}{T_{b,i}}(-\Delta V_{s,i} - k_{v,i}\Delta f) \tag{3.4.8}$$

where $T_{b,i}$ represents time constant of battery power adjustment. Thus, the V2G power of PEV_i responding to frequency regulation is

$$\Delta P_{V2G,i} = \frac{k_{b,i}}{1 + sT_{b,i}} \Delta f \tag{3.4.9}$$

where $k_{b,i} = -k_{v,i} I^o_{dc,i}$ is the battery gain, which represents the sensitivity of V2G power with respect to frequency deviation. It is decided by considering a tradeoff between the effect of frequency regulation and the constraint of battery state of charge (SOC) [135] as following:

$$k_{b,i} = \begin{cases} k_{max,i}[1 - (\frac{SOC_i - SOC_{low,i}}{SOC_{max,i} - SOC_{low,i}})^2], & \Delta f > 0, SOC_{low,i} \leq SOC_i \leq SOC_{max,i} \\ k_{max,i}[1 - (\frac{SOC_i - SOC_{high,i}}{SOC_{min,i} - SOC_{high,i}})^2], & \Delta f < 0, SOC_{min,i} \leq SOC_i \leq SOC_{high,i} \end{cases} \tag{3.4.10}$$

where $k_{max,i}$ and SOC_i are the maximum battery gain and current battery SOC, respectively. In the charging status, the $SOC_{max,i}$ and $SOC_{low,i}$ are allowable SOC limits; Meanwhile, in the discharging status, the $SOC_{high,i}$ and $SOC_{min,i}$ are allowable SOC limits [65]. The $SOC_{min,i}$ also represents the SOC needed for driving a PEV. If the PEV participates in frequency regulation by discharging power, $k_{b,i}$ will increase with the SOC increasing. If the PEV participates in frequency regulation by charging power, $k_{b,i}$ will decrease with the SOC increasing. However, when the SOC is not in allowable limits, $k_{b,i} = 0$, the PEV does not participate in frequency regulation [65].

Assume that there are N PEVs in the smart grid discussed in this chapter can be used to provide frequency support, and consider that the $T_{b,i}$ in (3.4.9) is not very sensitive to frequency deviation, then the aggregated V2G power can be approximately presented as following:

$$\Delta P_{V2G} = \sum_{i=1}^{N} \Delta P_{V2G,i} = \frac{k_{ev}}{1 + sT_{ev}} \Delta f \tag{3.4.11}$$

where the aggregated PEVs gain $k_{ev} = \sum_{i=1}^{N} k_{b,i}$, and the aggregated time constant $T_{ev} = \sum_{i=1}^{N} \frac{T_{b,i}}{N}$.

3.5 General DLC Model

The general dynamic model for DLC model is introduced in this section based on [25]. This model is investigated as general as possible and includes communication time delay in DLC loop as shown in Figure 3.5. The $K_1(s)$ and $K_2(s)$ are the PID type controller used in LFC scheme and DLC control loop.

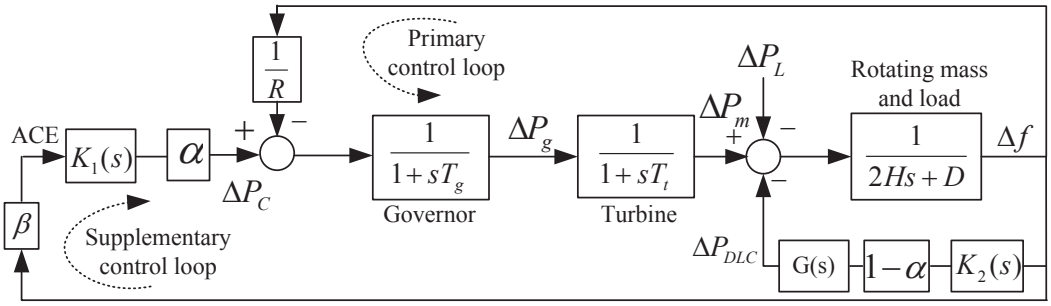

Figure 3.5: Single-area LFC with DLC model

The $Padé$ approximation is used in this model. In control engineering, the $Padé$ approximation is widely used to linearize system with time delays [136]. In Pade approximation, the time delay changed to $e^{-s.\tau_d} \approx R_{pq}(-s.T_d)$ is defined as follows [25, 137]:

$$R_{pq}(e^{-s.\tau_d}) = D_{pq}(e^{-s.\tau_d})^{-1} N_{pq}(e^{-s.\tau_d}) \tag{3.5.1}$$

where

$$D_{pq}(e^{-s.\tau_d}) = \sum_{k=0}^{q} \frac{(p+q-k)!q!}{(p+q)!k!(q-k)!}(s.\tau_d)^k \tag{3.5.2}$$

$$N_{pq}(e^{-s.\tau_d}) = \sum_{k=0}^{p} \frac{(p+q-k)!p!}{(p+q)!k!(p-k)!}(-s.\tau_d)^k \tag{3.5.3}$$

The D_{pq} and N_{pq} are polynomials of the order q and p, respectively. Usually, the order for this numerator and denominator of the fractional function is same and varies between 5 and 10 [25]. Assume the time delay in this model is 0.1 s. The 5th-order $Padé$ approximation is accepted and used in the general DLC model. Figure 3.6 shows signal flow graph for LFC with DSR model with 5th-order $Padé$ approximation and Table 3.1 shows the gains of the feed-forward and feedback value

for 5th order $Padé$ approximation, where the T_d is the communication time delay in DLC loop.

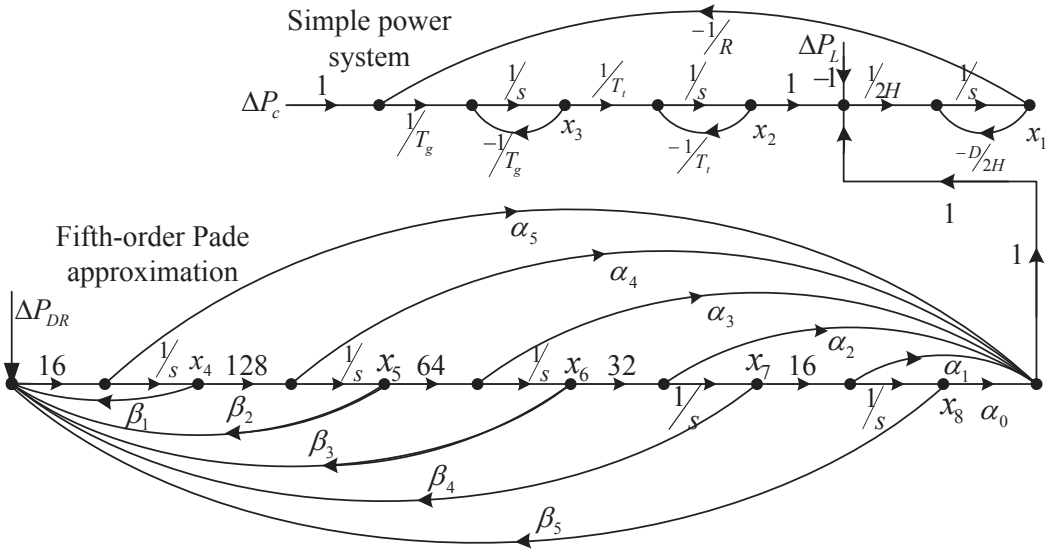

Figure 3.6: Signal flow figure of the single area power system with 5th-order Pade approximation [25]

Table 3.1: $Padé$ approximation s feed-forward and feedback value for signal flow graph [25]

α_0	α_1	α_2	α_3	α_4	α_5
$\frac{945}{2^{21}T_d^5}$	$\frac{-945}{2^{22}T_d^4}$	$\frac{105}{2^{17}T_d^3}$	$\frac{-105}{2^{15}T_d^2}$	$\frac{15}{2^9T_d}$	$\frac{-1}{2^4}$
	β_1	β_2	β_3	β_4	β_5
	$\frac{-15}{2^3T_d}$	$\frac{-105}{2^9T_d^2}$	$\frac{-105}{2^{12}T_d^3}$	$\frac{-945}{2^{18}T_d^4}$	$\frac{-945}{2^{21}T_d^5}$

From Figure 3.5, the power balance equation in the frequency domain is shown:

$$\Delta f(s) = \frac{1}{2Hs + D}[\Delta P_m(s) - \Delta P_L - G(s)(1-\alpha)\Delta P_{DLC}(s)] \tag{3.5.4}$$

where

$$\Delta P_m(s) = B(s)[\Delta P_c(s) - \frac{1}{R}\Delta f(s)], \tag{3.5.5}$$

$$B(s) = \frac{1}{(1+sT_g)(1+sT_t)} \tag{3.5.6}$$

$$G(s) = \frac{N_{pq}(e^{-s.\tau_d})}{D_{pq}(e^{-s.\tau_d})} = \frac{-s^5 + \frac{30}{T_d}s^4 - \frac{420}{T_d^2}s^3 + \frac{3360}{T_d^3}s^2 - \frac{15120}{T_d^4}s + \frac{30240}{T_d^5}}{s^5 + \frac{30}{T_d}s^4 + \frac{420}{T_d^2}s^3 + \frac{3360}{T_d^3}s^2 + \frac{15120}{T_d^4}s + \frac{30240}{T_d^5}} \tag{3.5.7}$$

and $p = q = 5$ in polynomials $N_{pq}(e^{-s.\tau_d})$ and $D_{pq}(e^{-s.\tau_d})$. Assume $\psi(s) = 2Hs + D + \frac{B(s)}{R}$ and substitute (3.5.5) to (3.5.4). The frequency deviation can be obtained:

$$\Delta f(s) = \frac{1}{\psi(s)}[H(s)\Delta P_m(s) - G(s)\Delta P_{DLC}(s)] - \frac{1}{\psi(s)}\Delta P_L(s) \tag{3.5.8}$$

The step load disturbance, $\Delta P_L(s)$, is commonly used in the LFC analysis as follows:

$$\Delta P_L(s) = \frac{\Delta P_L}{s} \tag{3.5.9}$$

Based on the final value theorem and substituting (3.5.9) into (3.5.8), the steady state value of the system frequency deviation is as follows:

$$\Delta f_{ss} = \lim_{s\to 0} s\Delta f(s) = \frac{\Delta P_{m,ss} - \Delta P_{DLC,ss} - \Delta P_L}{\psi(0)} \tag{3.5.10}$$

where

$$\Delta P_{m,ss} = \lim_{s\to 0} sB(s)\Delta P_m(s) \tag{3.5.11}$$

$$\Delta P_{DLC,ss} = \lim_{s\to 0} sG(s)\Delta P_{DLC}(s) \tag{3.5.12}$$

$$\psi(0) = D + \frac{B(0)}{R} = D + \frac{1}{R} \tag{3.5.13}$$

When the power system is in steady state, it means the supplementary control and DSR can reserve at the time of load disturbance. Finally, the steady state value of $\Delta P_{m,ss}$ and $\Delta P_{DSR,ss}$ can be obtained as follows:

$$\Delta P_{m,ss} = \alpha\Delta P_L \tag{3.5.14}$$

$$\Delta P_{DLC,ss} = -(1-\alpha)\Delta P_L \tag{3.5.15}$$

where $0 < \alpha < 1$ is the share of traditional regulation services in the LFC scheme. If $\alpha = 1$, it means the total required regulation will be provided by traditional regulation services. Oppositely, the total required regulation will be provided by DLC regulation services if $\alpha = 0$.

3.6 Model of Battery Energy Storage System

One alternative way for frequency regulation is to introduce the storage facilities, which provide energy stored in the low load condition for the smart grid during peak

load period. The battery energy storage system (BESS), as an important storage facility, can provide fast active power compensation so as to improve the performance of the frequency control based on [53, 125].

The main components of the BESS are a 12-pulse bridge converter, and the corresponding control scheme [53]. The ideal no load maximum d.c. voltage (E_{do}) of the 12-pulse converter is shown as follows:

$$E_{do} = E_{do1} + E_{do2} = \frac{6\sqrt{6}}{\pi} E_t \tag{3.6.1}$$

where E_t is the line to neutral (root-mean-squared) RMS voltage.

The equivalent circuit of the BESS can be represented as a converter connected to an equivalent battery, as shown in Figure 3.7.

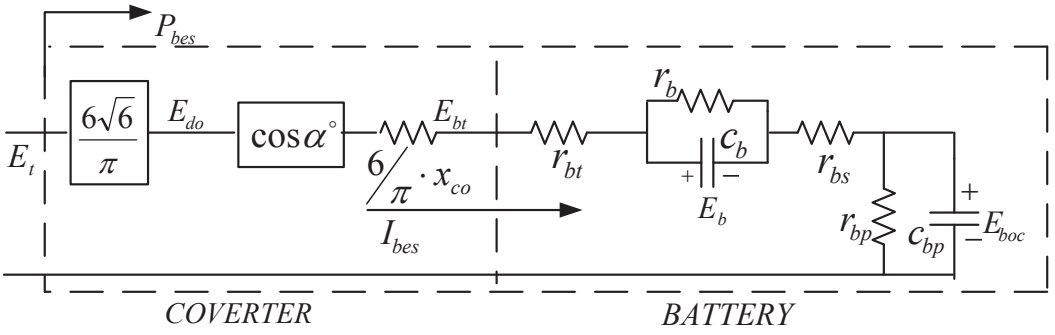

Figure 3.7: Equivalent circuit of the BESS [53]

In the battery equivalent circuit, the terminal voltage of the battery, E_{bt}, is obtained as

$$E_{bt} = E_{do}\cos\alpha^o - R_c I_{bes} = \frac{3\sqrt{6}}{\pi} E_t(\cos\alpha_1^o + \cos\alpha_2^o) - \frac{6}{\pi} X_{co} I_{bes} \tag{3.6.2}$$

where, α_1^o and α_2^o are the firing delay angle of converters 1 and 2, respectively, X_{co} is the commutating reactance, and I_{bes} stands for dc current flowing into battery, which can be given as follows:

$$I_{bes} = \frac{E_{bt} - E_{boc} - E_b}{r_{bt} + r_{bs}} \tag{3.6.3}$$

where E_{boc} is battery open circuit voltage, E_b is the battery overvoltage, r_{bt} and r_{bs} are the connecting resistance and the internal resistance, respectively.

In the converter equivalent circuits, the active and reactive power absorbed by the BESS are given as follows:

$$P_{BESS} = \frac{3\sqrt{6}}{\pi} E_t I_{bes} (\cos \alpha_1^o + \cos \alpha_2^o) \tag{3.6.4}$$

$$Q_{BESS} = \frac{3\sqrt{6}}{\pi} E_t I_{bes} (\sin \alpha_1^o + \sin \alpha_2^o) \tag{3.6.5}$$

For the control scheme, two strategies, P-Q modulation and P modulation, are usually used to control the converter. The frequency regulation only considers the active power, thus the P modulation ($\alpha^o := \alpha_1^o = -\alpha_2^o$) is considered in this chapter, namely

$$P_{BESS} = \frac{6\sqrt{6}}{\pi} E_t I_{bes} \cos \alpha^o = (E_{do} \cos \alpha^o) I_{bes} = E_{co} I_{bes} \tag{3.6.6}$$

$$Q_{BESS} = 0 \tag{3.6.7}$$

where $E_{co} = E_{do} \cos \alpha^o$ is the d.c. voltage without overlap.

Linearizing (3.6.6) and decomposing ΔE_{co} into two components, ΔE_p and ΔE_d, yield

$$\Delta P_{BESS} = E_{co}^o \Delta I_{bes} + I_{bes}^o \Delta E_p + I_{bes}^o \Delta E_d \tag{3.6.8}$$

where the second term is to compensate the power deviation caused by the current deviation, i.e., $I_{bes}^o \Delta E_p = -E_{co}^o \Delta I_{bes}$. Then,

$$\Delta P_{BESS} = I_{bes}^o \Delta E_d \tag{3.6.9}$$

in which ΔE_d is used to respond the system disturbance, i.e., frequency regulation task. In this chapter, the ACE signal is used as the feedback signal to control the BESS, i.e.,

$$\Delta E_d = \frac{K_{bes}}{1 + sT_{bes}} ACE \tag{3.6.10}$$

where K_{bes} and T_{bes} are the control loop gain and the measurement device time constant, respectively.

In the peak load time, the BESS is discharging mode. During the discharging mode, the ignition angle β^o, which $\beta^o = \pi - \alpha^o$, is used for the converter and the BESS power consumption as follows,

$$P_{BESS} = \frac{6\sqrt{6}}{\pi} E_t I_{bes} \cos \beta^o = -E_{do} I_{bes} \cos \alpha^o = -E_{co} I_{bes} \tag{3.6.11}$$

So the ΔP_{BESS} in discharging mode can be shown:

$$\Delta P_{BESS} = -I^o_{bes}\Delta E_d \tag{3.6.12}$$

From (3.6.9) and (3.6.12), the simplified model of the BESS for frequency regulation can be given as follows:

$$\Delta P_{BESS} = (sign)\frac{I^o_{bes}K_{bes}\beta}{1+sT_{bes}}\Delta f \tag{3.6.13}$$

When $sign = 1$, the BESS is in charging mode. Meanwhile, when $sign = -1$, the BESS is in discharging mode.

3.7 Conclusion

In this chapter, the BESS model and different kinds of DSR models have been recalled, including PEV model and DDC based air conditioner or HPWH model. These four models are constructed based on aggregated model of the individual small capacity component. The DLC controls the aggregated model supported the grid frequency in the smart grid. Details of these four models are described, respectively. Then, the general DLC model is described. This general model can represent different kind of controllable load and the time delay is considered via $Padé$ approximation. The time delay LFC model including BESS, PEVs and DDC based on air conditioners and HPWHs is also obtained.

Chapter 4

Robust Load Frequency Control with Demand Side Response for Deregulated Power System Considering Communication Delays

4.1 Introduction

LFC maintains the frequency of each control area and regulates the tie-line power flows between neighbouring control areas [41,138,139]. In a deregulated environment, the power system consists of Gencos, transmission companies (Transcos) and distribution companies (Discos) and is operated in an open assess policy [140–142]. The purpose of deregulation of the power industry is to restructure the electric industry so that power production and distribution are competitive, but the delivery is still regulated monopoly franchise business [78, 143]. Thus, the independent operator needs to develop a more reliable LFC service.

Traditionally, the Gencos are designed to provide enough backup generation capacity to meet the peak load, which makes substantial backup capacity idle for most hours within a year. Instead of providing enough generation capacity, DSR controls the load to balance the demand and the supply and becomes a promising

smart grid technology, especially for accommodating intermittent renewable generations [22, 25, 43]. DDC is one promising DSR technology which can provide the following two benefits in frequency control markets, providing an additional control [130] and reducing the spinning capacity [131]. DDC seeks to reduce the peak demands during a period when the frequency stability is under threaten or electricity market prices are high. Market performance benefits refer to demand response's value in mitigating suppliers ability to exercise market power by raising electricity prices significantly above the production costs. Then market-wide financial benefit is the lower wholesale market prices because demand response averts the need to use the most costly-to-run power plants during periods of otherwise high demand, driving production costs and prices down for all wholesale electricity purchasers [21]. These savings may be passed onto most retail customers as bill savings.

Lots of efforts have been devoted to investigate the DDC for the LFC scheme [25, 43, 79]. Reference [43] investigates whether a degree of built-in frequency stability could be provided by incorporating DDC into certain consumer appliances. In [25], it introduces demand response control loop in the traditional single-area LFC scheme. This LFC with DSR model has the feature of optimal operation through optimal power between the supply side and the demand side. Conventionally, most DDC employs the TCAs, such as EWHs [71, 72], refrigerators [43, 78] and air conditioners [79, 82]. Compared with active energy storage device, for example, a battery or flywheel, the main advantage is that TCAs do not require expensive auxiliary equipment such as power converters to provide the service, while the disadvantage is that it is not energy source and cannot provide electricity to other end users when the grid power is lost [28, 85]. The potential of DSR for facilitating the integration of wind power in the power system has been investigated [113, 115]. Most of those results have been carried out for the traditional LFC. To the best of authors' knowledge, the LFC with DDC in the deregulated environment has not received many efforts, while most DDC/DSR services are naturally expected to operate in the deregulated environment and competitive market.

Both the LFC scheme and the aggregation of DDC will use the communication channels to transmit the measurements and control commands, which will introduce

time delays [33, 37]. Time delays will deteriorate the dynamic performance or even cause instability of the closed-loop system [34, 35, 38–40]. The maximum time delay which allows an LFC scheme embedded with controllers to retain stable is denoted as delay margin for stability analysis [33, 41]. The delay margin of the LFC scheme has been calculated and applied in the design of load frequency controller [35, 42]. The impact of the time delay on the DDC scheme has been investigated as well [37, 43]. However, to the best of authors' knowledge, the impact of multiple delays for the LFC with the DDC has not been investigated yet.

This chapter targets to investigate the modelling and controller design of the LFC together with DDC, considering the impact of multiple delays in the control loops. A robust PID load frequency controller is designed to handle multiple delays in the control loops, through the H_∞ performance analysis and the PSO searching algorithm, guaranteeing robustness to time delay and load disturbances. Case studies are based on a three-area LFC scheme in deregulated environment. The effectiveness of the designed controller and the robustness of controller against to parameters uncertainties and delays are verified in simulation studies. Delay margins of the LFC scheme equipped with a PID-type controller have been obtained via trial-error simulation method. And the first and second delay stable region have been found, which reveals the fact that some large delays will stabilise the system again.

The rest of this chapter is organised as follows. The time delay model of the deregulated multi-area LFC with DDC is obtained in Section 4.2. Section 4.3 develops a method to design a robust PID controller. In section 4.4, case studies on a three-area deregulated LFC system with DDC are presented. Conclusions are drawn in Section 4.5.

4.2 Time Delay Model of LFC with DDC

The model of power system with N frequency control area in deregulated environment is concerned in this section. Figure 4.1 shows the control diagram of the i-th control area, in which the deregulated multi-area LFC scheme with n Gencos and m Discos, discussed in [35], and the DDC are included. In Figure 4.1, the AC

block stands for the DDC via controlling the air conditioners, where AC is short from air conditioners. τ_{1i} and τ_{2i} are the communication delay in LFC control loop and DDC control loop, respectively. The communication delay τ_{ji} is represented by $e^{-s\tau_{ji}}$ in Figure 4.1. The DDC model is introduced in Chapter 3.3.1. The following gives the model of LFC part, and the state-space model of the whole closed-loop system.

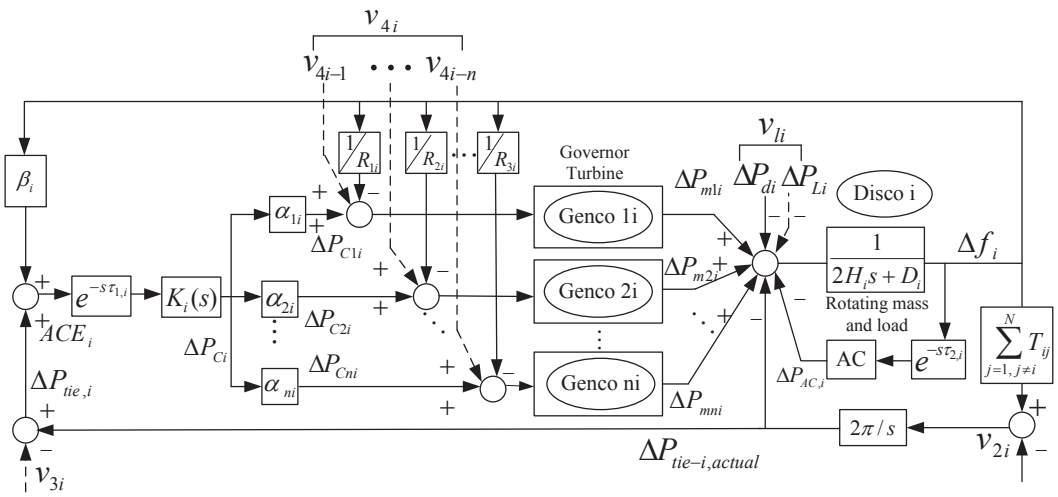

Figure 4.1: Diagram of the ith control area of the multi-area deregulated power system

4.2.1 Model of Deregulated Multi-area LFC

Without loss of generality, all generators are assumed to equip with non-reheat turbines. The details model of deregulated multi-area LFC scheme including N control areas with n Gencos and m Discos in each area have been given in our previous work [35]. Here, we just recall some important parts strongly linked to following sections.

For a modern power system under deregulated environment, each Genco can contract with various Discos located in or out of the area this Genco belonging to. Those bilateral contracts are visualized by an augmented generation participation

matrix (AGPM) [144]:

$$\mathrm{AGPM} = \begin{bmatrix} AGPM_{11} & \cdots & AGPM_{1N} \\ \vdots & \ddots & \vdots \\ AGPM_{N1} & \cdots & AGPM_{NN} \end{bmatrix} \tag{4.2.1}$$

where

$$\mathrm{AGPM_{ij}} = \begin{bmatrix} gpf_{s_i+1,z_j+1} & \cdots & gpf_{s_i+1,z_j+m} \\ \vdots & \ddots & \vdots \\ gpf_{s_i+n,z_j+1} & \cdots & gpf_{s_i+n,z_j+m} \end{bmatrix} \tag{4.2.2}$$

$s_i = n(i-1), z_j = m(j-1)$. The $\mathrm{gpf_{ij}}$ denotes the 'generation participation factor' of the Genco i in the total load following requirement of the Disco j based on the possible contracts. As there are many Gencos in each area, the relationship of $\mathrm{gpf_{ij}}$ is $\sum_{i=1}^{n_i} gpf_{ij} = 1$.

In Figure 4.1, the dashed line represents the new load demand signals corresponding to the possible contracts. The υ_{1i} contains the total contracted and uncontracted demand in area i; The interface effects between each control area and other areas is shown as the υ_{2i}; The scheduled tie-line power change is shown as the υ_{3i}; The υ_{4i} is a vector that contains contracted demands of other Discos from Gencos of area i [41]. They can be treated as additional disturbances of the traditional LFC scheme as follows [35, 144]:

$$\upsilon_{1i} = \Delta P_{Li} + \Delta P_{di} = \sum_{j=1}^{m} \Delta P_{Lj-i} + \sum_{j=1}^{m} \Delta P_{ULj-i} \tag{4.2.3}$$

$$\upsilon_{2i} = \Sigma_{j=1, j\neq i}^{N} T_{ij} \Delta f_j \tag{4.2.4}$$

$$\upsilon_{3i} = \Delta P_{tie,ik,sch} \sum_{k=1,k\neq i}^{N} \Delta P_{tie,ik,sch} \tag{4.2.5}$$

$$\Delta P_{tie,ik,sch} = \sum_{j=1}^{n} \sum_{t=1}^{m} gpf_{s_i+j,z_k+t} \Delta P_{Lt-k} - \sum_{j=1}^{n} \sum_{t=1}^{m} gpf_{s_k+j,z_i+t} \Delta P_{Lt-i} \tag{4.2.6}$$

$$\Delta P_{tie,i} = \Delta P_{tie-i,actual} - \upsilon_{3i} \tag{4.2.7}$$

$$\upsilon_{4i}^{T} = [\upsilon_{4i,1} \cdots \upsilon_{4i,k} \cdots \upsilon_{4i,n}] \tag{4.2.8}$$

$$\upsilon_{4i,k} = \sum_{j=1}^{N}[\sum_{t=1}^{m} gpf_{s_i+k,z_j+t}\Delta P_{Lt-j}] \tag{4.2.9}$$

$$\Delta P_{mk-i} = \upsilon_{4i,k} + \alpha_{ki}(\sum_{j=1}^{m} \Delta P_{UL_{j-i}} + \Delta P_{AC,i}) \tag{4.2.10}$$

where ΔP_{Li} and ΔP_{di} are the total contracted and un-contracted demand in area i, respectively; ΔP_{Lj-i} and ΔP_{ULj-i} are the contracted and un-contracted demand of Disco j in area i, respectively; $\Delta P_{tie,ik,sch}$ and $\Delta P_{m,k-i}$ are the scheduled tie-line power exchange between area i and area k and the desired total power generation of Genco k in area i. The range of integration for j and t from Equations (4.2.5) to (4.2.8) depend on the number of Gencos and Discos in the one control area.

In multi-area LFC, the ACE is defined as

$$ACE_i = \beta_i \Delta f_i + \Delta P_{tie,i} \tag{4.2.11}$$

where Δf_i and β_i are deviation of frequency and frequency bias factor in area i, respectively. The β_i can be shown as follows:

$$\beta_i = D_i + \frac{1}{R_{sys,i}} \tag{4.2.12}$$

where D_i is the load damping coefficient in area i and $R_{sys,i}$ is the equivalent system drooping characteristic which can be expressed $R_{sys,i} = \sum_{k=1}^{n} \frac{1}{R_{ki}}$.

4.2.2 Closed-loop State Space Model of LFC with DDC

When the DDC is included, based on the new power energy balance equation, the dynamic equation of the frequency deviation will be changed as follows:

$$\frac{d}{dt}\Delta f_i = \frac{1}{2H_i}[\sum_{j=1}^{n} \Delta P_{mji} - (\Delta P_{di} - \Delta P_{Li}) - \Delta P_{tie-i,actual} - \Delta P_{DDC,i} - D_i \Delta f_i] \tag{4.2.13}$$

Based on the transfer function of DDC, (3.3.5), dynamic model of DDC considering the time delay can be expressed as following:

$$\begin{aligned}\frac{d}{dt}\Delta P_{AC,i} =&(0.5K_I - D_{ac,i}\frac{2\pi D_i}{2H_i})\Delta f_i(t-\tau_{2,i}) + \frac{2\pi D_{ac,i}}{2H_i}[\sum_{j=1}^{n}\Delta P_{mji}(t-\tau_{2,i})\\ &- \frac{2\pi D_{ac,i}}{2H_i}\Delta P_{tie-i,actual}(t-\tau_{2,i}) - \frac{2\pi D_{ac,i}}{2H_i}\Delta P_{DDC,i}(t-\tau_{2,i})\\ &- \frac{2\pi D_{ac,i}}{2H_i}(\Delta P_{di} + \Delta P_{Li})\end{aligned} \tag{4.2.14}$$

In [35], it presents the multi-area deregulated LFC scheme in state-space. Based on this reference and dynamic equations (4.2.13) and (4.2.14), the state-space model of multi-area LFC with DDC in deregulated environment can be obtained as:

$$\begin{cases}\dot{x}_i(t) &= A_i x_i(t) + A_{di}x_i(t-\tau_{2i}) + B_i u_i(t-\tau_{1i}) + F_i\nu_i\\ y_i(t) &= C_i x_i(t) + E_i\nu_i\end{cases} \tag{4.2.15}$$

where

$$x_i^T = [\Delta f_i, \Delta P_{\text{tie}-i}, \Delta P_{\text{m}1i}, \cdots, \Delta P_{\text{m}ni}, \Delta P_{\text{g}1i}, \cdots, \Delta P_{\text{g}ni}, \Delta P_{DDC,i}]$$

$$y_i = ACE_i, \nu_i^T = [\nu_{1i}, \nu_{2i}, \nu_{3i}, \nu_{4i}]$$

$$A_i = \begin{bmatrix} A_{11i} & A_{12i} & 0_{2\times n} & A_{14i}\\ 0_{n\times 2} & A_{22i} & A_{23i} & 0_{n\times 1}\\ A_{31i} & 0_{n\times n} & A_{33i} & 0_{n\times 1}\\ 0_{1\times 2} & 0_{1\times n} & 0_{1\times n} & 0\end{bmatrix}, A_{di} = \begin{bmatrix} 0_{2\times 2} & 0_{2\times n} & 0_{2\times n} & 0\\ 0_{n\times 2} & 0_{n\times n} & 0_{n\times n} & 0\\ 0_{n\times 2} & 0_{n\times n} & 0_{n\times n} & 0\\ A_{41di} & A_{42di} & 0_{1\times n} & -\frac{2\pi D_{ac,i}}{2H_i}\end{bmatrix}$$

$$B_i = \begin{bmatrix} 0_{2\times 1}\\ 0_{n\times 1}\\ B_{3i}\\ 0\end{bmatrix}, F_i = \begin{bmatrix} F_{11i} & F_{12i} & 0_{2\times 1} & 0_{2\times n}\\ 0_{n\times 1} & 0_{n\times 1} & 0_{n\times 1} & 0_{n\times n}\\ 0_{n\times 1} & 0_{n\times 1} & 0_{n\times 1} & F_{33i}\\ -\frac{2\pi D_{ac,i}}{2H_i} & 0 & 0 & 0\end{bmatrix}, C_i = \begin{bmatrix} \beta_i & 1 & 0_{1\times 2n} & 0\end{bmatrix}$$

$$E_i = \begin{bmatrix} 0 & 0 & -1 & 0_{1\times n}\end{bmatrix}^T,$$

$$A_{11i} = \begin{bmatrix} -\frac{D_i}{2H_i} & -\frac{1}{2H_i} \\ 2\pi \sum_{j=1,j\neq i}^{N} T_{ij} & 0 \end{bmatrix}, A_{12i} = \begin{bmatrix} \frac{1}{2H_i} & \cdots & \frac{1}{2H_i} \\ 0 & \cdots & 0 \end{bmatrix}$$

$$A_{14i} = \begin{bmatrix} -\frac{1}{2H_i} \\ 0 \end{bmatrix}, A_{22i} = -A_{23i} = \mathrm{diag}\{ -\tfrac{1}{T_{\mathrm{t}1i}}, \cdots, -\tfrac{1}{T_{\mathrm{t}ni,}} \}$$

$$A_{31i} = \begin{bmatrix} \frac{-1}{T_{\mathrm{g}1i}R_{1i}} & \cdots & \frac{-1}{T_{\mathrm{g}ni}R_{ni}} \\ 0 & \cdots & 0 \end{bmatrix}^T, A_{33i} = -F_{33i} = \mathrm{diag}\{ \tfrac{-1}{T_{\mathrm{g}1i}}, \cdots, \tfrac{-1}{T_{\mathrm{g}ni}} \}$$

$$A_{41di} = \begin{bmatrix} 0.5K_I - \frac{2D_{ac,i}\pi D_i}{2H_i} & -\frac{2\pi D_{ac,i}}{2H_i} \end{bmatrix}, A_{42di} = \begin{bmatrix} \frac{2\pi D_{ac,i}}{2H_i} & \cdots & \frac{2\pi D_{ac,i}}{2H_i} \end{bmatrix}$$

$$B_{3i} = \begin{bmatrix} \frac{\alpha_{1i}}{T_{\mathrm{g}1i}} & \cdots & \frac{\alpha_{ni}}{T_{\mathrm{g}ni}} \end{bmatrix}^T, F_{11i} = \begin{bmatrix} \frac{-1}{2H_i} & 0 \end{bmatrix}^T, F_{12i} = \begin{bmatrix} 0 & -2\pi \end{bmatrix}^T$$

$$F_{33i} = \mathrm{diag}\{ \tfrac{1}{T_{\mathrm{g}1i}}, \cdots, \tfrac{1}{T_{\mathrm{g}ni}} \}$$

The $\Delta P_{\mathrm{g}ki}$ is valve position. The $2H_i$, D_i, $T_{\mathrm{g}ki}$, $T_{\mathrm{t}ki}$ and R_{ki} are the moment of inertia of generator unit, generator unit damping coefficient, time constant of the governor, time constant of the turbine and speed drop in area i, respectively. The α_{ki} is participation factor. $v_i (i = 1, 2, 3, 4)$ are the disturbances of area i caused by the possible contracts and load changing (Refer to [34] for more details).

To obtain the state space model of the closed-loop system, the PID-type control problem should be transformed into a static output feedback control problem. Define the following virtual vectors $\bar{x}_i = [x_i^T \ \int y_i^T]^T$ and $\bar{y}_i = [y_i \ \int y_i dt \ (d/dt)y_i]^T$, the closed-loop system can be rewritten as

$$\begin{cases} \dot{\bar{x}}_i(t) &= \bar{A}_i\bar{x}_i(t) + \bar{A}_{di}\bar{x}_i(t-\tau_{2i}) - \bar{B}_iK_i\bar{C}_ix(t-\tau_{1i}) + (\bar{F}_i - \bar{B}_iK_i\bar{D}_i)\nu_i \\ \bar{y}_i(t) &= \bar{C}_i\bar{x}_i(t) + \bar{D}_i\nu_i \end{cases} \tag{4.2.16}$$

where

$$\bar{A}_i = \begin{bmatrix} A_i & 0 \\ C_i & 0 \end{bmatrix}, \bar{A}_{di} = \begin{bmatrix} A_{di} & 0 \\ 0 & 0 \end{bmatrix}, \bar{B}_i = \begin{bmatrix} B_i \\ 0 \end{bmatrix}, \bar{C}_i = \begin{bmatrix} C_i & 0 \\ 0 & 1 \\ C_iA_i & 0 \end{bmatrix}$$

$$\bar{F}_i = \begin{bmatrix} F_i \\ 0 \end{bmatrix}, \bar{E}_i = \begin{bmatrix} E_i \\ 0 \\ C_iF_i \end{bmatrix}, K_i = \begin{bmatrix} K_{Pi} & K_{Ii} & K_{Di} \end{bmatrix}$$

4.3 Robust Controller Design

This section develops a method to design a robust PID controller through the H_∞ performance analysis and the PSO searching algorithm. Firstly, a performance criterion is derived to construct to the relationships among the delay, robust performance index, and PID gains. Then, the tuning of the PID gains is transformed into an optimisation problem solved by PSO algorithm.

4.3.1 A Performance Criterion

In [146], it improves the PID controller for the LFC with PEV system based on H_∞ performance analysis and PSO searching algorithm. Based on this reference and assuming the time delays in LFC and DDC loops be identical and defining the concerned output $z(t) = [\Delta f_i, \Delta P_{tie,i}]^T$, the closed-loop system for control areas shown in (4.2.16) can be described by the following general form:

$$\begin{cases} \dot{x}(t) &= Ax(t) + (A_d - BKC_y)x(t-h) + (B_\omega - BKD)\omega(t) \\ z(t) &= C_z x(t) \end{cases} \tag{4.3.1}$$

where $x(t) = \bar{x}_i(t)$, $h = \tau_{1i} = \tau_{2i}$, $\omega(t) = v_i(t)$, $B_\omega = \bar{F}_i$, $C_y = \bar{C}_i$, and $C_z = \left[\ I_{2\times 2}, 0_{2\times(2+2n)}\ \right]$.

The following criterion is derived by using the Lyapunov-Krasovskii functional (LKF) method and the Jensen integral inequality.

Theorem 4.1. For the given the delay h, the H_∞ performance index γ, and the controller gains $K = [K_P, K_I, K_D]$, the closed-loop system (4.3.1) is stable and has performance index, γ, against a non-zero disturbance for any delays smaller than h, if there exist symmetric matrices P, Q, and R, such that the following linear matrix inequalities hold

$$P > 0, Q > 0, R > 0 \tag{4.3.2}$$

$$\Phi = e_1^T P e_s + e_s^T P e_1 + e_1^T (Q + C_z^T C_z) e_1 - e_2^T Q e_2 + h^2 e_s^T R e_s - \gamma^2 e_3^T e_3 - (e_1 - e_2)^T R (e_1 - e_2) < 0 \tag{4.3.3}$$

where $e_s = \left[\ A,\ A_d - BKC_y,\ B_w - BKD\ \right]$, $e_1 = \left[\ I,\ 0,\ 0\ \right]$, $e_2 = \left[\ 0,\ I,\ 0\ \right]$, and $e_3 = \left[\ 0,\ 0,\ I\ \right]$,

Proof: Choose an LKF candidate as follows:

$$V(t) = x^T(t)Px(t) + \int_{t-h}^{t} x^T(s)Qx(s)ds + h\int_{-h}^{0}\int_{t+\theta}^{t} \dot{x}^T(s)R\dot{x}(s)dsd\theta \quad (4.3.4)$$

where P, Q and R are real symmetric and positive-define $n \times n$ matrices (n depends on the defined power system), which indicates $V(t) > 0$ for all x ($x \neq 0$). Calculating the derivative of LKF and using Jensen integral inequality yield

$$\begin{aligned} \dot{V}(t) &= 2x^T(t)P\dot{x}(t) + x^T(t)Qx(t) - x^T(t-h)Qx(t-h) \quad (4.3.5)\\ &+ h^2\dot{x}^T(t)R\dot{x}(t) - h\int_{t-h}^{t} \dot{x}^T(s)R\dot{x}(s)ds \\ &\leq 2x^T(t)P\dot{x}(t) + x^T(t)Qx(t) - x^T(t-h)Qx(t-h) \\ &+h^2\dot{x}^T(t)R\dot{x}(t) - (x(t)-x(t-h))^T R(x(t)-x(t-h)) \quad (4.3.6) \end{aligned}$$

where $\zeta(t) = \left[\ x(t),\ x(t-h),\ \omega(t)\ \right]$. It follows from linear matrix inequality (LMI) (4.3.3) that

$$\dot{V}(t) + z^T(t)z(t) - \gamma^2\omega^T(t)\omega(t) < \zeta^T(t)\Phi\zeta(t) \quad (4.3.7)$$

where Φ is defined in (4.3.3). Then, the following holds

$$\Phi < 0 \Rightarrow \int_0^{\infty} [z^T(s)z(s) - \gamma^2\omega^T(s)\omega(s)]ds \leq 0 \quad (4.3.8)$$

Therefore, the holding of LMI (4.3.3) leads to $\frac{\|z(t)\|}{\|\omega(t)\|} \leq \gamma$, which means the system is stable and has a H_∞ performance index, γ. This completes the proof.

4.3.2 PID Gain Tuning via the PSO Algorithm

Based on [146], Theorem 4.1 gives the relationships among the delay h, the H_∞ performance index γ, and the PID gains K. As discussed in [34], for fixed delay h and the controller gain K, one can find the minimal value of the performance index γ_{min} through the conditions of Theorem 4.1. That is, the minimal value γ_{min} is a function of the delay h and the controller gains K, as described as follows

$$\gamma_{min} = f(h, K_P, K_I, K_D) \quad (4.3.9)$$

How to calculate the minimal value, γ_{min}, for fixed delay bound h and the controller gains K can be found in [34] and is omitted here due to page limitation.

To provide the optimal robust performance against to the delays and the disturbances, control gains tuning can be transformed to the following optimisation problem:

$$Minimize: \quad \gamma_{min} = f(h, K_P, K_I, K_D) \tag{4.3.10}$$

$$subjectto: \quad K_{Pmin} \leq K_P \leq K_{Pmax} \tag{4.3.11}$$

$$K_{Imin} \leq K_I \leq K_{Imax} \tag{4.3.12}$$

$$K_{Dmin} \leq K_D \leq K_{Dmax} \tag{4.3.13}$$

The above optimisation problem can be solved by various algorithms. This chapter chooses the PSO searching algorithm as it is a meta-heuristic algorithm and has been widely used due to its decent performance in numerical optimisation [163]. The details are omitted here since the PSO is the standard algorithm and can be easily achieved by Matlab.

4.4 Case Studies

Case studies are based on a deregulated three-area LFC system, as shown in Figure 4.2. Each control area consists of two Gencos, two Discos, and one DDC. The related parameters are given in [79, 144] and listed in Table 4.1. The robust PID controllers for each control area are designed based on the linear time-delay model given in Section 2 and the method proposed in Section 3, and their effectiveness, robustness against to parameter uncertainties and time delays as well, is verified via simulation studies completed based on Figure 4.2 with some nonlinearities, including the generation rate constraint (GRC) and the dead bands. GRC is an important physical constraint which is on the rate of change of power generation due to the limitation of thermal and mechanical movements [41]. For speed governor, when the input signal changes, it may not immediately react until the input reaches a specified value. So all governors a have dead band. The dead band is defined the total magnitude of a sustained speed change, in which there is no resulting change in val-

ue position [41]. All calculations and simulations are carried out by using Matlab 7.10.0 (R2010a) running on a PC.

Table 4.1: Parameters of the concerned system

	Gencos							Areas				Areas		
	1-1	2-1	1-2	2-2	1-3	2-3		1	2	3		1	2	3
T_{T}	0.32	0.30	0.30	0.32	0.31	0.34	H	0.0833	0.1042	0.0800	c_p	1.01	1.01	1.01
T_{G}	0.06	0.08	0.06	0.07	0.08	0.06	D	0.0083	0.0083	0.0080	m	0.25	0.05	0.15
R	2.4	2.5	2.5	2.7	2.8	2.4	β	0.4250	0.3966	0.3522	k	8	15	10
α	0.5	0.5	0.5	0.5	0.6	0.4	$T_{12} = 0.0389, T_{13} = 0.0337, T_{23} = 0$				$D_{ac,i}$	0.025	0.015	0.01

4.4.1 Controller Design and Its Verification

Control Design:

To simplify the design procedure, the time delays of three-area are preseted as the same value, 0.2 s. The search regions for PID gains are set to be [-1,1]. By using the robust performance index (RPI)-based objective function calculated by the method in [34] and the standard PSO-based search method, all achieved through Matlab platform, the PID gains for three-area are obtained as follows:

$$K_1 = [0.79133, -0.56537, -0.19693]$$
$$K_2 = [-0.05968, -0.96936, -0.26727]$$
$$K_3 = [-0.13721, -0.84983, -0.41357]$$

Simulation Verification

During the construction of simulation platform of the concerned three-area LFC, the linear model of governor and turbine in Figure 4.1 is replaced by the nonlinear model shown in Figure 4.3, in which the GRC is assumed to be 0.1 pu/min and the dead band range is assumed to be 0.036 Hz for this model [41]. The communication time delays in LFC and DDC loops are given as 0.2s in scenario 1 and scenario 2.

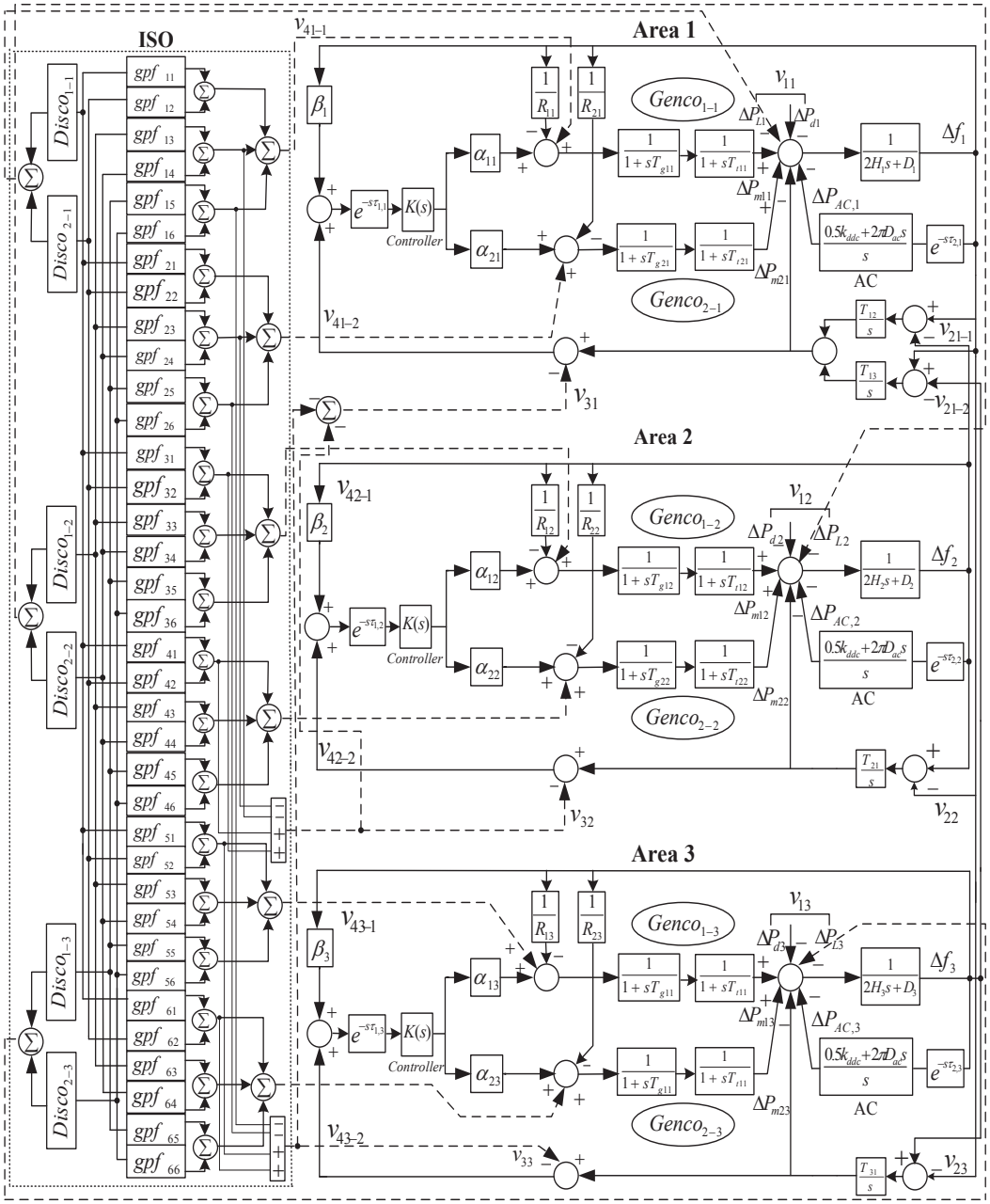

Figure 4.2: Three-area deregulated LFC test system [144]

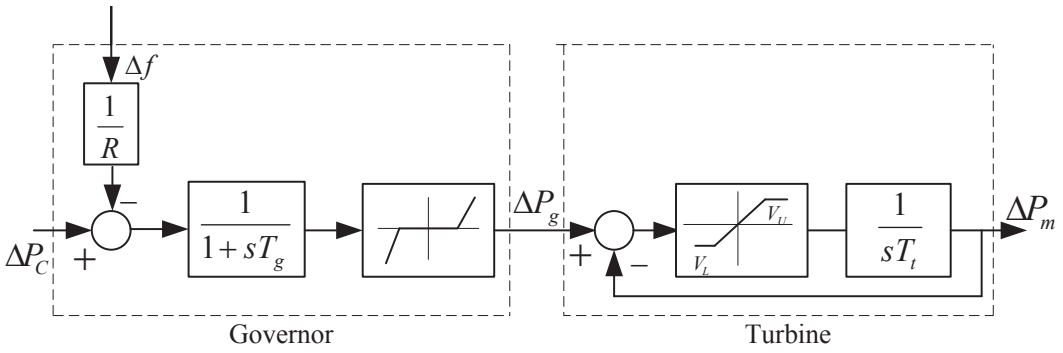

Figure 4.3: Non-reheat generator unit model with GRC and dead band

1) Scenario I: Poolco based transactions [41, 144]

In this scenario, Gencos only participate in the load following of their control area and Discos in area 1 and 2 are assumed a large step load of 0.1pu [144]. The Poolco based contracts between Discos and the available Gencos are simulated based on the following AGPM, which implies the Gencos in control area 3 do not participate in the LFC task.

$$\mathrm{AGPM} = \begin{bmatrix} 0.6 & 0.5 & 0 & 0 & 0 & 0 \\ 0.4 & 0.5 & 0 & 0 & 0 & 0 \\ 0 & 0 & 0.5 & 0.5 & 0 & 0 \\ 0 & 0 & 0.5 & 0.5 & 0 & 0 \\ 0 & 0 & 0 & 0 & 0 & 0 \\ 0 & 0 & 0 & 0 & 0 & 0 \end{bmatrix} \tag{4.4.1}$$

The frequency deviation and tie-line power exchange is shown in Figure 4.4. As the frequency deviation and tie-line power recover quickly to schedule values, the designed PID controller is effective. It can be found that the LFC with DDC can provide a better regulation transient dynamics, with a faster settling time and smaller overshoot, compared with those provided by LFC without DDC. As there are no contracts between areas, the scheduled steady state power flows over the tie-line are zero.

Mechanical power changing of Gencos properly converges to the specified value in the steady state is shown in Figure 4.5. Because the DDC participates in LFC of the deregulated power system, the mechanical power change of each Genco is small-

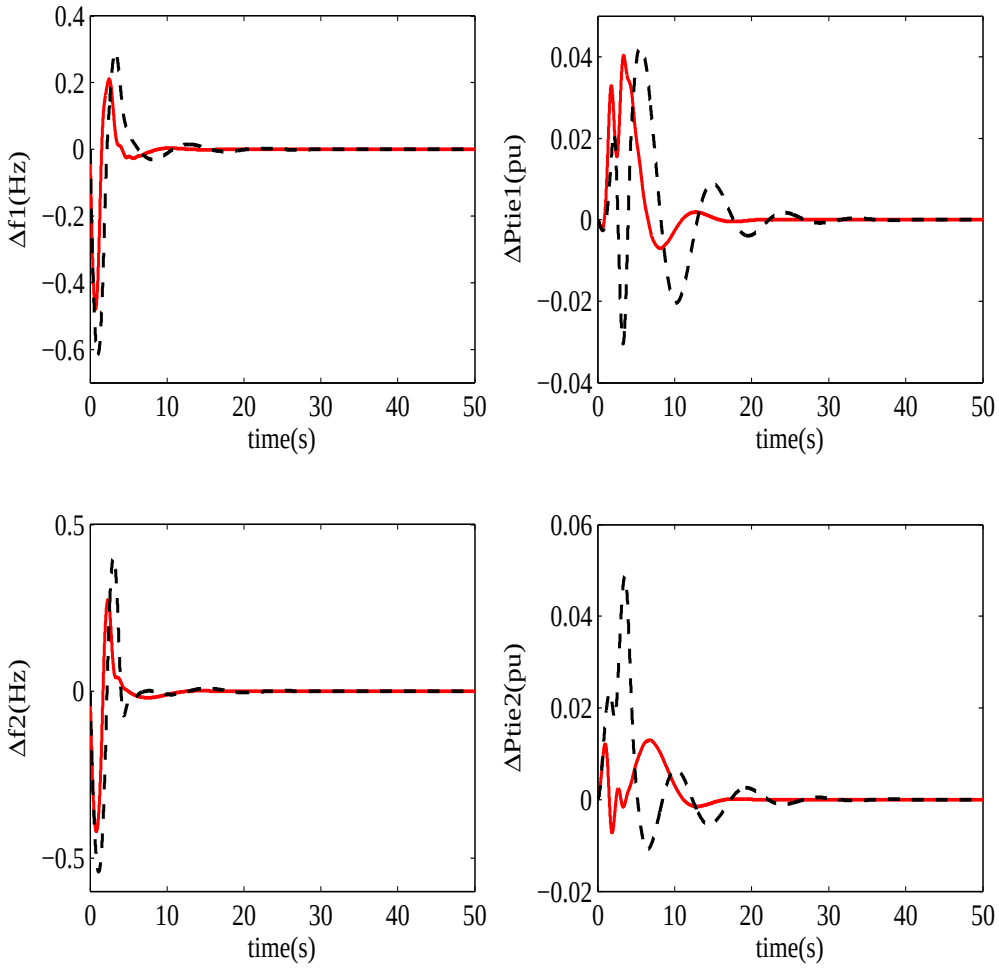

Figure 4.4: Frequency deviation and tie-line power exchange of the three-area power system in Scenario I: Solid (with DDC), Dashed (without DDC)

er than LFC without DDC. The $\Delta P_{AC,i}$ can be obtained via solving the equilibrium point from state space equation (4.2.15) as following: $\Delta P_{\mathrm{AC},1} = 0.066$ pu MW and $\Delta P_{\mathrm{AC},2} = 0.025$ pu MW. According to equation (4.2.10), the value of mechanical power change of each Genco in LFC with DDC is obtained as: $\Delta P_{\mathrm{m}11} = 0.077$ pu MW, $\Delta P_{\mathrm{m}21} = 0.057$ pu MW and $\Delta P_{\mathrm{m}12} = \Delta P_{\mathrm{m}22} = 0.088$ pu MW. Simulation results show DDC can enhance the transient response of freuqency regulation under Scenario I.

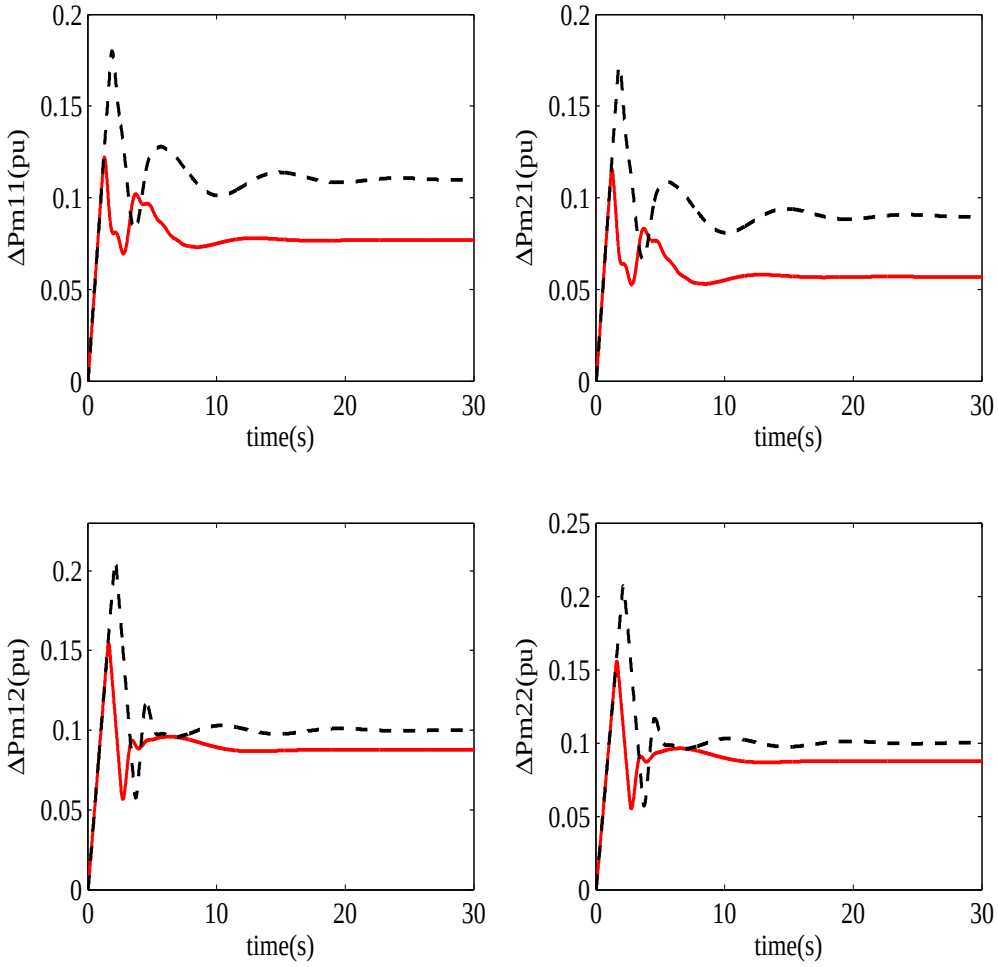

Figure 4.5: Response of four Gencos mechanical power of the three-area power system in Scenario I: Solid (with DDC), Dashed (without DDC)

2) Scenario II: Contract Violation [41, 144]

In this scenario, Discos have the freedom to have a contract with Gencos in their own or other areas, meanwhile Discos may violate a contract by demanding more power than that specified in the contract [144]. The excess power demand is reflected as a local load of the area, which is called the un-contracted demand. The purpose of this scenario is to test the effectiveness of the DDC to LFC scheme against small uncertainties as well as large load disturbance. The power supply contract among all Discos and Gencos related follows the following AGPM [144]:

$$\text{AGPM} = \begin{bmatrix} 0.25 & 0 & 0.25 & 0 & 0.5 & 0 \\ 0.5 & 0.25 & 0 & 0.25 & 0 & 0 \\ 0 & 0.5 & 0.25 & 0 & 0 & 0 \\ 0.25 & 0 & 0.5 & 0.75 & 0 & 0 \\ 0 & 0.25 & 0 & 0 & 0.5 & 0 \\ 0 & 0 & 0 & 0 & 0 & 1 \end{bmatrix} \tag{4.4.2}$$

Assume that a step load of 0.1 pu is demanded by each Disco in the areas, and Disco 1 in area 1 and area 2, and Disco 2 in area 3 demand 0.05 pu, 0.04 pu, and 0.03 pu as un-contracted loads, i.e., $\Delta P_{Lj-i} = 0.1pu, i = 1, 2, 3; j = 1, 2$; $\Delta P_{UL1-1} = 0.05pu$; $\Delta P_{UL1-2} = 0.04pu$; and $\Delta P_{UL1-3} = 0.03pu$.

The responses of the system are shown in Figure 4.6. The frequency deviation and tie-line power exchange are quickly convergent to schedule values, which means the designed PID controller is effective. Using equation (4.2.6), the value of tie-line power exchange is calculated and given as follows: $\Delta P_{tie1} = 0$ pu MW, $\Delta P_{tie2} = 0.025$ pu MW and $\Delta P_{tie3} = -0.025$ pu MW. Moreover, it can be found that the LFC with DDC can provide better dynamic performances, shorter settling time and smaller overshoot, compared with the one without DDC, which shows that the introducing of the DDC enhances the transient response of frequency regulation.

Mechanical power changing of Gencos in LFC with DDC and LFC without DDC is displayed in Figure 4.7. When the DDC part is participated in LFC deregulated power system, the mechanical power change of each Genco is smaller than LFC without DDC. Solving the equilibrium point of state-space equation (4.2.15) can obtain the value of $\Delta P_{AC,i}$ as follows: $\Delta P_{\text{AC},1} = 0.054$ pu MW, $\Delta P_{\text{AC},2} = 0.010$

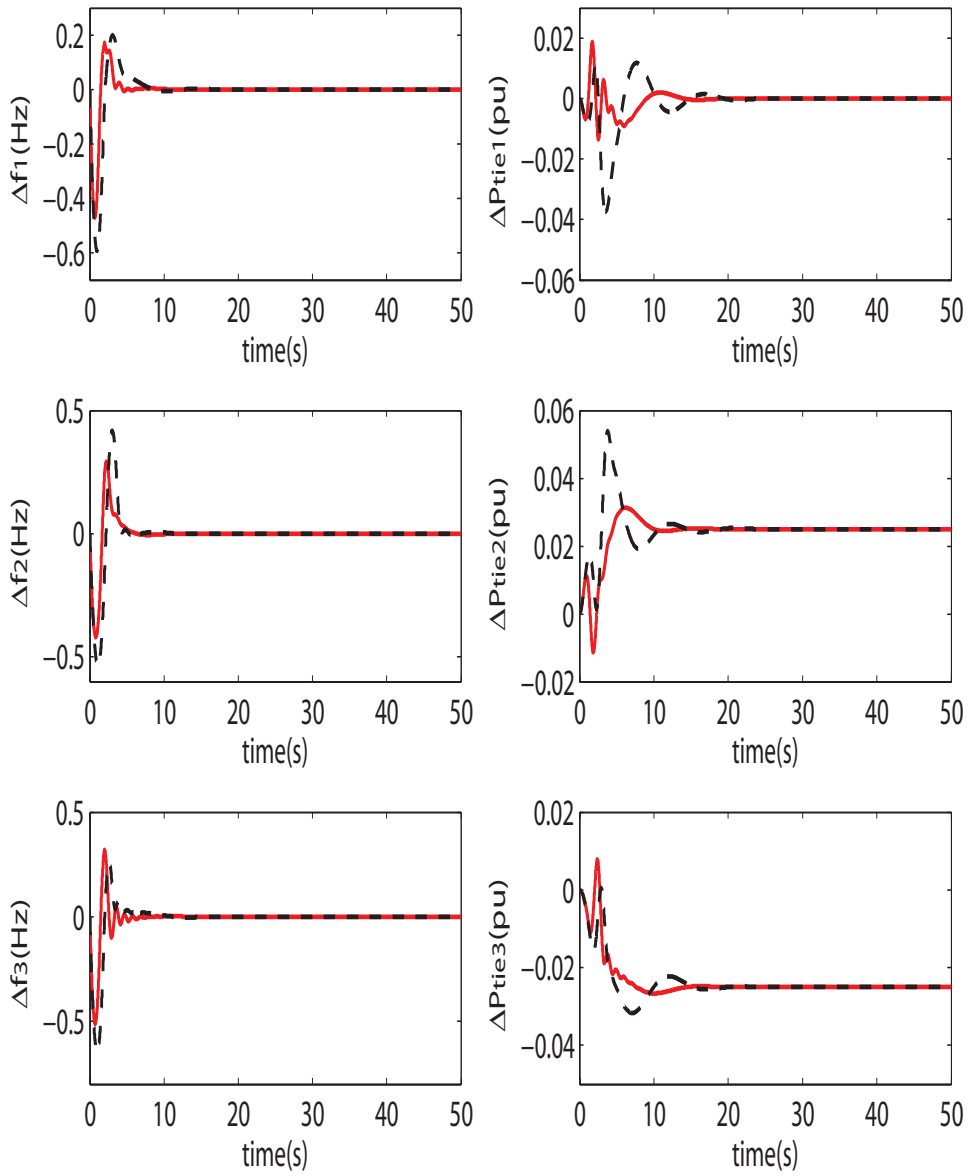

Figure 4.6: Frequency deviation and tie-line power exchange of the three-area power system in Scenario II: Solid (with DDC), Dashed (without DDC)

pu MW and $\Delta P_{\mathrm{AC},3} = 0.064$ pu MW. Then using equation (4.2.10), the value of mechanical power change of each Genco in LFC with DDC is calculated and given as follows: $\Delta P_{\mathrm{m11}} = \Delta P_{\mathrm{m21}} = 0.098$ pu MW, $\Delta P_{\mathrm{m12}} = 0.090$ pu MW, $\Delta P_{\mathrm{m22}} = 0.165$ pu MW, $\Delta P_{\mathrm{m13}} = 0.061$ pu MW and $\Delta P_{\mathrm{m23}} = 0.080$ pu MW. The simulation results reveal that the LFC scheme with the DDC can drive the power system in stable faster and have smaller fluctuation.

Then the random un-contracted loads in the power system in Scenario II is tested. Assume that un-contracted load in [-0.1 0.1] pu is demanded by in each Disco and the contracted load in each area is same as above. The communication time delays in LFC and DDC loops are given as 0.2 s. The response of power system is shown in Figure 4.8. Because the random un-contracted load is variable, the frequency deviation and tie-line power exchange are quickly convergent within a narrow band around schedule value. These results show the robustness of the designed PID controller against to random load change. Moreover, the LFC with DDC has better dynamic performances.

4.4.2 Robustness against to Parameters Uncertainties

The PID controller aforementioned is tuned for the nominal systems parameters. However, in reality, there exist uncertainties in the system parameters due to measurement errors etc., as well in the controller gains during the implementation procedure. Therefore, the robustness against those parameters uncertainties also is tested. To indicate the dynamic performances, the following two indexes, the integral of the time multiplied absolute value of the error (ITAE) and integral of the time multiplied square of the error (ITSE), with respect to ACE (ACE_i) are defined:

$$\mathrm{ITAE} = \int_0^{\mathrm{t}} \mathrm{t}(|\mathrm{ACE}_1| + |\mathrm{ACE}_2| + |\mathrm{ACE}_3)|)\mathrm{dt} \tag{4.4.3}$$

$$\mathrm{ITSE} = \int_0^{\mathrm{t}} \mathrm{t}(\mathrm{ACE}_1^2 + \mathrm{ACE}_2^2 + \mathrm{ACE}_3^2)\mathrm{dt} \tag{4.4.4}$$

Two cases, including uncertainties in system parameters (within $\pm 25\%$), and uncertainties in both system parameters and controller gains (within $\pm 25\%$), are simulated in Scenario I and Scenario II, respectively. Note that other operation conditions (time delays, load changes) are the same to ones given in Section 4.4.1. When only

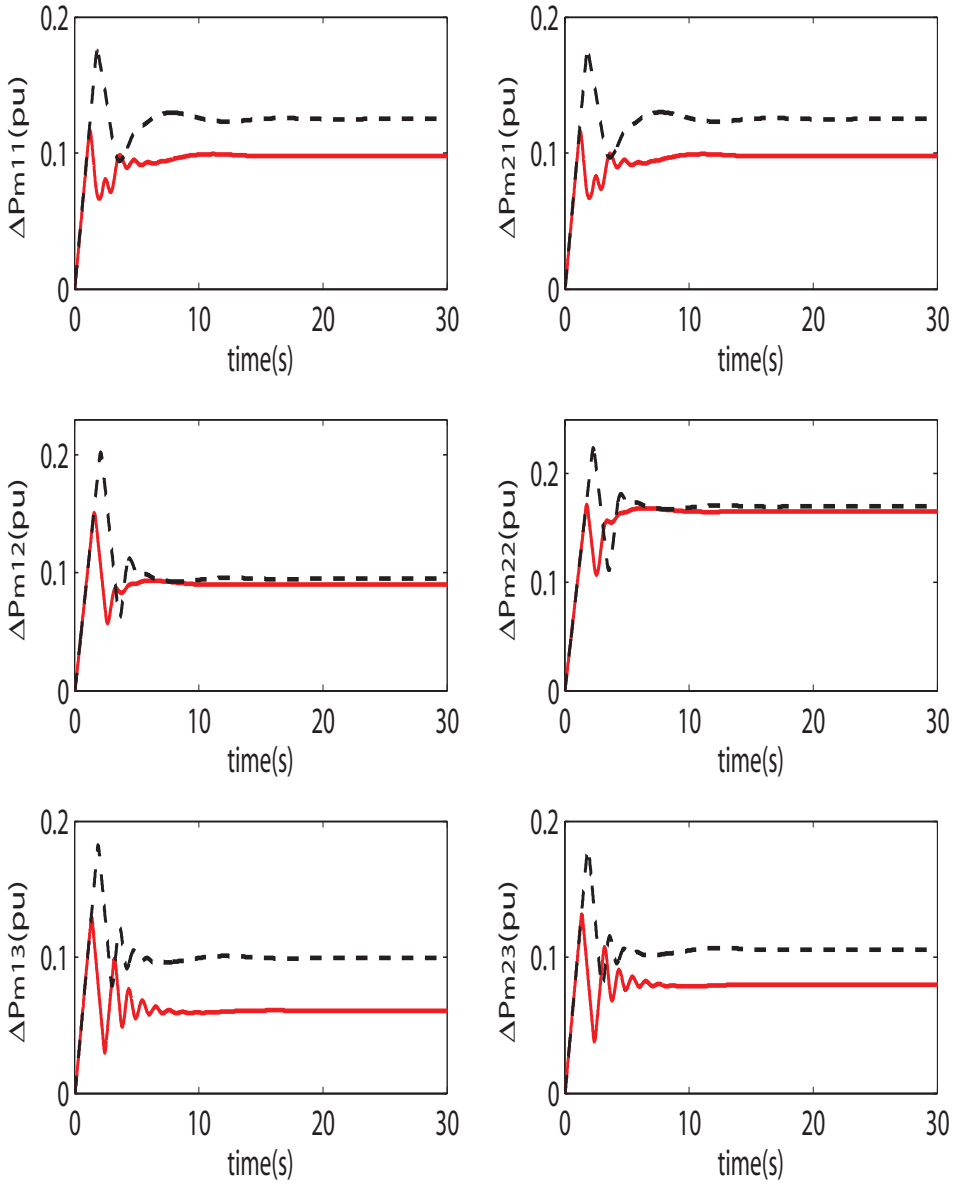

Figure 4.7: Response of six Gencos mechanical power of the three-area power system in Scenario II: Solid (with DDC), Dashed (without DDC)

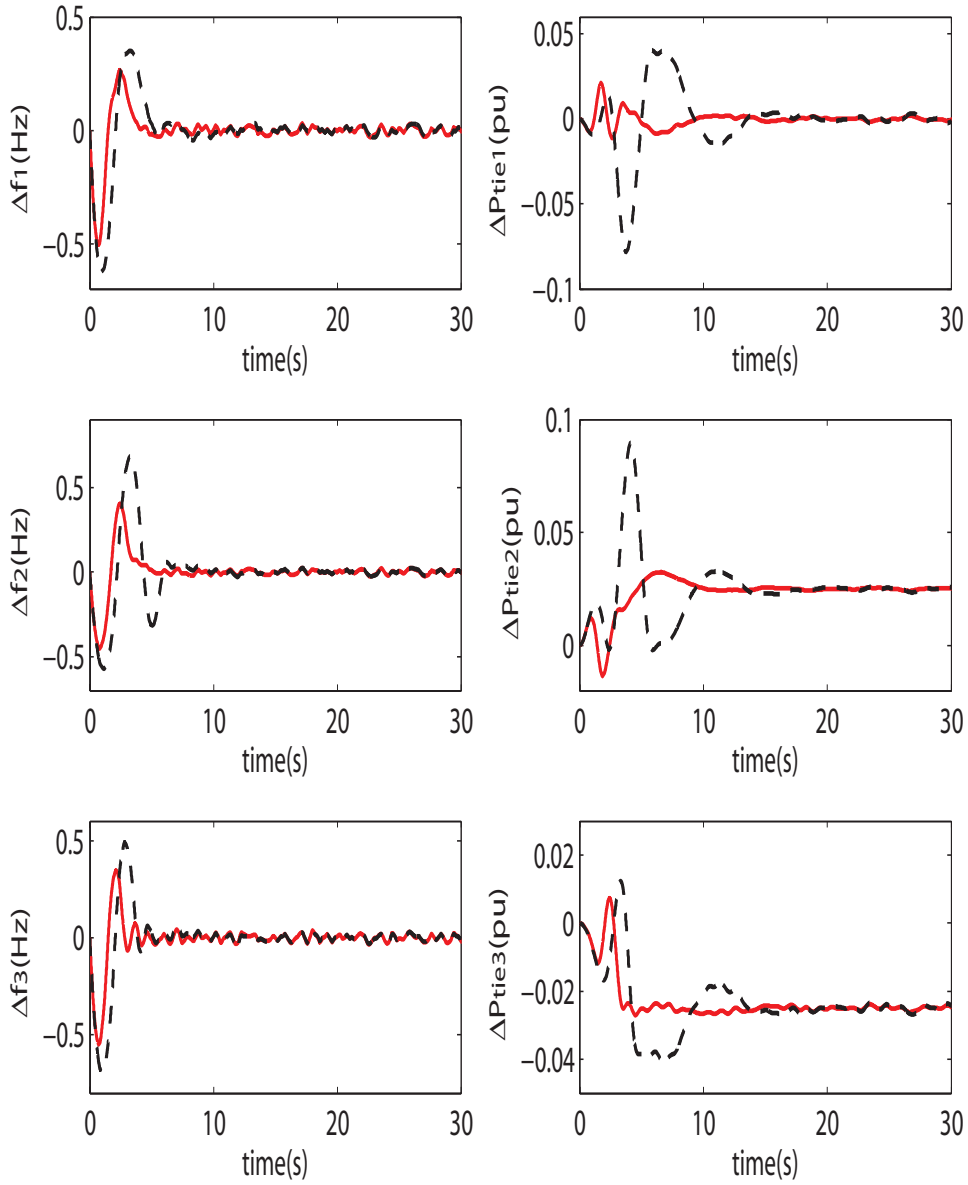

Figure 4.8: Frequency deviation and tie-line power exchange of the three-area power system in Scenario II: Solid (with DDC), Dashed (without DDC)

the system parameter uncertainties are considered, the values of ITAE and ITSE for some typical uncertainties are given in Table 4.3 and Table 4.2. Figures 4.9 to 4.11 are examples, which show uncertainties in parameter gain, controller gain or both of these two gains in control area 2 of this model in Scenario II. Figure 4.9 shows the frequency deviation of control area 2 in Scenario II for system parameters in normal value, increasing, and decreasing 25%, respectively. Figure 4.10 displays the frequency deviation of control area 2 in Scenario II for control parameters in normal value, increasing and decreasing 25%, respectively. When the uncertainties exist in both system parameters and controller gains, Figure 4.11 shows the frequency deviation of control area 2 in Scenario II for system parameters in normal value, increasing, and decreasing 25%, respectively.

From Table 4.3, Table 4.2, and Figures 4.9 to 4.11, it can be found that the designed PID controller stabilizes the LFC system even the uncertainties exist, which shows the robustness of controller against to parameter uncertainties. In Figure 4.9 (b) and 4.10 (b), when parameter or controller increase 25%, the LFC without DDC maintaining stable needs long time but the LFC with DDC is in stable very quickly. Meanwhile, it can be found that the introducing of DDC can stabilise LFC system more quickly with smaller fluctuation and provide better performance indexes. Furthermore, from Figure 4.11 (b), which shows that, when both system and controller parameters increase 25%, the LFC without DDC can not maintain stable while the LFC with DDC is still stable, it is concluded that the DDC can not only improve the transient responses of the system but also provide better robustness against to parameter uncertainties.

4.4.3 Robustness against to Time Delays

The PID controller designed in Section 4.4.1 is tuned by setting all delays to be constant, 0.2s. However, in reality, there usually exist time-varying delays and the delays for different areas and loops are not identical. Therefore, this subsection tests the robustness against to time-varying/random delays and finds the delay margin for different areas.

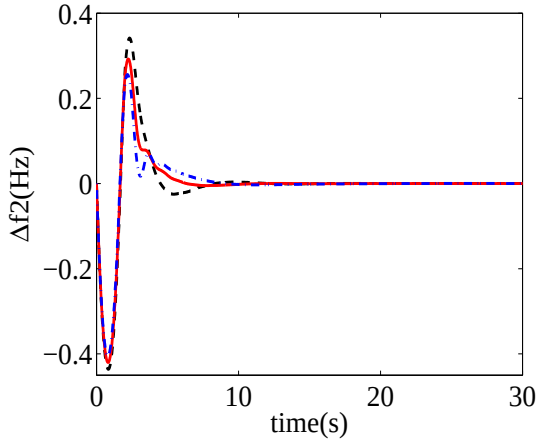

(a) LFC with DDC

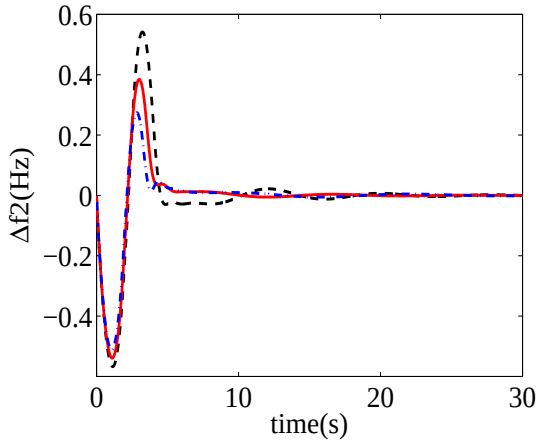

(b) LFC without DDC

Figure 4.9: Frequency deviation of area 2 in Scenario II under system parameters variation: Solid (normal value), Dashed (increased 25%)

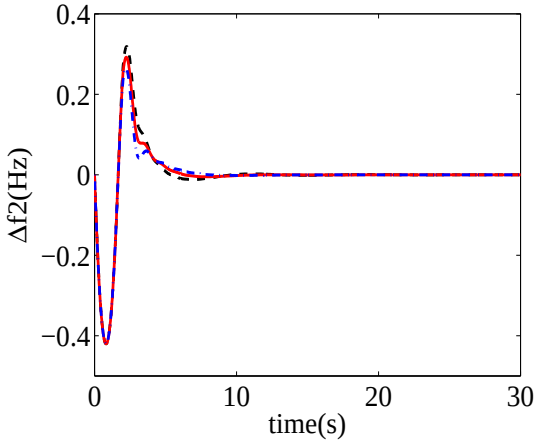

(a) LFC with DDC

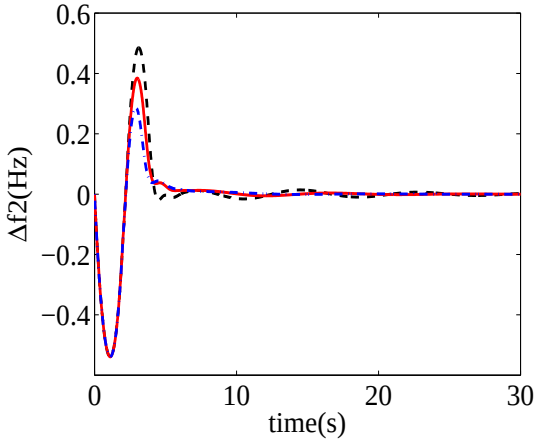

(b) LFC without DDC

Figure 4.10: Frequency deviation of area 2 in Scenario II under controller parameters variation: Solid (normal value), Dashed (increased 25%), Dashdotted (decreased 25%)

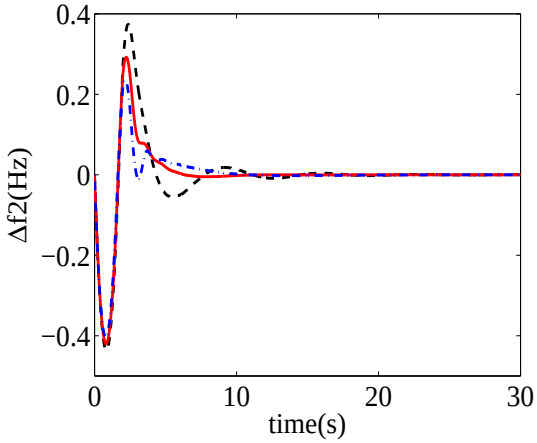

(a) LFC with DDC

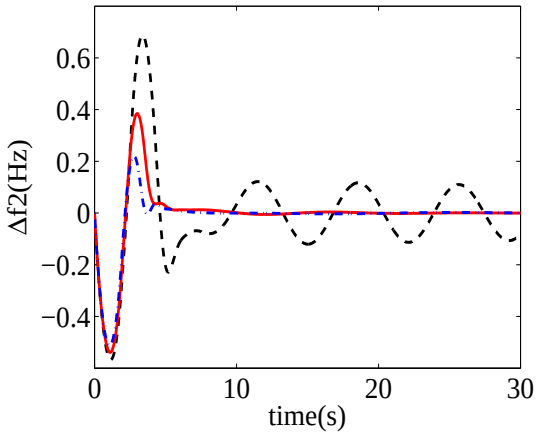

(b) LFC without DDC

Figure 4.11: Frequency deviation of area 2 in Scenario II for system and controller uncertainties: Solid (normal value), Dashed (increased 25%), Dashdotted (decreased 25%)

Table 4.2: Dynamic performance indices (ITAE and ITSE) in Scenario I

Parameter change (%)	Parameter Change				Controller Parameter Change			
	without DDC		with DDC		without DDC		with DDC	
	ITAE	ITSE	ITAE	ITSE	ITAE	ITSE	ITAE	ITSE
0%	2.510	0.152	4.773	0.453	2.510	0.152	4.773	0.453
+5	2.580	0.176	4.874	0.550	2.563	0.155	4.991	0.479
-5	2.480	0.132	4.709	0.379	2.485	0.149	4.581	0.429
+10	2.732	0.206	5.131	0.683	2.653	0.159	5.237	0.509
-10	2.498	0.167	4.669	0.322	2.489	0.148	4.431	0.408
+15	2.952	0.243	5.978	0.868	2.785	0.164	5.516	0.543
-15	2.455	0.104	4.680	0.276	2.522	0.147	4.327	0.390
+20	3.234	0.289	7.445	1.140	2.961	0.171	5.831	0.582
-20	2.330	0.094	4.734	0.239	2.581	0.147	4.265	0.375
+25	3.640	0.347	9.795	1.500	3.189	0.178	6.199	0.626
-25	2.761	0.086	4.904	0.209	2.670	0.148	4.243	0.361

1) Random delays: The different random delays within the range [0s, 0.4s] are added into the LFC and DDC loops of three areas in Scenario I and Scenario II. The responses of the LFC system in these two scenarios are given in Figures 4.12 and 4.13, respectively. Although the upper bound of the random delay (0.4s) is bigger than the delay (0.2s) for control design in Section 4.4.1, the frequency deviation is still quickly back to zero and tie-line power exchanges back to schedule value with short setting time, which shows the robustness of the designed PID controller against to time-vary and random delays. Moreover, the LFC with DDC has better dynamic performance in these two scenarios.

2) Multiple delay stable regions:

The contribution of the DDC to improve the dynamic performances of LFC systems has been revealed in the previous simulation results. During testing such contribution, an important factor needed to consider is the time delay. If the time delay is too big, the introducing of DDC may be no contribution to improve the performance and even leads to instability phenomenon. The time delays in LFC loop of

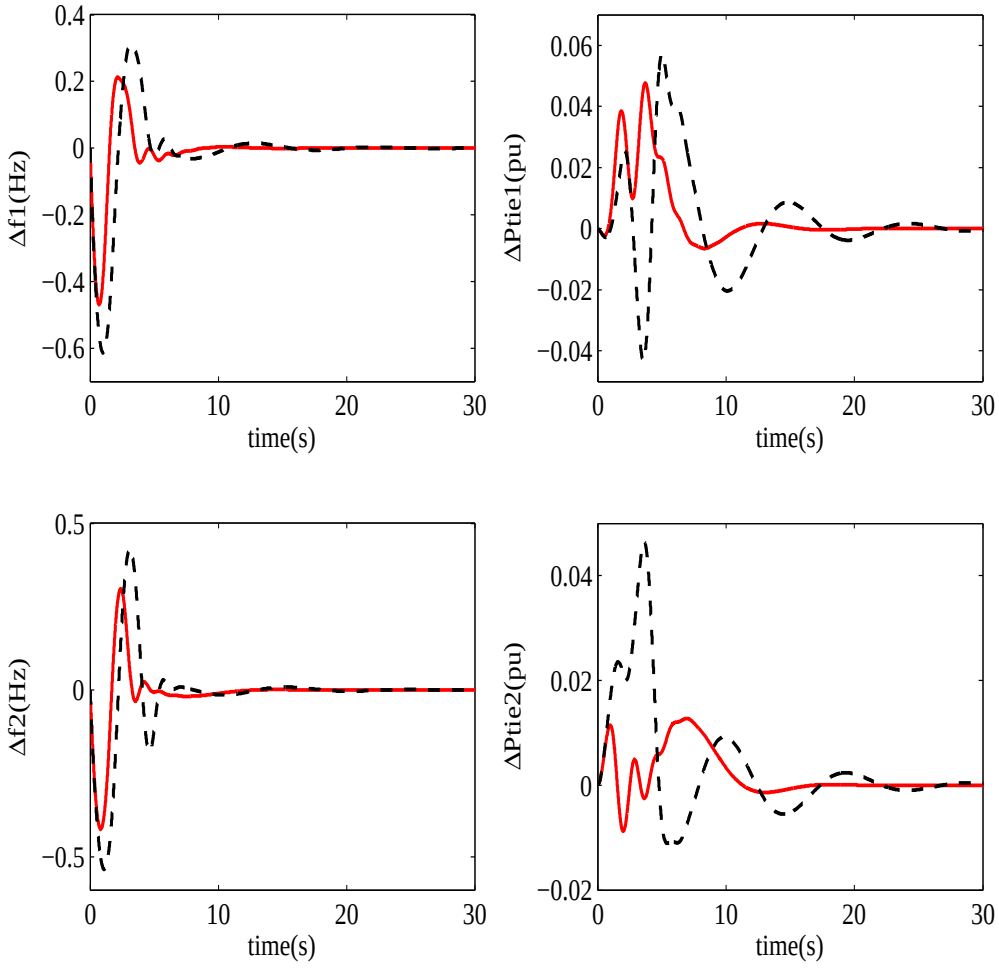

Figure 4.12: Deviation of frequency and and tie-line power exchange of the three-area power system with time-varying delay in Scenario I: Solid (LFC with DDC), Dashed (LFC without DDC)

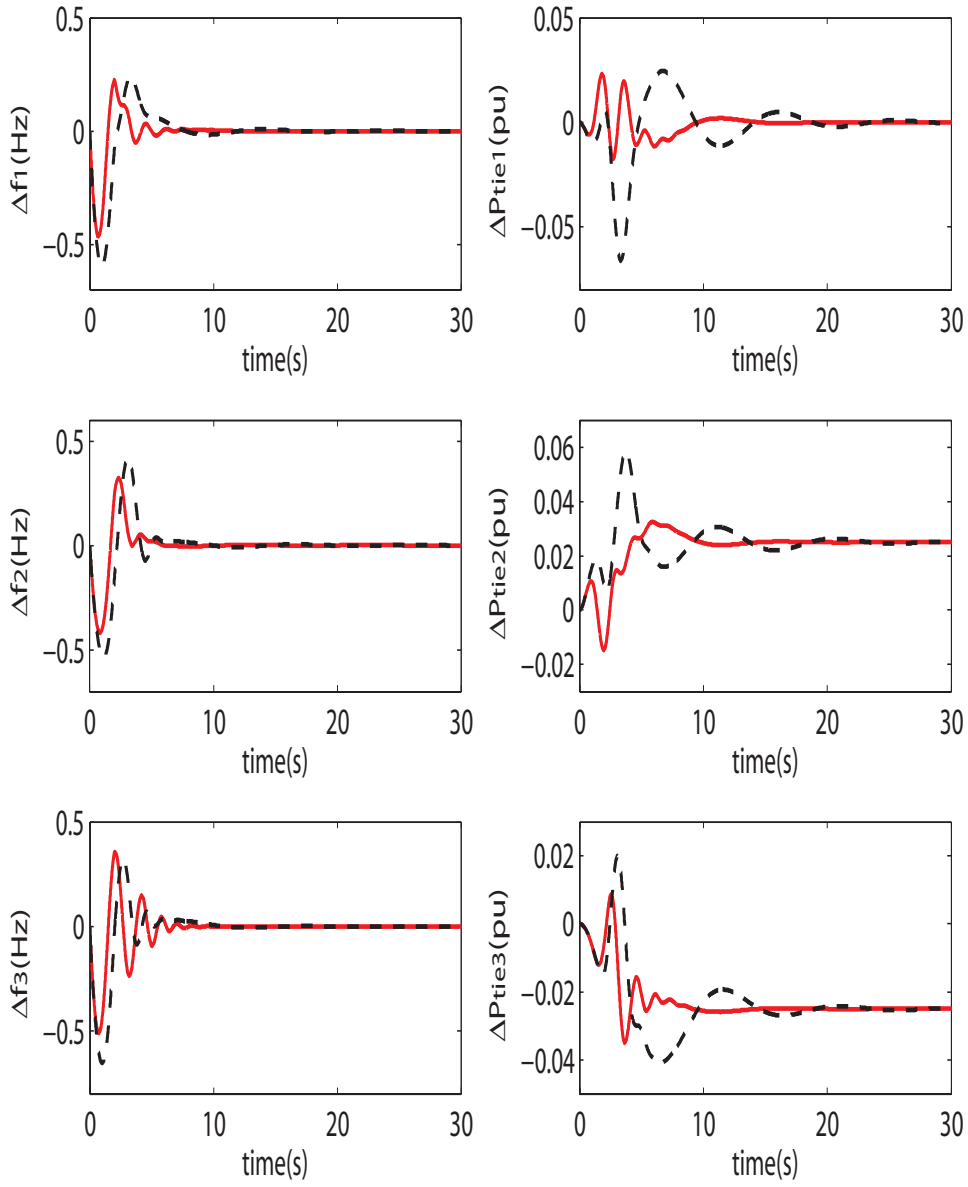

Figure 4.13: Deviation of frequency and and tie-line power exchange of the three-area power system with time-varying delay in Scenario II: Solid (LFC with DDC), Dashed (LFC without DDC)

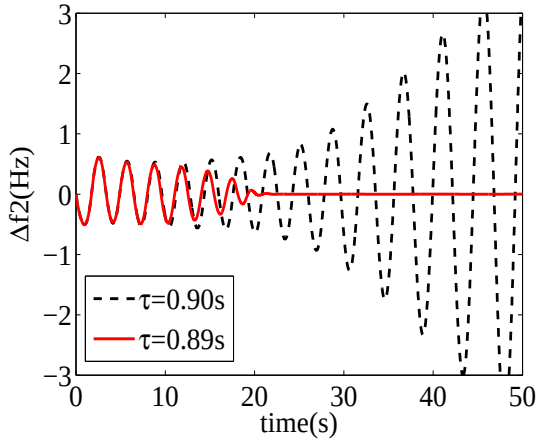

(a) FSR

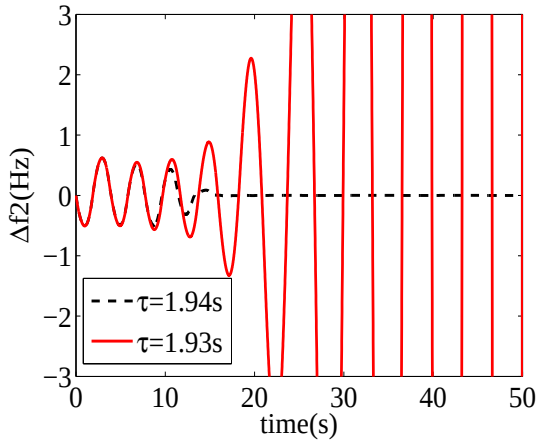

(b) SSR

Figure 4.14: Frequency deviation of control area 2 in Scenario II for different delay in DDC loop

Table 4.3: Dynamic performance indices (ITAE and ITSE) in Scenario II

Parameter change (%)	Parameter Change				Controller Parameter Change			
	without DDC		with DDC		without DDC		with DDC	
	ITAE	ITSE	ITAE	ITSE	ITAE	ITSE	ITAE	ITSE
0%	1.742	0.114	4.640	0.329	1.742	0.114	4.640	0.329
+5	1.904	0.132	4.864	0.396	1.814	0.117	5.134	0.350
-5	1.626	0.099	4.588	0.279	1.682	0.112	4.262	0.311
+10	2.109	0.154	5.422	0.487	1.902	0.119	5.809	0.374
-10	1.560	0.088	4.591	0.238	1.633	0.110	3.961	0.296
+15	2.356	0.181	6.541	0.615	2.009	0.123	6.744	0.403
-15	1.528	0.078	4.665	0.205	1.594	0.108	3.713	0.281
+20	2.657	0.214	8.497	0.805	2.140	0.126	8.072	0.440
-20	1.554	0.069	4.820	0.178	1.565	0.107	3.497	0.269
+25	3.022	0.256	11.560	1.102	2.301	0.130	10.060	0.488
-25	1.646	0.062	5.013	0.154	1.54	0.106	3.311	0.257

each area are assumed to be 0.3s. This part tests the admissible delay ranges, under which the LFC with DDC remains stable, by manual increasing the delay in the DDC loop step by step and observing the whole system stability. Figure 4.14 shows one example for control area 2 under different time delays in Scenario II. The results from Scenario I and Scenario II are found and listed in Table 4.4 and Table 4.5, respectively. It is found that there are multiple delay stable regions, only two of them are given in this chapter, defined as the first stability region (FSR) and the second stability region (SSR) respectively.

Table 4.4: Delay stable regions for each area in Scenario I

Control Area	First Stable Region (s)	Second Stable Region (s)
1	[0 3.15]	[5.74 11.30]
2	[0 0.86]	[2.11 12.50]
3	[0 0.48]	[2.10 10.00]

Table 4.5: Delay stable regions for each area in Scenario II

Control Area	First Stable Region (s)	Second Stable Region (s)
1	[0 3.15]	[5.70 11.10]
2	[0 0.89]	[1.94 11.50]
3	[0 0.48]	[1.87 11.00]

4.5 Conclusion

In this chapter, the PID-type controller for LFC with DDC in a deregulated multi-area power system is investigated. A robust PID controller design method has been proposed, through the H_∞ performance analysis and the PSO searching algorithm, to design a PID load frequency controller providing the robustness to the step and random load disturbances, the parameter and controller uncertainties, and the multiple delays in the LFC loop and the DDC loop. Case studies are based on a deregulated three-area LFC of the power system in two scenarios. Simulation results demonstrate that the effectiveness of the proposed PID controller, and robustness against parameter uncertainties and multiple time delays. It also shows that the LFC with DDC can provide better dynamic performance, in terms of performance index ITAE and ITSE. Moreover, delay margins of LFC with DDC are obtained via trial-and-error simulation method, and multiple stability regions have been found, which shows that large delay may re-stabilise the LFC system. It also found that the DDC can increase the delay margin of the LFC scheme.

Chapter 5

Frequency Regulation of Smart Grid via Direct Load Control and Battery Energy Storage System

5.1 Introduction

The momentary imbalance between the power generation side and the demand side will lead to frequency deviation of a power system [43]. In order to ensure the frequency stability, frequency regulation through matching the supply and the demand is an important topic in the operation of electricity markets [140]. In traditionally regulated environment, the elimination of frequency deviation is achieved by adjusting the power output of generator units to track the demand changes [41]. In the current power grid, with the increasing development of the wind power generation system, wind power has become one of the main power supplies [147]. However, the wind power generation depends on the weather condition and the wind speed and is time-varying, stochastic and intermittent. Therefore, the control and dispatch of wind power generators are not so easy as conventional generators. The improper control of wind power generators can result in the imbalance of supply and demand. Moreover, for a power grid working in the isolated mode and with high penetration of wind power, the intermittent wind power injection would become an

important factor of causing frequency deviation. Therefore, it is a challenging task to achieve the frequency regulation of the power grid with a high penetration level of wind power generations.

To integrate intermittent wind power into a power grid, spinning generation reserve with enough capacity are required to cover the period of no wind power outputs and thus will increase the operational cost [11]. Design of an advanced LFC scheme is an alternative way to integrate more intermittent wind power, such as multi-stage fuzzy logic control based LFC scheme designed to guarantee the robustness against the disturbance caused by the intermittent wind power [148–150]. The grid-scale energy storage system, such as BESS, is an effective alternative of the backup generation capacity by charging or discharging based on frequency deviation [109, 151], such as the BESS equipped with a controller based on ACE [53]. However, the grid-scale of BESS requires some expensive auxiliary equipment and thus still not a feasible solution due to its high cost.

As PEVs have drawn increasing attention in the transportation electrification in recent years, and considering most time PEVs are parked at home or workplaces, the battery of PEVs can be used as distributed energy storage to provide support of the grid operation, called V2G service [133]. One function of the V2G services is to aggregate a large number of small batteries of individual PEV as an equivalent grid-scale BESS and then provide frequency regulation of smart grid via controlling the charging/discharging of these batteries [60, 65–67, 135, 152]. Moreover, the PEVs have been adopted to suppress the frequency fluctuation in the power system with high penetration of renewable energy sources [153].

DSR, such as DDC, can provide controllability from the load-side to frequency regulation, rather than the conventional frequency regulation from the generator side, and is an effectively way to reduce the spinning generation capacity [43]. The DDC method can self-adjust the usage of electricity based on the frequency deviation of the power system [25]. In [70], the combination of the DDC and the BESS was proposed for frequency control, which has several advantages over other resources used for energy balancing and ancillary services, including relatively fast response time and high ramp rate, as well as low cost and high efficiency [12].

In order to implement the frequency regulation, inter-area power exchange and frequency derivation should be measured and transmitted to the control centre, and then the corresponding control signal calculated at the control centre should be transmitted to generation units taking part in the frequency regulation. In the traditional LFC scheme, the dedicate communication channel is usually used to transmit those signals, and the time delays arising are generally small and can be ignored due to the slow dynamic of frequency regulation [33]. However, in the modern smart power grids operating under deregulated environment, open communication networks are tended to be applied for transmitting those related signals, because of the feasibility, low cost and the bilateral contracts. With the introduction of the open communication channels, both constant delay and time-varying delay will be arisen in LFC problem [154]. Considering the characteristic of the communication channel, LFC scheme is a typical time delay system. The stability analysis and controller design problems considering the communication delays have been investigated for traditional and/or deregulated power systems [33–35, 155, 156].

The usage of the DDC and the PEVs to support the frequency regulation usually require aggregated a large number of smaller units by a third-party aggregator via the communication networks. Open communication networks are preferred for communication between the aggregator and a large number of individually controllable loads or the PEVs, which will introduce time delays into the frequency control loops. In [25], the time delays in the DDC loops are treated by using the different orders $Padé$ approximation. The field demonstration report shows that the delay between the aggregator and a PEV is less than two seconds via wireless communication [157]. Communication delays in the control loop have important impacts on the frequency regulation performance of the V2G service [65] and a large time delay may even destabilise the power grid with PEVs [66].

This chapter carries out the modelling, stability analysis and control design of frequency regulation of a smart power grid including wind farms, BESS, DDC and PEVs by considering the impact caused by time delays from communication networks in the control loops. Firstly, the state-space model of the closed-loop LFC scheme with/without communication delays for the smart power grid is develope-

d based on the simplified models of wind farms equipped with variable-speed wind turbines (VSWTs), the simple BESS, air-conditioners based DDC, and the distributed PEVs. Secondly, the Lyapunov stability theory based stability analysis method are given for the closed-loop LFC system with different embedded controller. Thirdly, a PID-type load frequency controller is tuned based on the H_∞ performance analysis and the PSO searching algorithm. Case studies based on single area smart power grid are carried out to investigate the contribution of the BESS, the PEVs, and the DDC to the frequency regulation and to verify the robustness of the designed PID controller against the power imbalance disturbances, the time delays, and the parameters uncertainties.

The rest of this chapter is organised as follows. The dynamic model of a single area LFC scheme is presented in Section 5.2. Section 5.3 introduces the stability analysis methods for LFC system with time delays. Section 5.4 develops a tuning method to design a robust PID controller. In section 5.5, case studies based on single area smart power grid are presented. Conclusions are drawn in Section 5.6.

5.2 Dynamic Model of Smart Grid for Frequency Regulation

This section describes the dynamic model of the smart grid including the wind farms, the BESS, the DDC, and the PEVs. The simplified models of BESS, the DDC, and the PEVs are introduced in the Chapter 3. The structure of the frequency regulation and the simplified model of the wind farm are given at first. Then, the state-space models of the closed-loop LFC scheme equipped with a PID controller are constructed by with and without the communication delays, respectively.

5.2.1 Structure of Frequency Regulation

The smart power grid used in this paper is shown in Figure 5.1, which can be operated in two alternative modes, i.e.,grid-connect and island model mode [158]. When the smart grid is in grid connected mode, the majority of the loads can be

supplied by the connected main grid and the system could be controlled by distribution management system (DMS). When the smart power grid is in island operating mode, the system power flow is balanced by local generation, and the system is controlled by the local smart-grid dispatch system (SGDS). The signals of the system state are measured by distributed sensors and transmitted to the SGDS through the communication channel. These signals are processed by the SGDS to generate control signals and sent back to each unit [158].

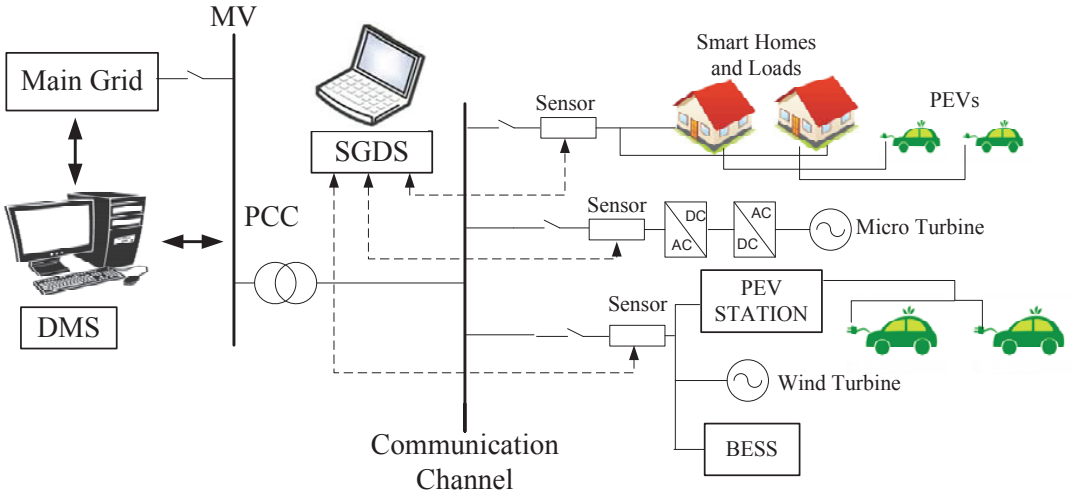

Figure 5.1: Smart grid with wind turbines, the PEVs, the smart homes, and the BESS

This chapter discusses the case where the smart power grid is in island operating mode, and the capacity of the micro traditional generator is not adequate to provide the local demands. The wind turbines can provide active power to local loads, while the wind power injection depends on the wind speed and is usually intermittent and uncontrollable, which may often lead to the imbalance and result in the frequency deviation. The PEVs, the BESSs and the controllable loads in the smart homes are used to compensate such unbalance. Then the structure of the frequency regulation for smart grid is given as Figure 5.2, in which the micro turbine is assumed to be a non-reheat turbine with the time constant, T_t.

From Figure 5.2, the relationship between the energy imbalance and the corre-

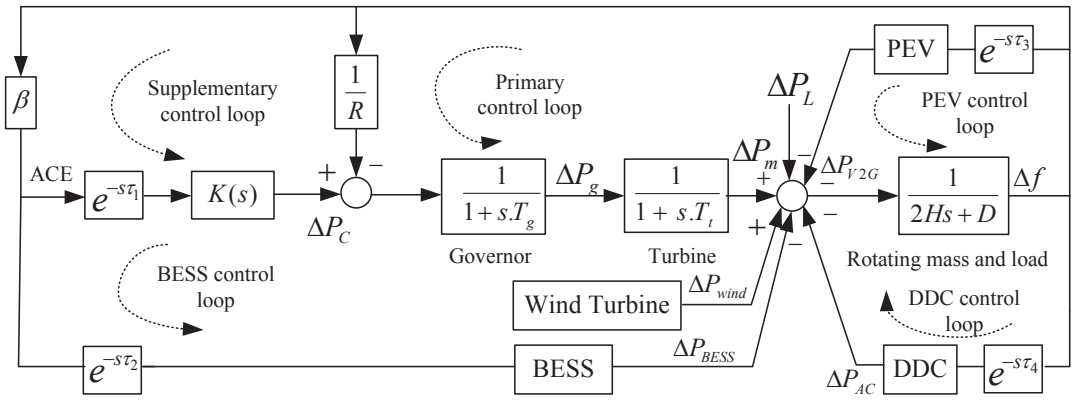

Figure 5.2: The structure of the frequency regulation

sponding frequency deviation can be given as follows:

$$\begin{aligned} & \Delta P_m(s) + \Delta P_{wind}(s) - \Delta P_{BESS}(s) - \Delta P_L(s) - \Delta P_{AC}(s) - \Delta P_{V2G}(s) \\ = \; & 2Hs\Delta f(s) + D\Delta f(s) \end{aligned} \tag{5.2.1}$$

where ΔP_m is the generator mechanical output, ΔP_{wind} is the deviation of the wind power energy from the wind farm, ΔP_{BESS} is the power deviation from the BESS, ΔP_{AC} is the power deviation from the DDC based on air conditioners, ΔP_{V2G} is the power deviation from the PEVs, ΔP_L is the load change, $2H$ is the equivalent inertia constant, D is the equivalent load-damping coefficient, and Δf is the frequency deviation of smart grid.

As shown in Figure 5.2, there are five control loops taking part in the frequency regulation, including two generator-side loops (traditional primary and supplementary loops) and three demand-side loops (BESS, PEVs, and DDC loops). When sudden drop happens in the frequency, the primary control loop can maintain frequency deviation closely to 0. The supplementary control loop (usually called LFC) is required to eliminate the steady state error of the frequency deviation [25]. The parameters in primary control loop and supplementary control loop are introduced in Chapter 3.2.1. The load frequency controller, $K(s)$, commonly used in practice is the PID controller.

Three additional control loops are introduced for compensating the energy unbalance caused by the intermittent wind power injection. In the BESS loop, the

BESS is controlled for charging or discharging based on the ACE signal, and the DDC and PEV loops are responding directly to the frequency deviation.

The measurements and control commands are transmitted through open communication channels, and the time delays may be introduced during the procedure of the transition. In Figure 5.2, the τ_1, τ_2, τ_3 and τ_4 show the communication time delays in LFC, the BESS, the PEV and the DDC control loops, respectively.

5.2.2 Wind Farm with Variable-Speed Wind Turbines

The wind power energy is developing very fast in recent years, and its intermittent characteristic may cause the energy imbalance of the smart grid. The part presents the dynamic model of a pitch angle controlled VSWT [159–161]. The VSWT model is a complex nonlinear system and consists of aerodynamics, turbine mechanics, generator dynamics, and pitch actuator dynamics parts. Figure 5.3 shows the relationships among them.

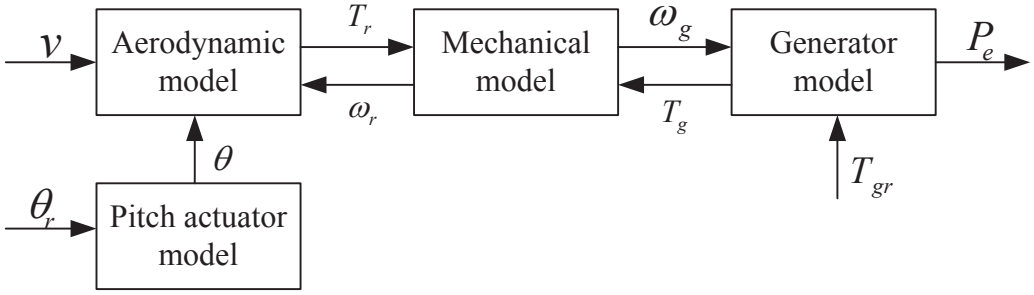

Figure 5.3: Interconnection of sub-models describing the characteristics of the wind turbine [159]

The aerodynamic blades on the rotor converts the kinetic energy of the wind into mechanical energy, effectively providing the torque, T_r, on the rotor:

$$T_r = \frac{P_r}{\omega_r} \tag{5.2.2}$$

where ω_r is the rotor speed, and the mechanical power absorbed from the wind P_r is given as:

$$P_r = \frac{1}{2}\rho\pi R_{wind}^2 v^3 C_p \tag{5.2.3}$$

where ρ is the air density, R_{wind} is the wind radius, v is the effective wind speed, and C_p is the power coefficient which is a function of the blade pitch angle, θ, and the tip speed ratio, λ, and the one used in this chapter is given as follows:

$$C_p(\lambda, \theta) = 0.22 \left(\frac{116}{\lambda_t} - 0.6\theta - 5 \right) e^{-\frac{12.5}{\lambda_t}} \tag{5.2.4}$$

where λ_t is defined as

$$\frac{1}{\lambda_t} = \frac{1}{\lambda^{-1} + 0.129} - \frac{0.035}{(1.5\theta)^3 + 1} \tag{5.2.5}$$

with $\lambda = v/(R_{wind}\omega_r)$.

The blade pitch angle, θ, is changed by a hydraulic/mechanical actuator. A simplified model of the blade dynamics is presented by the following first order linear model:

$$\dot{\theta} = -\frac{1}{\tau_\theta}\theta + \frac{1}{\tau_\theta}\theta_r \tag{5.2.6}$$

where θ_r is the reference and the one control input for the wind turbine.

The mechanical model includes two parts, i.e., the rotor side and generator side. The dynamic on the two sides are described as follows:

$$\dot{\omega_r} J_r = T_r - T_{sr} \tag{5.2.7}$$

$$\dot{\omega_g} J_g = T_{sg} - T_g \tag{5.2.8}$$

where J_r and J_g are the inertia on the rotor side and generator side, respectively; ω_r and ω_g are the rotational speeds on the rotor side and generator side, respectively; T_r and T_g represent for the rotor torque and generator torque, respectively; T_{sg} and T_{sr} are the torques on each side of the transmission, which are related by the gear ratio, N_g:

$$T_{sr} = T_{sg} N_g \tag{5.2.9}$$

and the torque at the rotor side of the transmission can be described by the twist of the flexible shaft:

$$T_{sr} = D_s\dot{\delta} + K_s\delta \tag{5.2.10}$$

where D_s is the damping and K_s is the spring constant, which can illustrate the dynamic nature of the shaft; and the twist of the flexible shaft, δ, is determined by

$$\dot{\delta} = \omega_r - \frac{\omega_g}{N_g} \tag{5.2.11}$$

The generator power, P_e, is given by:

$$P_e = T_g \omega_g \tag{5.2.12}$$

where the generator torque, T_g, is controlled, however, it cannot be changed instantaneously. The dynamic response of the generator has therefore been modelled by a first order linear model with time constant, τ_t:

$$\dot{T}_g = -\frac{1}{\tau_t} T_g + \frac{1}{\tau_t} T_{gr} \tag{5.2.13}$$

where T_{gr} is the reference and one of the control inputs for the wind turbine.

Some individual wind turbines are aggregated to represent a wind farm. It assumes the wind speed for each wind turbine is same at the same time. Considering the clustering effect of wind turbines, the active power produced by a large scale wind farm introduced by [161] is expressed as:

$$\Delta P_{wind} = \sum_{j=1}^{N_{wind}} P_{e,j} - P_{wind,desired} \tag{5.2.14}$$

where $P_{wind,desired}$ is the desired active power output of the wind farm, ΔP_{wind} is the deviation of the active power out from the desired value, $P_{e,j}$ is active power output of the jth wind turbines and N_{wind} is the total number of wind turbines in the wind farm [161].

5.2.3 State-Space Model of Closed-Loop LFC scheme

By taking into account the aforementioned models of the BESS, PEVs and the DDC, and the model of single area traditional LFC scheme discussed in [33], the dynamic model of the LFC scheme shown in Figure 5.2 can be obtained as follows:

$$\begin{cases} \dot{x}(t) = Ax(t) + A_b x(t-\tau_2) + A_c x(t-\tau_3) + A_d x(t-\tau_4) + Bu(t-\tau_1) + Fv \\ y(t) = Cx(t) \end{cases} \tag{5.2.15}$$

where

$$x = [\Delta f \ \ \Delta P_{\mathrm{m}} \ \ \Delta P_{\mathrm{g}} \ \ \Delta P_{BESS} \ \ \Delta P_{V2G} \ \ \Delta P_{AC}]^T$$

$$y = ACE$$

$$v = \Delta P_L - \Delta P_{wind}$$

$$A = \begin{bmatrix} -\frac{D}{2H} & \frac{1}{2H} & 0 & -\frac{1}{2H} & -\frac{1}{2H} & -\frac{1}{2H} \\ 0 & -\frac{1}{T_t} & \frac{1}{T_t} & 0 & 0 & 0 \\ -\frac{1}{RT_g} & 0 & -\frac{1}{T_g} & 0 & 0 & 0 \\ 0 & 0 & 0 & 0 & 0 & 0 \\ 0 & 0 & 0 & 0 & 0 & 0 \\ 0 & 0 & 0 & 0 & 0 & 0 \end{bmatrix}$$

$$A_b = \begin{bmatrix} 0 & 0 & 0 & 0 & 0 & 0 \\ 0 & 0 & 0 & 0 & 0 & 0 \\ 0 & 0 & 0 & 0 & 0 & 0 \\ \frac{I^0_{bes} K_{bes} \beta}{T_{bes}} & 0 & 0 & -\frac{1}{T_{bes}} & 0 & 0 \\ 0 & 0 & 0 & 0 & 0 & 0 \\ 0 & 0 & 0 & 0 & 0 & 0 \end{bmatrix}$$

$$A_c = \begin{bmatrix} 0 & 0 & 0 & 0 & 0 & 0 \\ 0 & 0 & 0 & 0 & 0 & 0 \\ 0 & 0 & 0 & 0 & 0 & 0 \\ 0 & 0 & 0 & 0 & 0 & 0 \\ \frac{k_{ev}}{T_{ev}} & 0 & 0 & 0 & -\frac{1}{T_{ev}} & 0 \\ 0 & 0 & 0 & 0 & 0 & 0 \end{bmatrix}$$

$$A_d = \begin{bmatrix} 0 & 0 & 0 & 0 & 0 & 0 \\ 0 & 0 & 0 & 0 & 0 & 0 \\ 0 & 0 & 0 & 0 & 0 & 0 \\ 0 & 0 & 0 & 0 & 0 & 0 \\ 0 & 0 & 0 & 0 & 0 & 0 \\ 0.5K_{ddc} - \frac{2\pi D D_{ac}}{2H} & \frac{2\pi D_{ac}}{2H} & 0 & -\frac{2\pi D_{ac}}{2H} & -\frac{2\pi D_{ac}}{2H} & -\frac{2\pi D_{ac}}{2H} \end{bmatrix}$$

$$B = \begin{bmatrix} 0 & 0 & \frac{1}{T_g} & 0 & 0 & 0 \end{bmatrix}^T$$

$$F = \begin{bmatrix} -\frac{1}{2H} & 0 & 0 & 0 & 0 & -\frac{2\pi D_{ac}}{2H} \end{bmatrix}^T$$

$$C = \begin{bmatrix} \beta & 0 & 0 & 0 & 0 & 0 \end{bmatrix}$$

And the load frequency controller, $K(s)$, used in this chapter is the PID type controller with the following form:

$$u(t) = -K_P ACE - K_I \int ACE dt - K_D \frac{d}{dt} ACE \tag{5.2.16}$$

where K_P, K_I, and K_D stand for proportional, integral and derivative gains, respectively; and ACE is the area control error as shown in Equation (5.4.8).

In order to simplify the analysis, the closed-loop system with a PID controller is transformed into a new system with a static output feedback controller. By defining the following virtual state vector and the output vector

$$\bar{x} = \begin{bmatrix} x^T & \int y^T dt \end{bmatrix}^T \tag{5.2.17}$$

$$\bar{y} = \begin{bmatrix} y^T & \int y^T dt & \frac{d}{dt} y^T \end{bmatrix}^T \tag{5.2.18}$$

the closed-loop system can be rewritten as:

$$\begin{cases} \dot{\bar{x}}(t) = \bar{A}\bar{x}(t) + \bar{A}_b\bar{x}(t-\tau_2) + \bar{A}_c\bar{x}(t-\tau_3) + \bar{A}_d\bar{x}(t-\tau_4) - \bar{B}K\bar{C}\bar{x}(t-\tau_1) \\ \qquad\qquad + (\bar{F} - \bar{B}K\bar{Q})v \\ \bar{y}(t) = \bar{C}\bar{x}(t) + \bar{Q}v \end{cases} \tag{5.2.19}$$

where

$$\bar{A}=\begin{bmatrix} A & 0 \\ C & 0 \end{bmatrix},\quad \bar{A}_b=\begin{bmatrix} A_b & 0 \\ 0 & 0 \end{bmatrix},\quad \bar{A}_c=\begin{bmatrix} A_c & 0 \\ 0 & 0 \end{bmatrix},\quad \bar{A}_d=\begin{bmatrix} A_d & 0 \\ 0 & 0 \end{bmatrix}$$

$$\bar{B}=\begin{bmatrix} B \\ 0 \end{bmatrix},\quad \bar{C}=\begin{bmatrix} C & 0 \\ 0 & 1 \\ CA & 0 \end{bmatrix},\quad \bar{F}=\begin{bmatrix} F \\ 0 \end{bmatrix},\quad \bar{Q}=\begin{bmatrix} 0 \\ 0 \\ CF \end{bmatrix}$$

$$K=[K_P\ \ K_I\ \ K_D]$$

By using the similar deriving procedure, the dynamic models for the special cases can be obtained. Firstly, for the case that only primary and supplementary control loops (i.e., traditional LFC) are included, the closed-loop model is given as

$$\begin{cases} \dot{\bar{x}}_1(t)=\bar{A}_1\bar{x}_1(t)-\bar{B}_1K\bar{C}_1\bar{x}_1(t-\tau_1)+(\bar{F}_1-\bar{B}_1K\bar{Q}_1)v \\ \bar{y}(t)=\bar{C}_1\bar{x}_1(t)+\bar{Q}_1v \end{cases} \tag{5.2.20}$$

where

$$\bar{x}_1=\left[\Delta f\ \ \Delta P_{\mathrm{m}}\ \ \Delta P_{\mathrm{g}}\ \ \int y^T dt\right]^T$$

$$\bar{A}_1=\begin{bmatrix} A_1 & 0 \\ C_1 & 0 \end{bmatrix},\ A_1=\begin{bmatrix} -\frac{D}{2H} & \frac{1}{2H} & 0 \\ 0 & -\frac{1}{T_t} & \frac{1}{T_t} \\ -\frac{1}{RT_g} & 0 & -\frac{1}{T_g} \end{bmatrix},\ C_1=\begin{bmatrix} \beta & 0 & 0 \end{bmatrix}$$

$$\bar{B}_1=\begin{bmatrix} B_1^T & 0 \end{bmatrix}^T,\ B_1=\begin{bmatrix} 0 & 0 & \frac{1}{T_g} \end{bmatrix}^T,\ \bar{C}_1=\begin{bmatrix} C_1 & 0 \\ 0 & 1 \\ C_1A_1 & 0 \end{bmatrix}$$

$$\bar{F}_1=\begin{bmatrix} F_1^T & 0 \end{bmatrix}^T,\ F_1=\begin{bmatrix} -\frac{1}{2H} & 0 & 0 \end{bmatrix}^T,\ \bar{Q}_1=[0\ \ 0\ \ C_1F_1]^T.$$

Secondly, for the case of traditional LFC with the DDC part, the closed-loop model is given as

$$\begin{cases} \dot{\bar{x}}_2(t)=\bar{A}_2\bar{x}_2(t)+\bar{A}_{d2}\bar{x}_2(t-\tau_4)-\bar{B}_2K\bar{C}_2\bar{x}_2(t-\tau_1)+(\bar{F}_2-\bar{B}_2K\bar{Q}_2)v \\ \bar{y}(t)=\bar{C}_2\bar{x}_2(t)+\bar{Q}_2v \end{cases} \tag{5.2.21}$$

where

$$\bar{x}_2 = \left[\Delta f \;\; \Delta P_{\mathrm{m}} \;\; \Delta P_{\mathrm{g}} \;\; \Delta P_{AC} \;\; \int y^T dt\right]^T$$

$$\bar{A}_2 = \begin{bmatrix} A_2 & 0 \\ C_2 & 0 \end{bmatrix}, \quad A_2 = \begin{bmatrix} -\frac{D}{2H} & \frac{1}{2H} & 0 & -\frac{1}{2H} \\ 0 & -\frac{1}{T_t} & \frac{1}{T_t} & 0 \\ -\frac{1}{RT_g} & 0 & -\frac{1}{T_g} & 0 \\ 0 & 0 & 0 & 0 \end{bmatrix}, \quad C_2 = \begin{bmatrix} C_1 & 0 \end{bmatrix}$$

$$\bar{A}_{d2} = \begin{bmatrix} 0 & 0 & 0 & 0 & 0 \\ 0 & 0 & 0 & 0 & 0 \\ 0 & 0 & 0 & 0 & 0 \\ 0.5K_{ddc} - \frac{2\pi D D_{ac}}{2H} & \frac{2\pi D_{ac}}{2H} & 0 & -\frac{2\pi D_{ac}}{2H} & 0 \\ 0 & 0 & 0 & 0 & 0 \end{bmatrix}$$

$$\bar{B}_2 = \begin{bmatrix} B_1^T & 0 & 0 \end{bmatrix}^T, \quad \bar{C}_2 = \begin{bmatrix} C_2 & 0 \\ 0 & 1 \\ C_2 A_2 & 0 \end{bmatrix}, \bar{F}_2 = \begin{bmatrix} F_2^T & 0 \end{bmatrix}^T$$

$$F_2 = \left[F_1^T \;\; -\frac{2\pi D_{ac}}{2H}\right]^T, \quad \bar{Q}_2 = \begin{bmatrix} 0 & 0 & C_2 F_2 \end{bmatrix}^T.$$

Thirdly, for the case that both the DDC and the BESS are introduced into the traditional LFC, the closed-loop model is given as:

$$\begin{cases} \dot{\bar{x}}_3(t) = \bar{A}_3 \bar{x}_3(t) + \bar{A}_{b3} \bar{x}_3(t-\tau_2) + \bar{A}_{d3} \bar{x}_3(t-\tau_4) - \bar{B}_3 K \bar{C}_3 \bar{x}_3(t-\tau_1) \\ \qquad\qquad + (\bar{F}_3 - \bar{B}_3 K \bar{Q}_3) v \\ \bar{y}(t) = \bar{C}_3 \bar{x}_3(t) + \bar{Q}_3 v \end{cases} \tag{5.2.22}$$

where

$$\bar{x}_3 = \left[\Delta f \;\; \Delta P_{\mathrm{m}} \;\; \Delta P_{\mathrm{g}} \;\; \Delta P_{BESS} \;\; \Delta P_{AC} \;\; \int y^T dt\right]^T$$

$$\bar{A}_3 = \begin{bmatrix} A_3 & 0 \\ C_3 & 0 \end{bmatrix}, \quad A_3 = \begin{bmatrix} -\frac{D}{2H} & \frac{1}{2H} & 0 & -\frac{1}{2H} & -\frac{1}{2H} \\ 0 & -\frac{1}{T_t} & \frac{1}{T_t} & 0 & 0 \\ -\frac{1}{RT_g} & 0 & -\frac{1}{T_g} & 0 & 0 \\ 0 & 0 & 0 & 0 & 0 \\ 0 & 0 & 0 & 0 & 0 \end{bmatrix}$$

$$\bar{A}_{b3} = \begin{bmatrix} 0 & 0 & 0 & 0 & 0 & 0 \\ 0 & 0 & 0 & 0 & 0 & 0 \\ 0 & 0 & 0 & 0 & 0 & 0 \\ \frac{I^0_{bes} K_{bes} \beta}{T_{bes}} & 0 & 0 & -\frac{1}{T_{bes}} & 0 & 0 \\ 0 & 0 & 0 & 0 & 0 & 0 \\ 0 & 0 & 0 & 0 & 0 & 0 \end{bmatrix}$$

$$\bar{A}_{d3} = \begin{bmatrix} 0 & 0 & 0 & 0 & 0 & 0 \\ 0 & 0 & 0 & 0 & 0 & 0 \\ 0 & 0 & 0 & 0 & 0 & 0 \\ 0 & 0 & 0 & 0 & 0 & 0 \\ 0.5K_{ddc} - \frac{2\pi D D_{ac}}{2H} & \frac{2\pi D_{ac}}{2H} & 0 & -\frac{2\pi D_{ac}}{2H} & -\frac{2\pi D_{ac}}{2H} & 0 \\ 0 & 0 & 0 & 0 & 0 & 0 \end{bmatrix}$$

$$\bar{B}_3 = \begin{bmatrix} B_1^T & 0 & 0 & 0 \end{bmatrix}^T, \quad \bar{C}_3 = \begin{bmatrix} C_3 & 0 \\ 0 & 1 \\ C_3 A_3 & 0 \end{bmatrix}, \quad C_3 = \begin{bmatrix} C_1 & 0 & 0 \end{bmatrix}$$

$$F_3 = \begin{bmatrix} F_1^T & 0 & -W \end{bmatrix}^T, \quad \bar{F}_3 = \begin{bmatrix} F_3^T & 0 \end{bmatrix}^T, \quad \bar{Q}_3 = [0 \ 0 \ C_3 F_3]^T$$

5.3 Delay-Dependent Stability Analysis

The system stability is the basic requirement of the smart power grid, and the communication time delays arising from the model (5.2.19) will degrade the system performance even cause instability. In this section, a delay-dependent stability analysis method is developed based on the Lyapunov functional method and the LMI, including the proof of the stability criterion and the procedure of the calculation of the delay margin.

In model (5.2.19), the time delays of different control loops are different, which makes the analysis complex. Hence, some modifications are made to simplify the analysis. That is, the time delays in LFC and BESS control loops caused from the measurement and the transmission of the ACE signal are assumed to be identical, and the time delays in PEV and DDC control loops arising due to the measurement of the frequency deviation are also assumed to be identical, i.e., $\bar{\tau}_1 = \tau_1 = \tau_2$ and $\bar{\tau}_2 = \tau_3 = \tau_4$. This chapter investigates the initial stability, thus the disturbance is not taken into account. In another word, it assumes the initial state of the power system in not stable. Then the internal stability of the power system is analyzed without considering the external disturbance. It means the external disturbance "$(\bar{F} - \bar{B}K\bar{Q})v$" of Equation (5.2.19) is ignored. So the closed-loop system shown in Equation (5.2.19) can be rewritten as:

$$\dot{\bar{x}}(t) = \bar{A}\bar{x}(t) + (\bar{A}_b - \bar{B}K\bar{C})\bar{x}(t - \bar{\tau}_1) + (\bar{A}_c + \bar{A}_d)\bar{x}(t - \bar{\tau}_2) \tag{5.3.1}$$

5.3.1 Delay-Dependent Stability Criterion

The stability criterion is important to judge the system stability. By using the Lyapunov stability theory and the Wirtinger inequality and following the similar procedure of [35], the following delay-dependent stability criterion can be obtained.

Theorem 5.1. Consider the following time-delay system:

$$\dot{x}(t) = A_0 x(t) + A_1 x(t - \tau_1) + A_2 x(t - \tau_2) \tag{5.3.2}$$

For given scalars τ_i satisfying $0 = \tau_0 \leq \tau_1 \leq \tau_2$, the above system is asymptotically stable if there exist symmetric positive definite matrices $P_1 > 0$, $Q_1 > 0$, $Q_2 > 0$, $R_1 \geq 0$ and $R_2 \geq 0$ such that the following LMI holds

$$\Xi = \Phi + \Phi_1 + \Phi_2 < 0 \tag{5.3.3}$$

where

$$\Phi = \begin{bmatrix} e_1 \\ \tau_1 e_4 \\ (\tau_2-\tau_1)e_5 \end{bmatrix}^T P_1 \begin{bmatrix} e_0 \\ e_1-e_2 \\ e_2-e_3 \end{bmatrix} + \begin{bmatrix} e_0 \\ e_1-e_2 \\ e_2-e_3 \end{bmatrix}^T P_1 \begin{bmatrix} e_1 \\ \tau_1 e_4 \\ (\tau_2-\tau_1)e_5 \end{bmatrix}$$

$$\Phi_1 = e_1^T Q_1 e_1 - e_2^T Q_1 e_2 + e_2^T Q_2 e_2 - e_3^T Q_2 e_3 + \tau_1^2 e_0^T R_1 e_0 + (\tau_2-\tau_1)^2 e_0^T R_2 e_0$$

$$\Phi_2 = -\begin{bmatrix} e_1-e_2 \\ e_1+e_2-2e_4 \end{bmatrix}^T \begin{bmatrix} R_1 & 0 \\ 0 & 3R_1 \end{bmatrix} \begin{bmatrix} e_1-e_2 \\ e_1+e_2-2e_4 \end{bmatrix}$$
$$-\begin{bmatrix} e_2-e_3 \\ e_2+e_3-2e_5 \end{bmatrix}^T \begin{bmatrix} R_2 & 0 \\ 0 & 3R_2 \end{bmatrix} \begin{bmatrix} e_2-e_3 \\ e_2+e_3-2e_5 \end{bmatrix}$$

$$e_0 = \begin{bmatrix} A_0, & A_1, & A_2, & 0, & 0 \end{bmatrix}$$
$$e_1 = \begin{bmatrix} I, & 0, & 0, & 0, & 0 \end{bmatrix}$$
$$e_2 = \begin{bmatrix} 0, & I, & 0, & 0, & 0 \end{bmatrix}$$
$$e_3 = \begin{bmatrix} 0, & 0, & I, & 0, & 0 \end{bmatrix}$$
$$e_4 = \begin{bmatrix} 0, & 0, & 0, & I, & 0 \end{bmatrix}$$
$$e_5 = \begin{bmatrix} 0, & 0, & 0, & 0, & I \end{bmatrix}$$

Proof: Construct a candidate Lyapunov function as

$$\begin{aligned} V(t) = &\begin{bmatrix} x(t) \\ \int_{t-\tau_1}^{t} x(s)ds \\ \int_{t-\tau_2}^{t-\tau_1} x(s)ds \end{bmatrix}^T P_1 \begin{bmatrix} x(t) \\ \int_{t-\tau_1}^{t} x(s)ds \\ \int_{t-\tau_2}^{t-\tau_1} x(s)ds \end{bmatrix} + \int_{t-\tau_1}^{t} x^T(s)Q_1 x(s)ds \\ &+ \tau_1 \int_{-\tau_1}^{0}\int_{t+\theta}^{t} \dot{x}^T(s)R_1\dot{x}(s)dsd\theta + \int_{t-\tau_2}^{t-\tau_1} x^T(s)Q_2 x(s)ds \\ &+ (\tau_2-\tau_1)\int_{-\tau_2}^{-\tau_1}\int_{t+\theta}^{t} \dot{x}^T(s)R_2\dot{x}(s)dsd\theta \end{aligned} \tag{5.3.4}$$

where $P_1,\ Q_1,\ Q_2,\ R_1$ and R_2 are positive definite symmetric matrices, which means the positive of the function, i.e., $V(t) \geq \varepsilon_1 ||x(t)||^2$ with $\varepsilon_1 > 0$.

Calculating the derivative of (5.3.4) yields

$$\begin{aligned}\dot{V}(t) &= 2\begin{bmatrix} x(t) \\ \int_{t-\tau_1}^{t} x(s)ds \\ \int_{t-\tau_2}^{t-\tau_1} x(s)ds \end{bmatrix}^T P_1 \begin{bmatrix} \dot{x}(t) \\ x(t)-x(t-\tau_1) \\ x(t-\tau_1)-x(t-\tau_2) \end{bmatrix} \\ &\quad +x^T(t)Q_1x(t)-x^T(t-\tau_1)Q_1x(t-\tau_1) \\ &\quad +x^T(t-\tau_1)Q_2x(t-\tau_1)-x^T(t-\tau_2)Q_2x(t-\tau_2) \\ &\quad +\tau_1^2\dot{x}^T(t)R_1\dot{x}(t)+(\tau_2-\tau_1)^2\dot{x}^T(t)R_2\dot{x}(t) \\ &\quad -\tau_1\int_{t-\tau_1}^{t}\dot{x}^T(s)R_1\dot{x}(s)ds-(\tau_2-\tau_1)\int_{t-\tau_2}^{t-\tau_1}\dot{x}^T(s)R_2\dot{x}(s)ds\end{aligned}$$

It follows from Wirtinger-based integral inequality [162] that

$$\begin{aligned}&\tau_1\int_{t-\tau_1}^{t}\dot{x}^T(s)R_1\dot{x}(s)ds+(\tau_2-\tau_1)\int_{t-\tau_2}^{t-\tau_1}\dot{x}^T(s)R_2\dot{x}(s)ds \qquad (5.3.5)\\ &\geq \begin{bmatrix} x(t)-x(t-\tau_1) \\ x(t)+x(t-\tau_1)-2\int_{t-\tau_1}^{t}\frac{x(s)}{\tau_1}ds \end{bmatrix}^T \begin{bmatrix} R_1 & 0 \\ 0 & 3R_1 \end{bmatrix} \\ &\quad \begin{bmatrix} x(t)-x(t-\tau_1) \\ x(t)+x(t-\tau_1)-2\int_{t-\tau_1}^{t}\frac{x(s)}{\tau_1}ds \end{bmatrix} \\ &\quad +\begin{bmatrix} x(t-\tau_1)-x(t-\tau_2) \\ x(t-\tau_1)+x(t-\tau_2)-2\int_{t-\tau_2}^{t-\tau_1}\frac{x(s)}{\tau_2-\tau_1}ds \end{bmatrix}^T \\ &\quad \begin{bmatrix} R_2 & 0 \\ 0 & 3R_2 \end{bmatrix} \begin{bmatrix} x(t-\tau_1)-x(t-\tau_2) \\ x(t-\tau_1)+x(t-\tau_2)-2\int_{t-\tau_2}^{t-\tau_1}\frac{x(s)}{\tau_2-\tau_1}ds \end{bmatrix}\end{aligned}$$

then applying (5.3.3) and (5.3.5) yields

$$\dot{V}(t) \leq \bar{\xi}^T(t)\Xi\bar{\xi}(t) \leq 0 \qquad (5.3.6)$$

where

$$\bar{\xi}(t) = \left[\ x^T(t),\ x^T(t-\tau_1),\ x^T(t-\tau_2),\ \int_{t-\tau_1}^{t}\frac{x^T(s)}{\tau_1}ds,\ \int_{t-\tau_2}^{t-\tau_1}\frac{x^T(s)}{\tau_2-\tau_1}ds\ \right]^T$$

Therefore, the system is asymptotically stable if $P_1 > 0$, $Q_1 \geq 0$, $Q_2 \geq 0$, $R_1 \geq 0$ and $R_2 \geq 0$ and (5.3.3) holds. This completes the proof.

5.3.2 Delay Margin Calculation

The aforementioned stability criterion (Theorem 5.1) shows the relationship between the stability and the value of the time delays. Based on this criterion, one can judge the stability of the system with the given time delays, and also find the admissible maximal delay value, so-called delay margin, that the system starts to become instability. As reported in [35], the calculation of the delay margin of the system is an important issue during the delay-dependent stability analysis.

There are two time delays in system (5.3.1). One can find the delay margin of the one of the delays, based on Theorem 5.1, by fixing the other time delay. That is, the delay margin of $\bar{\tau}_1$ (or $\bar{\tau}_2$) should be a function of the delay $\bar{\tau}_2$ (or $\bar{\tau}_1$), i.e.,

$$\bar{\tau}_{\max i} = f_s(\bar{\tau}_j), i = 1, j = 2;\ i = 2, j = 1 \tag{5.3.7}$$

As mentioned in [172], the method combining the $feasp$ solver in Matlab/LMI toolbox and the binary search algorithm can be applied to calculate the delay margin. The simplified procedure is described in Figure 5.4

5.4 Delay-Dependent Robust Controller Design

In this section, a PID controller tuning method is developed based on the delay-dependent H_∞ performance analysis and the PSO searching algorithm. The delay-dependent H_∞ performance analysis is carried out to derive a criterion, which constructs the relationships among the delay bound, the robust performance index, and the control gains. Then, based on the criterion, the tuning of the controller gains is transformed into an optimisation problem solved by standard PSO algorithm.

In model (5.2.19), four delays exist in the different control loops. To simplify the analysis, those delay are assumed to be identical, i.e., $h = \tau_1 = \tau_2 = \tau_3 = \tau_4$. Then, the closed-loop system shown in (5.2.19) can be rewritten as:

$$\begin{cases} \dot{x}(t) &= Ax(t) + (A_{bc} - \bar{B}KC_y)x(t-h) + (B_\omega - \bar{B}K\bar{Q})\omega(t) \\ z(t) &= C_z x(t) \end{cases} \tag{5.4.1}$$

where $x(t) = \bar{x}(t)$, $A = \bar{A}$, $A_{bc} = \bar{A}_b + \bar{A}_c + \bar{A}_d$, $\omega(t) = v(t)$, $B_\omega = \bar{F}$, $C_y = \bar{C}$, and $C_z = [1\ 0\ 0\ 0\ 0\ 0\ 0]$.

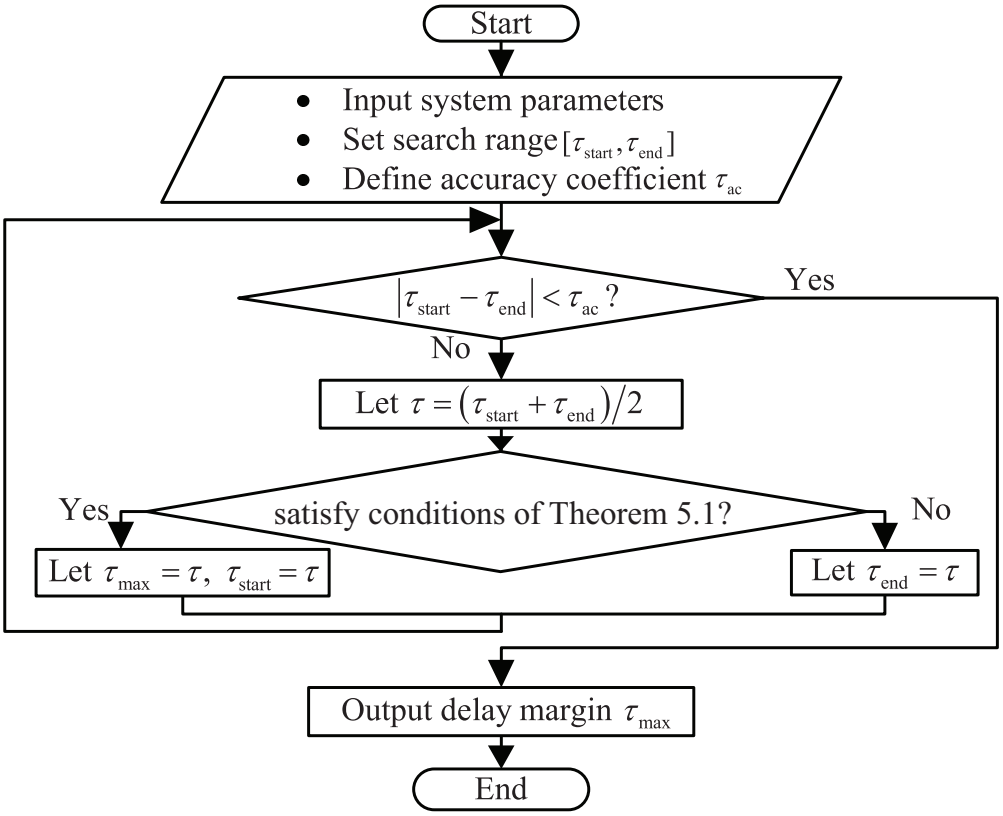

Figure 5.4: The simplified procedure of delay margin calculation

5.4.1 Delay-dependent H_∞ Performance Analysis

For the above system, by using the Lyapunov-Krasovskii functional method, the relationships among the delay bound, the robust performance index, and the control gains can be described by the following criterion.

Theorem 5.2: Consider the closed-loop system (5.4.1), for the delay bound h, the H_∞ performance index γ, and the controller gains $K = [K_\mathrm{P}\ K_\mathrm{I}\ K_\mathrm{D}]$, if there exist symmetric and positive-definite matrices P, Q, and R, such that the following

LMIs hold

$$\begin{aligned} P &> 0,\ Q>0,\ R>0 \qquad (5.4.2)\\ \Phi &= Sym\left\{ \begin{bmatrix} e_1 \\ he_3 \end{bmatrix}^T P \begin{bmatrix} e_s \\ e_1-e_2 \end{bmatrix} \right\} - \begin{bmatrix} e_1-e_2 \\ e_1+e_2-2e_3 \end{bmatrix}^T \begin{bmatrix} R & 0 \\ 0 & 3R \end{bmatrix} \\ &\quad \begin{bmatrix} e_1-e_2 \\ e_1+e_2-2e_3 \end{bmatrix} + e_1^T Q e_1 - e_2^T Q e_2 + h^2 e_s^T R e_s + e_1^T C_z^T C_z e_1 - \gamma^2 e_4^T e_4 \\ &< 0 \qquad (5.4.3) \end{aligned}$$

where $e_s = \big[A, A_d - \bar{B}KC_{\mathrm{y}}, 0, B_w - \bar{B}K\bar{Q}\big], e_1 = \big[I,0,0,0\big], e_2 = \big[0,I,0,0\big], e_3 = \big[0,0,I,0\big], e_4 = \big[0,0,0,I\big]$, then the system is stable and has H_∞ performance index, γ, against a non-zero disturbance for any delays smaller than h.

Proof: Choose an LKF candidate as follows:

$$\begin{aligned} V(x_t) &= \begin{bmatrix} x(t) \\ \int_{t-h}^{t} x(s)ds \end{bmatrix}^T P \begin{bmatrix} x(t) \\ \int_{t-h}^{t} x(s)ds \end{bmatrix} + \int_{t-h}^{t} x^T(s) Q x(s) ds \\ &\quad + h \int_{-h}^{0} \int_{t+\theta}^{t} \dot{x}^T(s) R \dot{x}(s) ds \end{aligned}$$

where P, Q, and R are symmetrical matrices. It can be found that the positive of the LKF, i.e. $(V(t) > 0)$, can be ensured if LMI (5.4.2) holds.

Calculating the derivative of LKF and using Wirtinger-based integral inequality [162] to estimate the yields

$$\begin{aligned} &\dot{V}(x_t) \\ &= 2 \begin{bmatrix} x(t) \\ \int_{t-h}^{t} x(s)ds \end{bmatrix}^T P \begin{bmatrix} \dot{x}(t) \\ x(t) - x(t-h) \end{bmatrix} \\ &\quad + x^T(t) Q x(t) - x^T(t-h) Q x(t-h) + h^2 \dot{x}^T(t) R \dot{x}(t) \\ &\quad - h \int_{t-h}^{t} \dot{x}^T(s) R \dot{x}(s) ds \qquad (5.4.4) \end{aligned}$$

$$
\begin{aligned}
\leq\ & 2\begin{bmatrix} x(t) \\ \int_{t-h}^{t} x(s)ds \end{bmatrix}^T P \begin{bmatrix} \dot{x}(t) \\ x(t)-x(t-h) \end{bmatrix} \\
& + x^T(t)Qx(t) - x^T(t-h)Qx(t-h) + h^2\dot{x}^T(t)R\dot{x}(t) \\
& - \begin{bmatrix} x(t)-x(t-h) \\ x(t)+x(t-h)-2\int_{t-h}^{t}\frac{x(s)}{h}ds \end{bmatrix}^T \begin{bmatrix} R & 0 \\ 0 & 3R \end{bmatrix} \\
& \begin{bmatrix} x(t)-x(t-h) \\ x(t)+x(t-h)-2\int_{t-h}^{t}\frac{x(s)}{h}ds \end{bmatrix}
\end{aligned} \tag{5.4.5}
$$

By defining the following notations

$$
\begin{aligned}
\zeta(t) &= \left[x(t),\ x(t-h),\ \int_{t-h}^{t}\frac{x(s)}{h}ds, \omega(t)\right] \\
\dot{x}(t) &= e_s\zeta(t),\ \ e_s = \left[A, A_d - \bar{B}KC_{\mathrm{y}}, 0, B_w - \bar{B}K\bar{Q}\right] \\
x(t) &= e_1\zeta(t),\ \ e_1 = \left[I,0,0,0\right] \\
x(t-h) &= e_2\zeta(t),\ \ e_2 = \left[0,I,0,0\right] \\
\int_{t-h}^{t}\frac{x(s)}{h}ds &= e_3\zeta(t),\ \ e_3 = \left[0,0,I,0\right] \\
\omega(t) &= e_4\zeta(t),\ \ e_4 = \left[0,0,0,I\right]
\end{aligned}
$$

it follows (5.4.5) and (5.4.3) that

$$
\dot{V}(x_t) + z^T(t)z(t) - \gamma^2\omega^T(t)\omega(t) \ < \ \zeta^T(t)\Phi\zeta(t) < 0 \tag{5.4.6}
$$

where Φ is defined in (5.4.3). Thus, based on (5.4.6) and $V(x_0) = 0$, $V(x_\infty) \geq 0$, the following holds

$$
\int_0^\infty \left[z^T(s)z(s) - \gamma^2\omega^T(s)\omega(s)\right]ds < V(x_0) - V(x_\infty) < 0 \tag{5.4.7}
$$

Therefore,

$$
\sqrt{\frac{\int_0^\infty z^T(s)z(s)ds}{\int_0^\infty \omega^T(s)\omega(s)ds}} \leq \gamma \tag{5.4.8}
$$

which means the the system is stable and has a H_∞ performance index, γ.

Based on above discussion, it can conclude that if LMIs (5.4.2) and (5.4.3) hold, the system is stable when without disturbance and has a H_∞ performance index, γ,

against a non-zero disturbance, for any delays smaller than h. This completes the proof.

Remark 5.1: Theorem 5.2 gives the relationships among the delay bound h, the H_∞ performance index γ, and the controller gains K. As discussed in [35], based on Theorem 5.2, for the fixed delay bound h and the controller gains K, one can find the minimal value of the performance index $\gamma_{\min}$, i.e., delay-dependent H_∞ performance analysis. That is, the minimal value $\gamma_{\min}$ is a function of the delay bound h and the controller gains K, as described as follows

$$\gamma_{\min} = f(h, K) = f(h, K_{\mathrm{P}}, K_{\mathrm{I}}, K_{\mathrm{D}}) \tag{5.4.9}$$

There are two methods can calculate the minimal value, $\gamma_{\min}$, for fixed delay bound h and designed controller gains K. One method is manually decreasing the value of γ step by step and then using the binary search technique to choose the $\gamma_{\min}$ [33]. Another method is introduced in [34] and used in this chapter because this method has higher efficiency. Figure 5.5 shows the simplified step for calculating $\gamma_{\min}$ as shown in below [34]:

- In the step 1, the search interval $[\gamma_{start}, \gamma_{end}]$ is initialized, in which γ_{start} is equal to 0. The γ_{end} is a big enough number and the accuracy coefficient γ_{ac} with sufficiently small value is chosen.
- In the step 2, the delay upper bound, h_{given}, is given, determine whether the system has a test value given as $\gamma_{test} = (\gamma_{start} + \gamma_{end})/2$ by checking the feasibility of Equation (5.4.3).
- In the step 3, the search interval is reduced to half by setting $\gamma_{end} = \gamma_{test}$ if Equation (5.4.3) is feasible or $\gamma_{start} = \gamma_{test}$ if Equation (5.4.3) is not feasible.
- In the step 4, the $\gamma_{\min}$ is obtained by letting $\gamma_{min} = \gamma_{test}$ when $|\gamma_{start} - \gamma_{end}| \leq \gamma_{ac}$.

5.4.2 Controller Gain Tuning Based on the PSO Algorithm

For a built communication channel, the time delay upper bound can be estimated from the transmitted data with time stamp. Then, for such delay bound, different

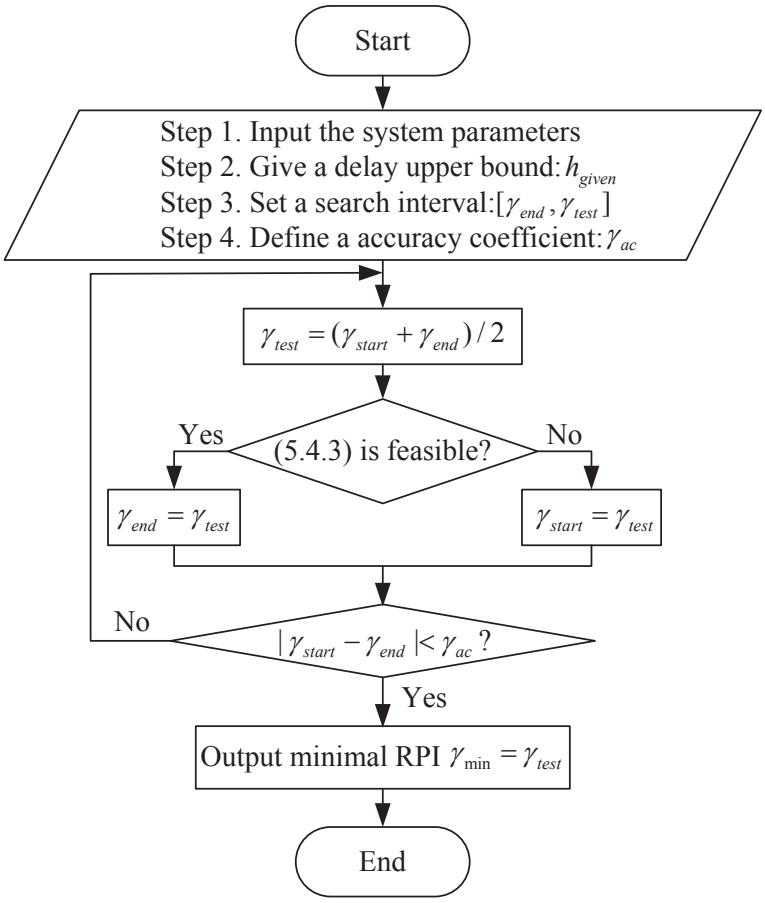

Figure 5.5: The simplified procedure for calculating γ_{min} of system with a given controller [34]

controller gains lead to different performance index calculated via (5.4.9). Thus, to provide the optimal robust performance for a preset time delay, the tuning of control gain can be transformed to the following optimisation problem:

$$\begin{aligned} Minimize: \quad & \gamma_{\min} = f(h, K_{\mathrm{P}}, K_{\mathrm{I}}, K_{\mathrm{D}}) \\ subject\ to: \quad & K_{Pmin} \leq K_P \leq K_{Pmax} \\ & K_{Imin} \leq K_I \leq K_{Imax} \\ & K_{Dmin} \leq K_D \leq K_{Dmax} \end{aligned} \tag{5.4.10}$$

The above optimisation problem can be solved by different optimisation algorithms. This chapter chooses the PSO searching algorithm as it is a meta-heuristic algorithm and has been widely used due to its decent performance in numerical op-

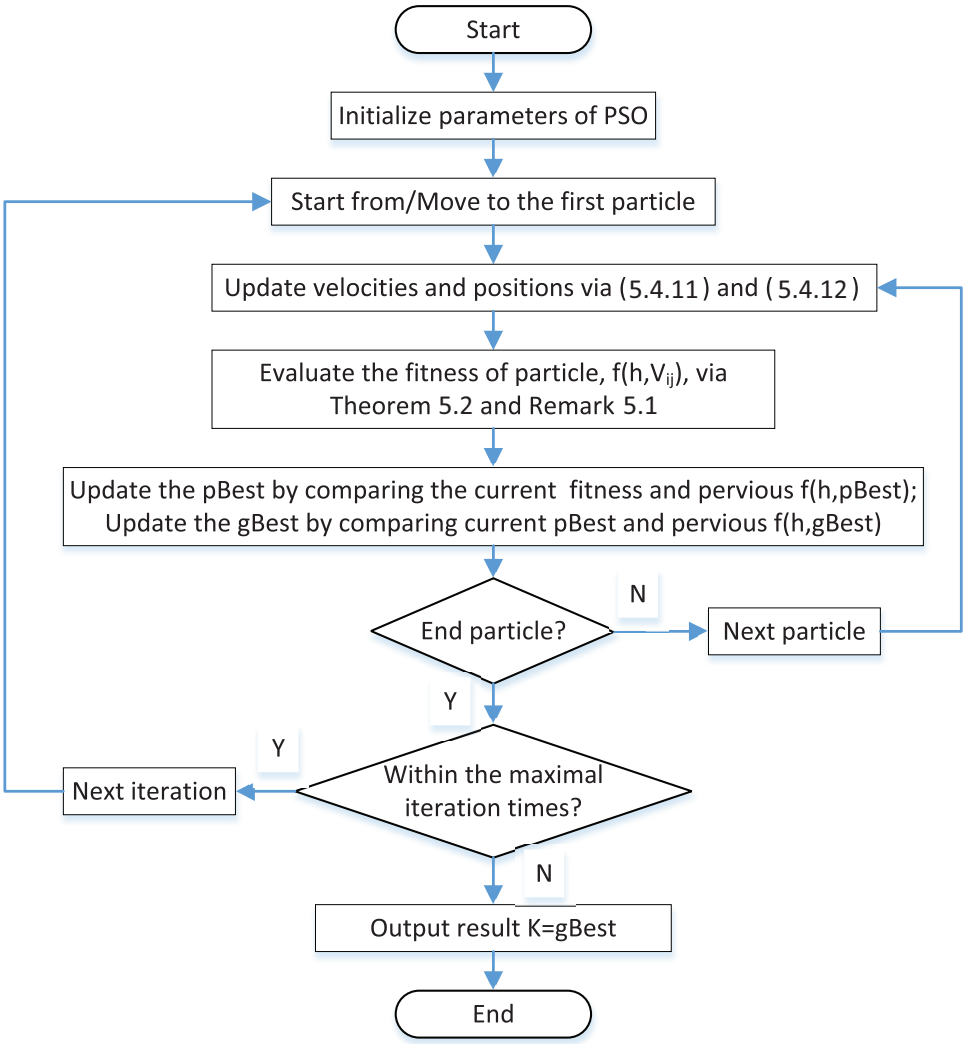

Figure 5.6: Simplified flowchart of the PID tuning.

timisation [163, 164]. The simplified flowchart of the PID gains tuning via the H_∞ performance index and the PSO algorithm is shown in Figure 5.6.

In Figure 5.6, for the initialization step, the following parameters should be given or calculated:

- Set the time delay upper bound, h.
- Set position bounds, $X_{\min}$ and $X_{\max}$, velocity bounds, $V_{\min}$ and $V_{\max}$ and the size of particles, N; and obtain random populations of the positions X_0 within $[X_{\min}, X_{\max}]$ (i.e., N sets of gains $K = [K_P \ K_I \ K_D]$) and the velocities V_0

within $[V_{\min}, V_{\max}]$.

- Set the maximal iteration times, $k_{\max}$, and the initial iteration times $i = 0$.
- Evaluate the fitness (i.e., H_∞ performance index, $\gamma_{\min}$ shown in (5.4.9)) for N particles, $f(h, X_{0,j}), j = 1, 2, \cdots, N$, via Theorem 5.2 and Remark 5.1.
- Find the best position for each particle, $pBest$, and the best position within all particles, $gBest$, i.e., set $f(h, pBest_j) = f(h, X_{0,j}), j = 1, 2, \cdots, N$ and $pBest = X_0$, and set $gBest = X_{o,k}, k \in \{1, 2, \cdots, N\}$ such that $f(h, gBest) = \min f(h, X_{0,j}), j = 1, 2, \cdots, N$.

For the step of updating the velocities and the positions, the following renewing conditions are applied:

$$V_{i+1} = \begin{cases} V_{\min}, & if \;\; V_{i+1} < V_{\min} \\ wV_i + c_1 \cdot \text{rand} \cdot (pBest - X_i) & \\ +c_2 \cdot \text{rand} \cdot (gBest - X_i), & if \;\; V_{i+1} \in [V_{\min}, V_{\max}] \\ V_{\max}, & if \;\; V_{i+1} > V_{\max} \end{cases} \tag{5.4.11}$$

where V_i and V_{i+1} are respectively the velocities in i-th and $(i+1)$-th iteration, w is the inertia weight, c_1 and c_2 are the acceleration constants, and rand is a value randomly generated between 0 and 1; and

$$X_{i+1} = \begin{cases} X_{\min}, & if \;\; X_{i+1} < X_{\min} \\ X_i + V_{i+1}, & if \;\; X_{i+1} \in [X_{\min}, X_{\max}] \\ X_{\max}, & if \;\; X_{i+1} > X_{\max} \end{cases} \tag{5.4.12}$$

where X_i and X_{i+1} are respectively the positions in i-th and $(i+1)$-th iteration.

5.5 Case Studies

Case studies are carried out based on the smart power grid operating in the island mode, shown in Figure 5.1, which consists of traditional micro generation, smart homes with controllable loads, a PEV station, and a wind farm. The micro generation equips with a non-heat turbine with the capacity of 800MW, and its GRC

is assumed to be ± 0.1 pu/min [41]. In the smart homes, there are 200 air conditioners that can provide the DDC service. Assume that there are total 60 PEVs in the considered area, and the ones parking in the PEV station or at smart homes can participate the frequency support service. The wind farm consists 88 variable-speed wind turbines and every turbine's capacity is around 2.25MW. The total wind farm output power is 198MW (about 20% of total output power). Assume that all wind turbines are identical and the cut-in wind speed, the rated wind speed, and the furling speed are 5m/s, 12m/s, and 25m/s, respectively [43]. The related parameters are listed in Table 5.1 and recalled from literatures [53, 65, 79]. All corresponding simulations are carried out by using Matlab 7.10.0 (R2011a) running on a PC.

Table 5.1: Parameters of test smart power grid

Parameter	Value	Parameter	Value	Parameter	Value
T_g (s)	0.08	D_{ac}	0.03	r_{bs} (Ω)	0.013
T_t (s)	0.38	EER	3.75	J_g $(kg \cdot m^2)$	10
R $(Hzpu)$	2.5	k_b (kW/Hz)	11.75	J_r $(kg \cdot m^2)$	90000
$2H$ (pus)	0.1667	T_b (ms)	50	k_s (N/m)	8×10^6
D (pu/Hz)	0.0083	$I^0_{bes}(kA)$	4.426	D_s (s^{-1})	8×10^4
β (pu/Hz)	0.55	$K_{bes}(kV/puMW)$	100	N_g	24.6
c_p (J/K)	1.01	$T_{bes}(s)$	0.026	R_{wind} (m)	14.5
m (pu/s)	0.35	$\alpha(^\circ)$	15	τ_θ (s)	0.15
K_{DDC}	10	r_{bt} (Ω)	0.0167	τ_T (s)	0.1

5.5.1 Robust Controller Design

At first, the robust LFC is designed based on the simplified state-space model developed in Section 5.2 and the robust PID controller design method presented in Section 5.4.

In order to simplify the design procedure, the time delays in different loops in the model are assumed to be identical and here it is preset to be 0.2s. And, the related initial parameters of the PSO mentioned in Section 5.4 are given as: position

bounds, $X_{\max} = 1$, $X_{\min} = -1$ (i.e., $\{K_P, K_I, K_D\} \in [-1, 1]$); velocity bounds, $V_{\max} = 1$, $V_{\min} = -1$; population size $N = 50$; maximum iteration times $k_{\max} = 50$ inertia weight, $w = 0.4$, acceleration constants, $c_1 = c_2 = 2$. By following the controller gains tuning method shown in Figure 5.6, the following PID controller can be obtained:

$$K = [-0.34438 \quad -0.07727 \quad -0.31065] \tag{5.5.1}$$

5.5.2 Contribution of the DDC, BESS, and PEV to Frequency Regulation

How the additionally connected DDC, BESS, and PEV contribute to improve the frequency control performance is shown in this part.

When the wind power is not connected in the power system, the frequency deviations for LFC with and without DDC, BESS, and PEV are shown in Figure 5.7. Compared with traditional LFC, the LFC with DDC, BESS, and PEV can provide better performance and shorter settling time. The DDC, BESS, and PEV participating in frequency regulation can improve the power system stability. Moreover, although the time delays of 0.2s are included in the control loops during the simulation, the frequency deviation is quickly convergent to schedule values, which shows the effectiveness of the proposed PID controller.

For the case where the DDC, BESS, and PEV do not participate in the frequency regulation, the responds of the frequency deviation for the system connected wind turbines with different output power (0.09 pu and 0.12 pu) are given in Figure 5.8. From these results, the frequency deviation can recover to small fluctuation range when the low penetration of wind power injects in the power system (0.09 pu); While the wind farm output power becomes to 0.12 pu, the frequency regulation is no longer in stable. It can be concluded that the traditional LFC scheme can only maintain the power system in steady state for the case of small intermittent wind power injection.

When the connected wind power is 0.198 pu, the same cases which are used in the above part are shown in Figure 5.9. It is easily found that, compared with

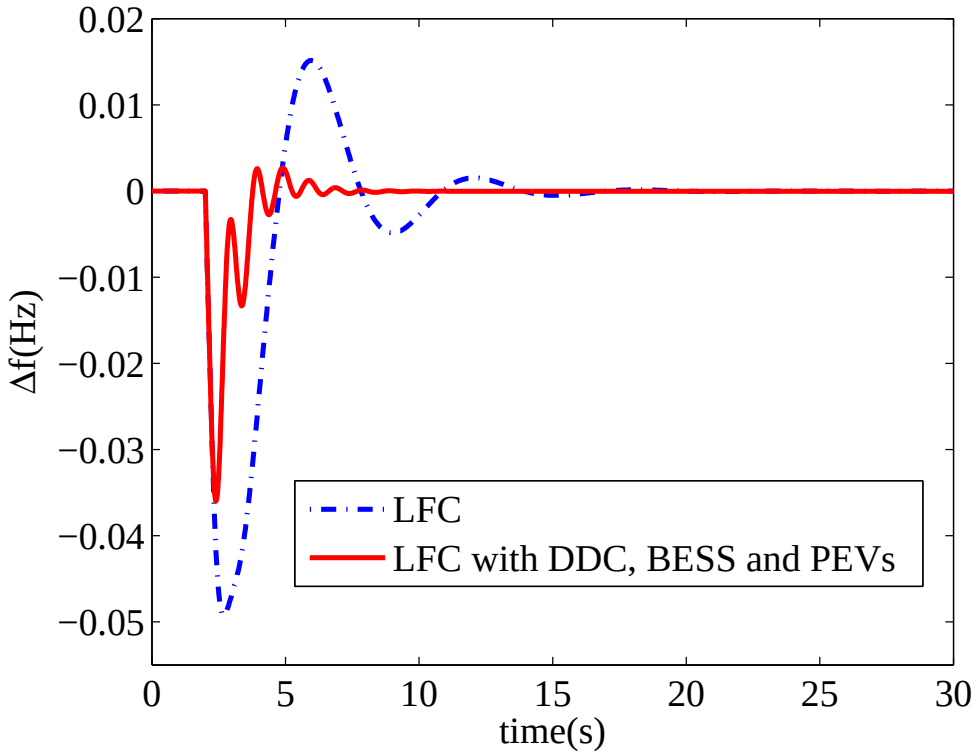

Figure 5.7: Frequency deviation in the LFC model without wind power energy

the case with only LFC, the case with DDC, BESS, and PEV can provide better dynamic performances, shorter settling time and smaller overshoot and effectively solved problem caused by the intermittent wind power energy, which shows that the introducing of the DDC, BESS, and PEVs enhances the transient response of frequency regulation and improves the frequency control performance.

The LFC scheme with different capacities of DDC, BESS, and PEV are also tested. Figures. 5.10 to 5.12 show the responds of the frequency deviation for those cases. From results, it can be found that the DDC/BESS with bigger capacity or more PEVs participating in frequency regulation can recover the frequency deviation in stable quicker and fluctuation smaller.

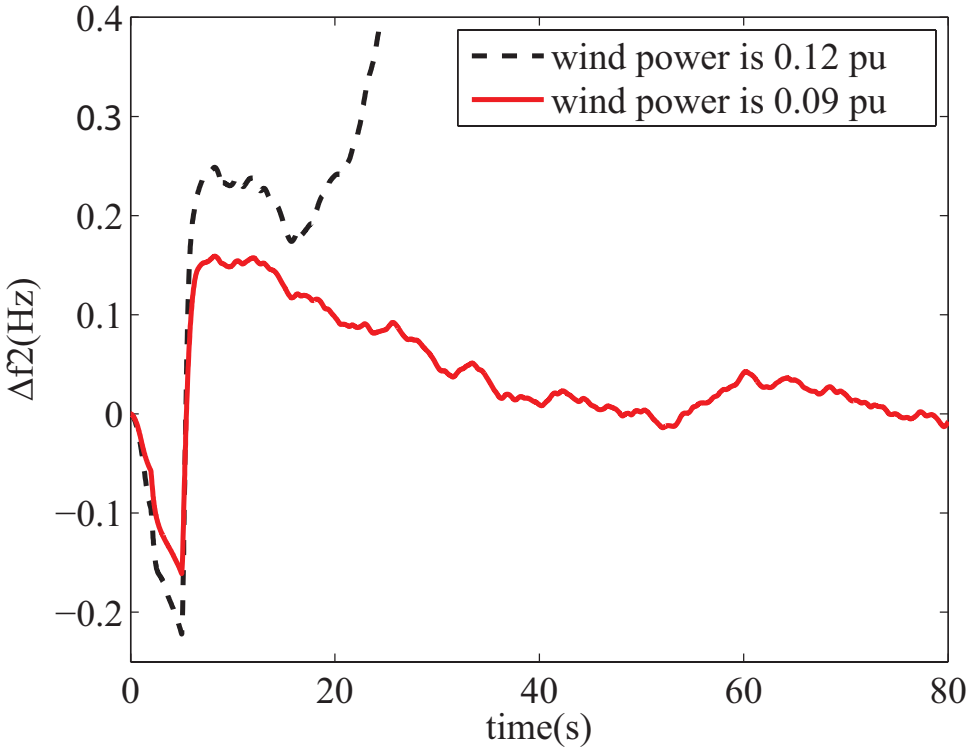

Figure 5.8: Frequency deviation in the LFC model when different value of wind power energy in the model

5.5.3 Robustness Against to Load Disturbances

The most important aim of the frequency regulation is to minimise the frequency derivation of the power system in the case where load disturbance occurs. And the time delays, if considered, also affect the frequency performance. Such disturbance rejection capability for different delays is described by the delay-dependent H_∞ performance index defined in Section 5.4.

Assume time delays in different control loops are identical. By using the method given in Section 5.4, the performance index, γ_{min}, of close-loop LFC scheme are calculated and some typical values are listed in Table. 5.2, where Cases A, B, and C respectively indicate the LFC with only DDC, with DDC and BESS, with DDC, BESS, and PEV. The γ_{min} is defined by Equation (5.4.8). The results show that the value of the performance index increases with the increasing of the time delay. The smaller performance index, γ_{min}, indicates that the closed-loop LFC scheme has

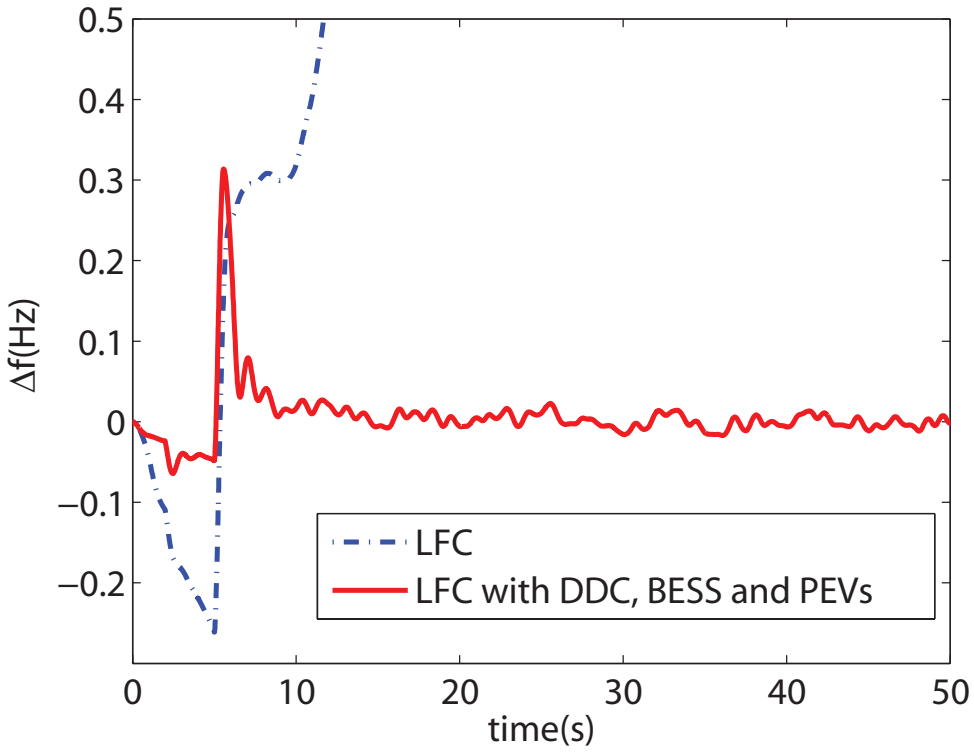

Figure 5.9: Frequency deviation in LFC and LFC with DDC, BESS and PEVs model

Table 5.2: γ_{min} for different time delays

Case A		Case B		Case C	
τ (s)	γ_{min}	τ (s)	γ_{min}	τ (s)	γ_{min}
0.001	1.4820	0.001	1.4820	0.001	1.4820
0.05	1.3470	0.05	1.3470	0.05	1.3470
0.10	1.3250	0.10	1.3240	0.10	1.3220
0.15	1.6240	0.15	1.6240	0.15	1.6240
0.20	2.4850	0.20	2.4810	0.20	2.4800
0.25	5.8870	0.25	5.6390	0.25	5.6380

better disturbance rejection capability, which means that the smart power grid can accept more load disturbances, such as intermittent wind power energy. Thus, the injection of the DDC, BESS, and PEV indeed improves the capability of introducing intermittent wind power energy.

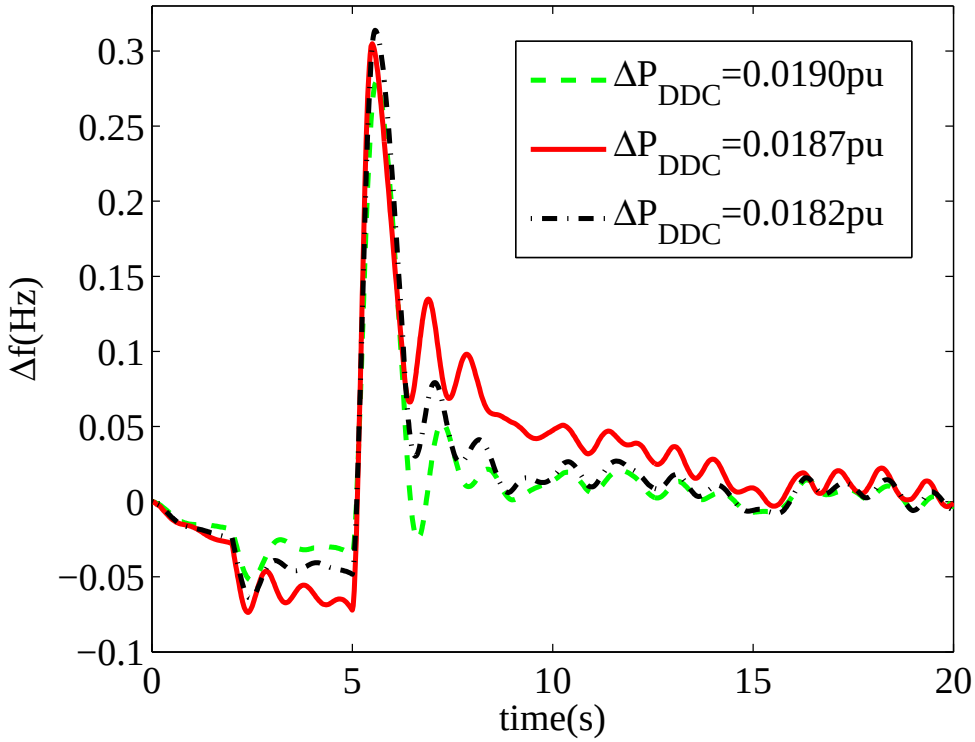

Figure 5.10: Frequency deviation from LFC with BESS, PEVs and different sizes of DDC model

5.5.4 Robustness Against to Parameters Uncertainties

The PID controller gains aforementioned are tuned for the nominal system parameters. However, in reality, there exist uncertainties in the system parameters due to measurement errors, operation condition change, ect., as well in the controller gains during the implementation procedure. Therefore, the robustness against to those parameter uncertainties also is tested. To indicate the dynamic performances, the ITAE and ITSE introduced in Chapter 4 are calculated by Equations (4.4.3) and (4.4.4).

For three cases defined in previous subsection, uncertainties in system parameters (within $\pm 20\%$) are simulated, and some typical values of the ITAE and the ITSE are given in Table 5.3. And, Figure 5.13 shows the frequency deviation of LFC with DDC, BESS, and PEV under system parameters in normal value, increasing, and decreasing 20%, respectively.

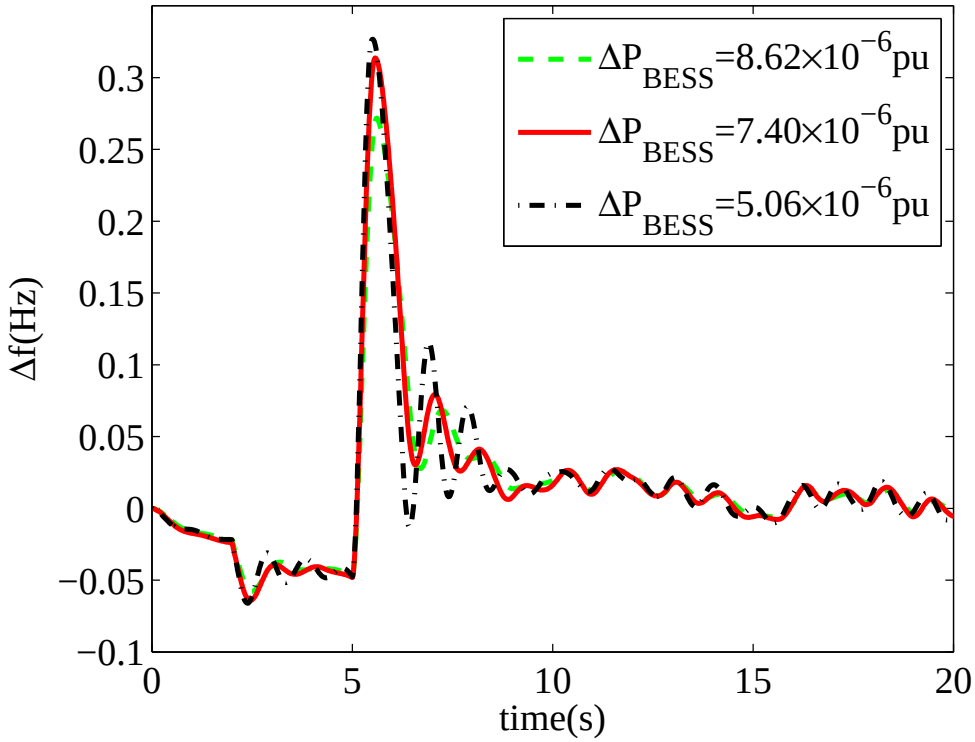

Figure 5.11: Frequency deviation from LFC with DDC, PEVs and different sizes of BESS model

From the results, it can be found that the designed PID controller stabilises the closed-loop LFC system even the uncertainties exist, which shows the robustness of the controller against to parameter uncertainties. Meanwhile, it can be found that the introducing of DDC, BESS, and PEV can stabilise the system more quickly with smaller fluctuation and provide better performance indexes.

5.5.5 Robustness Against to Time Delays

The PID controller gains given in Section 5.5.1 are tuned by setting all delays to be identical. However, in reality, there usually exist different delays for different loops. Assume that the time delays in LFC and BESS loops are same, and the ones in DDC and PEV loops are also same, i.e., $\bar{\tau}_1 = \tau_1 = \tau_2$ and $\bar{\tau}_2 = \tau_3 = \tau_4$. This part calculates the delay margins by using the method given in Section 5.3.

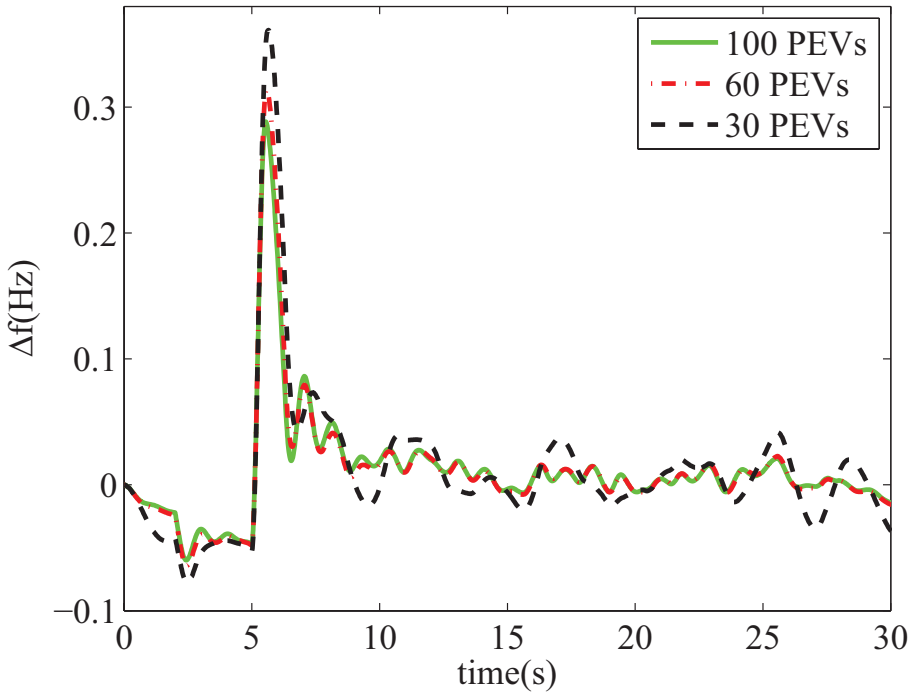

Figure 5.12: Frequency deviation from LFC with DDC, BESS and different number of PEVs model

Table 5.3: Dynamic performance indices, ITAE and ITSE

Parameter	Case A		Case B		Case C	
change(%)	ITAE	ITSE	ITAE	ITSE	ITAE	ITSE
+20	51.66	0.9890	35.43	0.5627	23.10	0.3215
+15	49.49	0.9085	34.72	0.5292	22.04	0.2933
+10	47.29	0.8325	33.86	0.4949	21.00	0.2667
+5	45.02	0.7591	32.89	0.4600	19.97	0.2415
0	42.74	0.6886	31.86	0.4256	18.96	0.2178
-5	40.54	0.6223	30.75	0.3917	17.99	0.1956
-10	38.40	0.5595	29.57	0.3585	17.05	0.1750
-15	36.31	0.4998	27.32	0.3261	16.12	0.1561
-20	34.26	0.4434	27.01	0.2947	15.21	0.1391

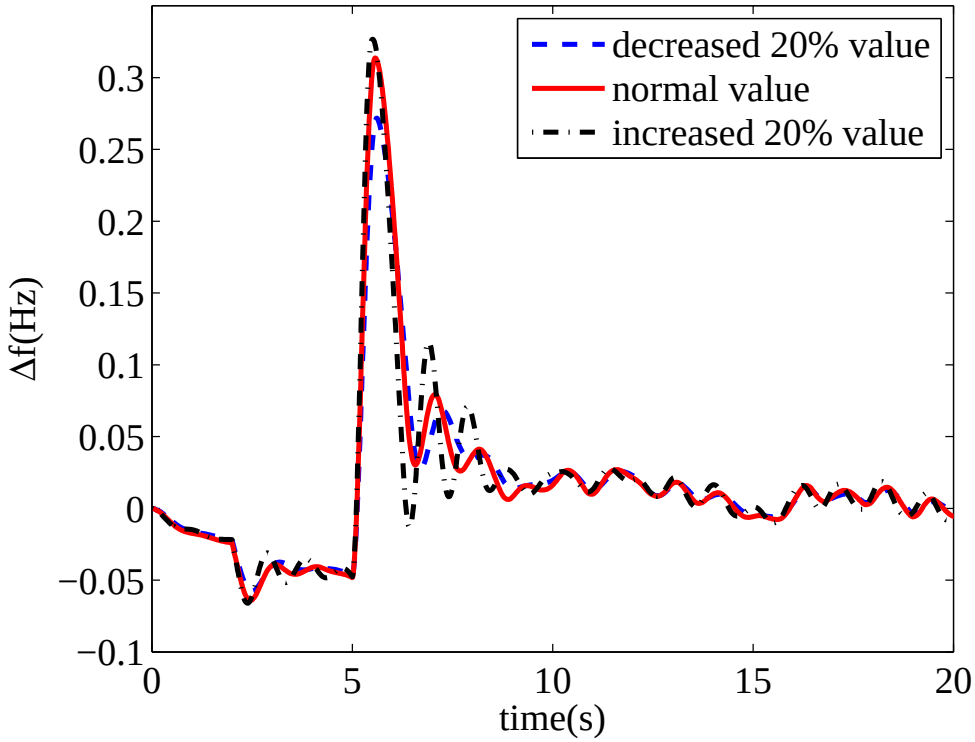

Figure 5.13: Frequency deviation of LFC with DDC, BESS and PEV under system parameters variation

The delay margins for the case of the LFC with DDC, BESS, and PEV are listed in Table 5.4, in which the delay margins obtained by using simulation method are also given. It is found that the calculated delay margins are smaller than simulated delay margins. Because the calculation condition for calculation method is sufficient condition, it has conservative property, which causes the calculated delay margins are smaller than simulation results. However, these two kinds of results are very similar, which shows that the method in Section 5.3 is feasible to calculated multiple delay margins.

5.6 Conclusion

In this chapter, the contribution of the DDC, the BESS and the PEV for frequency regulation has been investigated for a smart power grid operating in isolated mode

Table 5.4: The delay margins in LFC with DDC, BESS and PEV model

$\bar{\tau}_1$ (s)	calculated $\bar{\tau}_2$ (s)	$simulated\bar{\tau}_2$ (s)
0	1.20	1.39
0.05	1.13	1.40
0.10	1.14	1.42
0.15	1.11	1.44
0.20	1.31	1.45
0.25	1.30	1.46

with intermittent wind power injections. Firstly, the smart power grid, including the BESS, the DDC, the PEVs, and the wind farm, is modelled as a single area LFC system, and the state-space model considering the communication time delays in the control loops has been constructed. Secondly, the delay-dependent stability analysis has been developed by using the Lyapunov theory. Finally, gains of PID-type controllers are tuned based on the H_∞ performance analysis and the PSO searching algorithm. Case studies based on the single area power system with the DDC, the BESS and the PEV have been carried out. Analysis and simulation results have demonstrated that the LFC with the DDC, the BESS, and the PEV can provide better performance compared with other cases, which means the combined DDC, BESS, and PEVs can effectively alleviate the power unbalance caused by intermittent wind power. Moreover, simulation results have also demonstrated the effectiveness of the proposed PID controller, including the robustness against to the load disturbances, the parameter uncertainties, and multiple time delays. In addition, delay margins calculated based on the developed stability analysis method and the ones obtained via trial-and-error simulation method are very closed to each other, which shows that the proposed delay-dependent stability analysis method is effective and can be used to theoretically investigate the robustness of the controller to multiple time delays.

Chapter 6

Coordinated Frequency Regulation by Demand Side Response and Variable Speed Wind Turbines

6.1 Introduction

Considering the fossil fuel price increasing and environment pressure, the intermittent renewable energy has been developed rapidly in recent years, such as wind energy and solar energy. With the low penetration of wind power penetration in the power system, i.e., less than 20% of total capacity, thermal plants with abundant regulating capability can balance the active power of the power system between the generation side and the demand side. However, when the penetration of wind power is increased, the frequency stability will be progressively influenced due to the uncertainty of wind power and insufficient thermal power reserves [165]. Moreover, it may even cause one situation that the total power produced by wind power generators and traditional generators is less than the demand load required. Sometimes, the demand side load suddenly increased to require more power exceeds total produced power. For example, the demand loads required more electricity power in the summer because the number of using air conditioners' customers are increased. Therefore, balancing the active power between the generation side and the demand

side is a challenging problem when the penetration of wind power level increases to a certain level, which is more than 20% of the total capacity of the power system.

Many methods can be used to solve this imbalance problem caused by intermittent wind power. Traditionally, the spinning generation reserves with enough capacity can be used to meet this task. However, this solution makes substantial backup idle for most hours within a year. Thus it will increase the operation cost and reduces the advantages of wind power [11]. An alternative the grid-scale energy storage system, such as BESS, is another important way to keep the active power balance by charging or discharging based on the frequency deviation [109, 151]. For example, the BESS equipped with a controller based on area control error (ACE) successfully achieves the frequency regulation [53]. Disadvantages of the grid scale BESS are they require expensive auxiliary equipment and high installation and operation cost. Therefore, the BESS method is not a feasible solution due to the high cost.

With the increasing penetration of wind power, variable-speed wind turbines (VSWTs) are required to participate in frequency regulation via augmented additional controller, such as IC, PAC and RSC [24, 169]. When the grid frequency changes, not only the synchronous generators will response to this change, but also wind turbines will quickly change their output active power to follow the disturbance change [166]. The IC method used for frequency regulation can transiently release the large kinetic energy stored in the rotating mass of wind turbine to emulate inertia of wind generators for providing frequency regulation [24, 166, 167]. The PAC and RSC used in the VSWT to participate in the frequency control for an extended period are investigated [165, 166, 168]. In recent years, although IC, PAC and RSC have investigated, coordination between them is rarely considered [165, 166]. In this chapter, the VSWTs participating in frequency regulation via coordination of IC, RSC and PAC control methods in different wind speed in LFC system.

In recent years, the demand side response (DSR), which can control or shift the controllable loads, has become a promising smart grid technology for accommodating intermittent renewable generations [25, 43]. It also can solve the problem, in which the total produced power is less than the demand loads required because the

wind speed is intermittent. In recent year, the PEVs which reduce the greenhouse gas emission have drawn increasing attention in the transportation electrification. Considering battery charging/discharging dynamics, a battery of PEVs is proposed to contribute frequency regulation. Considering PEVs are parking at homes or workplaces at most time of a day, batteries of PEVs can be used as distributed energy storage to provide support of the grid operation, which is called vehicle-to-grid (V2G) technology [133]. V2G service requires a number of aggregated small batteries of the PEVs as an equivalent large scale BESS and then provides frequency support of the smart grid via controlling the charging/discharging of these batteries [60,65,67]. Usage of PEVs to suppress the fluctuation in renewable energy sources have been investigated in lots of literature [60,67]. The dynamic demand control (DDC) method, which controls the TCAs, can self-adjust the usage of appliances based on frequency deviation of power system [25]. Kowli and Meyn [114] investigate demand side load controlled by the electricity industry, which can provide a potential solution for the reliable integration of wind generation resources.

This chapter investigates combination wind turbines and DSR participating in frequency regulation in the power system to solve imbalance problem caused by high penetration of intermittent wind power. Model of LFC with VSWTs and DSR participating in frequency regulation is constructed. Combination wind turbines and DSR participating in frequency regulation to deal with high wind power penetration and the DSR to provide balance power when the traditional and wind power generation produced power can not provide enough power for demand load. Finally, wind turbines with different capacity of DSR supporting grid frequency is tested. This combination method has several advantages over other resources used for energy balancing and ancillary services, including relatively fast response time, providing enough capacity to adopt the high penetration of wind power and solving load suddenly increasing problem.

The rest of this chapter is organised as follows. The dynamic model of smart grid for frequency regulation is provided in Section 6.2. In Section 6.3, it introduces wind plant frequency regulation capability with PAC and RSC in conjunction with IC. Section 6.4 shows case studies based on the model of LFC with wind farm and

DSR. Section 6.5 is a conclusion.

6.2 Dynamic Model of Smart Grid for Frequency Regulation

The model LFC with a wind farm and DSR is investigated, which wind turbines and DSR participates in frequency regulation. The structure of the frequency regulation for the smart grid can be given as Figure 6.1.

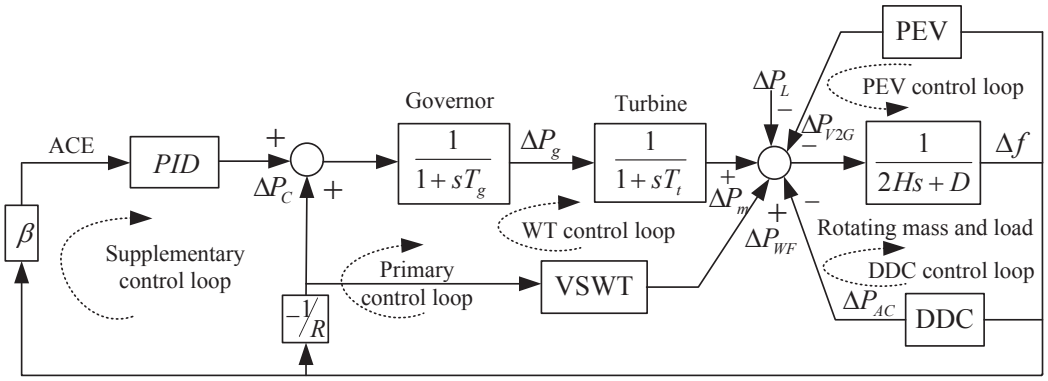

Figure 6.1: The structure of the frequency regulation of power system

From Figure 6.1, the relationship between the energy imbalance and the corresponding frequency deviation can be given as follows:

$$\begin{aligned}&\Delta P_m(s) + \Delta P_{wind}(s) - \Delta P_L(s) - \Delta P_{AC}(s) - \Delta P_{V2G}(s)\\&= 2Hs\Delta f(s) + D\Delta f(s)\end{aligned} \tag{6.2.1}$$

where ΔP_m is the generator mechanical output, ΔP_{wind} is the deviation of the wind power energy from the wind farm, ΔP_{AC} is the power deviation from the DDC based on air conditioners, ΔP_{V2G} is the power deviation from the PEVs, ΔP_L is the load change, $2H$ is the equivalent inertia constant, D is the equivalent load-damping coefficient, and Δf is the frequency deviation of the smart grid.

As shown in Figure 6.1, there are five control loops taking part in the frequency regulation, including two generator-side loops (traditional primary and supplementary loops), wind turbine control loop and two demand-side loops (PEVs and DDC

loops). $K(s)$ is the PID type controller used in LFC scheme. The frequency deviation is an input signal used in PEVs, DDC and wind turbines to participating in frequency regulation. The integral controller is used to control DDC scheme. PEVs in the power system are in charging state and constraint of battery SOC. The wind turbines are controlled by RSC, PAC and IC. The model of PEVs and the model of DDC based on air conditioners introduced in Chapter 3 are used, while the VSWT model described in Chapter 5 is used.

6.3 Control Design of wind turbine supported in frequency regulation

The IC, RSC and PAC control methods are introduced in this section, respectively. These control methods are related the grid frequency. IC is used for short-time grid frequency restoration and RSC and PAC are used for long-time grid frequency restoration.

6.3.1 Inertial Control for Short-time Grid Frequency Restoration

For a synchronous generator, the kinetic energy is released automatically from the rotating mass when the frequency drops. In the VSWT, the IC utilises the kinetic energy of wind turbine's rotor during grid frequency excursion [166]. The kinetic energy stored in the wind generator as shown in (6.3.1).

$$E_k = \frac{1}{2} J \omega_r^2 \tag{6.3.1}$$

where J is the equivalent inertia of wind power generators, including rotors of wind turbine and generator.

The power from the rotating mass is expressed wind power generators, including rotors of wind turbine and generator, as follows:

$$\Delta P_{ic} = \frac{dE_k}{dt} = J \omega_r \frac{d\omega_r}{dt} \tag{6.3.2}$$

Equation (6.3.2) shows that the extracted power is related to J, ω_r and $d\omega_r/dt$. To couple the grid frequency change, $d\omega_r/dt$ is replaced by the grid frequency change df_{sys}/dt for the inertial control loop. So the response of the inertial controller can be designed as:

$$\Delta P_{ic} = K_{ic}\frac{df_{sys}}{dt} \tag{6.3.3}$$

where control coefficient K_{ic} replaces the coefficient $J\omega_r$. Figure 6.2 shows the inertial control schematic for a VSWT, in which the P_0, ΔP_{ic} and P_{ref} are initial operating power point, per-unit response of the inertial controller and reference active power for the VSWT, respectively.

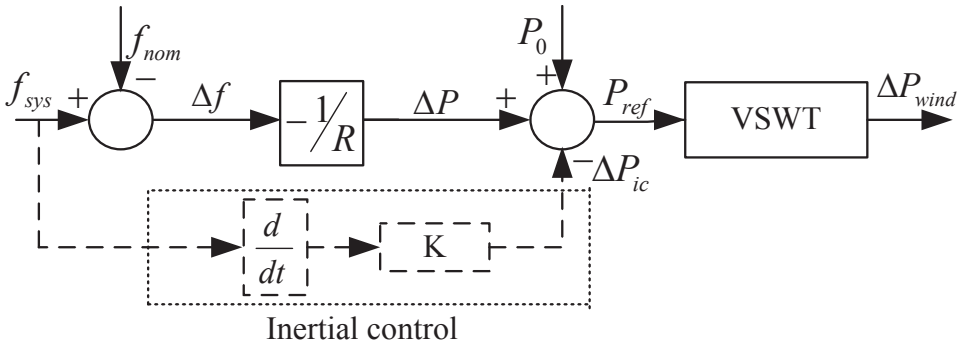

Figure 6.2: Inertial control schematic for VSWT

6.3.2 Rotor Speed Control for Grid-frequency Regulation [165]

The rotor speed control is based on the frequency drop characteristic of the VSWT, as shown in Figure 6.3. The controller adjusts the active power output in proportion to the frequency deviation with the ratio of $-\frac{1}{R}$ as following:

$$\Delta P = -\frac{1}{R}(f_{sys} - f_{ref}) = -\frac{1}{R}\Delta f \tag{6.3.4}$$

where f_{ref} is the nominal frequency and f_{sys} is the measured system frequency.

Figure 6.4 shows the RSC scheme schematic. The wind power $P_{e,ref}$ is the initial wind plant output power and is held constant during the grid frequency restoration period. ΔP from Equ. (6.3.4) uses its droop characteristic during a drop in the frequency.

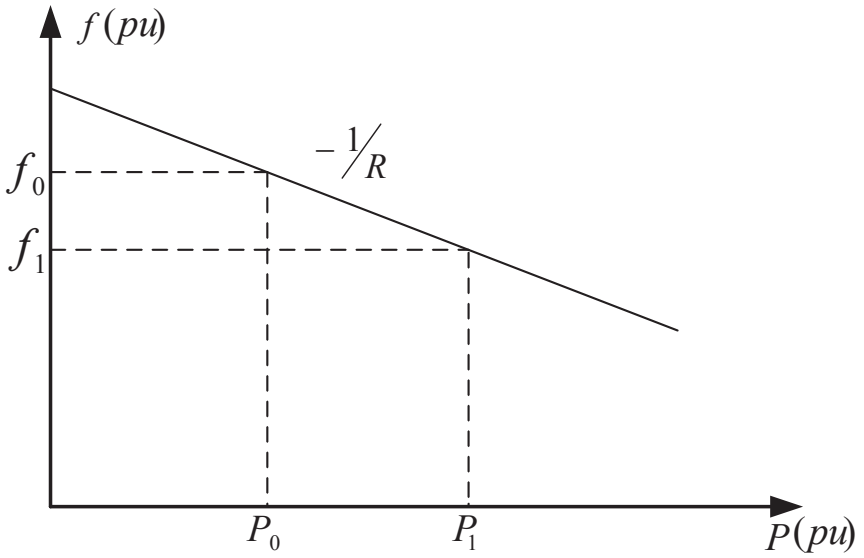

Figure 6.3: The variable speed wind turbine droop characteristic [165]

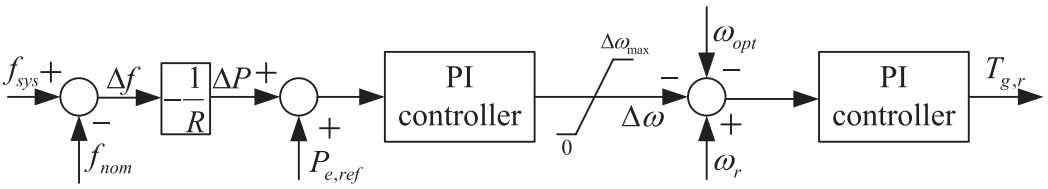

Figure 6.4: Rotor speed control schematic for VSWT

The relationship of mechanical power P_m, wind speed v and rotor speed ω_r is described in Figure 6.5. There are two 90% sub-optimal curves, under-speed curve (left curve) and over-speed curve (right curve). The left curve is unstable and undesirable which explained in [166]. So the 'sub-optimal curve' represents the right curve used in this chapter.

When the rotor speed control is used in the wind turbine, the wind turbine initially operates at point A which generates the mechanical power shown in Figure 6.5. When the grid frequency drops, the rotor speed reduces to point D and ΔP increases the electromagnetic power because of imbalance between the mechanical and electromagnetic power. The point C is the MPPT point, so the rotor speed can not be smaller than point C.

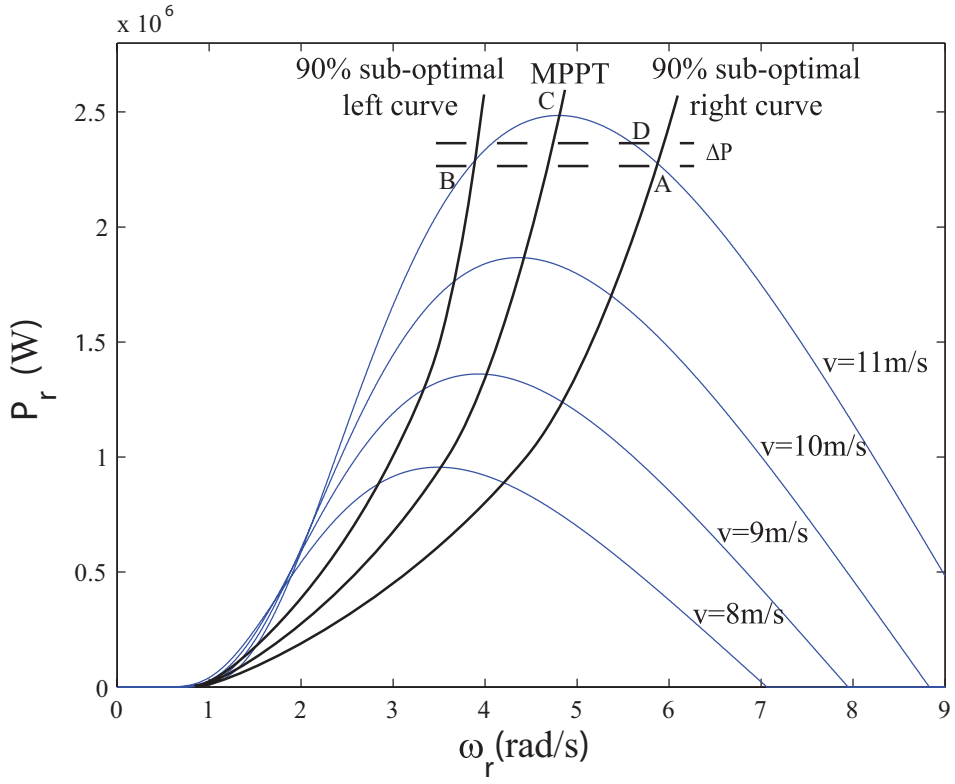

Figure 6.5: Sub-optimal operation

6.3.3 Pitch Angle Control for Grid-frequency Regulation

PAC used for the wind turbine is designed much like the governor control of a synchronous machine, which prevents the rotor speed from exceeding the nominal value [165].

Figure 6.6 shows the schematic of PAC and the input signal is Δf. The ΔP is obtained from Equation (6.3.4). By using the PAC method, the wind farm provides either higher or lower power to share in the frequency restoration strategy in the long term.

6.3.4 Coordinated Control Strategies

Figure 6.7 shows the wind turbine power output curve in different wind speed. In region 1, the wind turbine blades cannot rotate at very low wind speeds. While the wind turbine will start to rotate and generate the maximum electrical power from

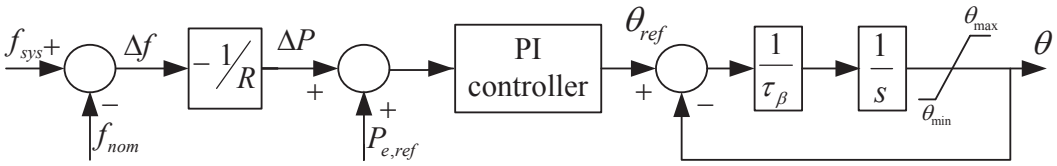

Figure 6.6: Pitch angle control schematic for VSWT [165]

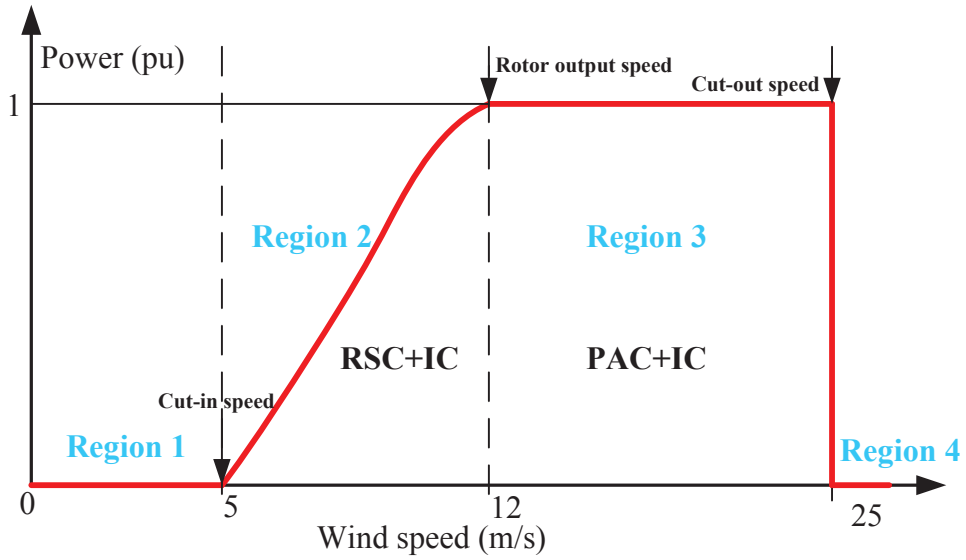

Figure 6.7: The wind turbine power output curve with different wind speed

the wind when the wind speed rises in region 2. In region 3, as the power generated by the wind turbine is higher than its rated output power, the wind turbine starts to regulate the pitch angle to limit the electrical power to its rated value. Finally, at the cut-out wind speed, a braking system is used to stop the wind turbine for the sake of protecting the wind turbine in region 4. In this chapter, it presents a novel frequency regulation by VSWT to coordinate IC, RSC and PAC under low or high wind mode.

When the wind speed is in 5 m/s to 12 m/s (in region 2), the output power can be achieved following the trajectory of the 90% sub-optimal operation curve as shown in Figure 6.5. The PAC do not need to be activated to down-regulate the wind turbine [165]. So the RSC is used to control wind turbine and the pitch angle is equal to 0. When the frequency drops, the RSC will control wind turbine to produce more active output power.

When the wind speed is in the range between 12 m/s and 25 m/s (in region 3), over-speed is impossible because the MPPT speed has been over maximum rotor speed. Therefore PAC is the only way to down-regulate the wind turbine. When the wind speed is above the rated, the pitch angle is increased to limit the mechanical power of a wind turbine to its rated value [166]. However, if the power grid requires less power than the rated, the pitch angle is further increased to satisfy the grid side power demand in order to minimise the frequency deviation of the power system.

The IC can support frequency control in transient. So the IC combined RSC or PAC to control wind turbines in different wind speed in this chapter. The IC combined RSC or PAC can maintain grid frequency in stable more quickly with smaller fluctuation.

6.4 Case Studies

The proposed wind turbine controllers test on a single area LFC scheme which includes a wind farm, aggregated DDC and PEVs. The micro generation equips with a non-heat turbine with the capacity of 800MW. In the smart homes, there are total 200 air conditioners that can provide the DDC service. Assume that there are total 100 PEVs in the considered area, and the ones parking in the PEV station or at smart homes can participate the frequency support service. The wind turbine's capacity is around 2.25 MW. Assume that all wind turbines are identical and the cut-in wind speed, the rated wind speed, and the cut-out speed are 5 m/s, 12 m/s, and 25 m/s, respectively. [43]. The related parameters are listed in Table 6.1 and recalled from literature [65, 79]. All corresponding simulations are carried out by using Matlab/Simulink. The following four cases are studied.

6.4.1 Low Penetration of Wind Power in Smart Grid

In this case, the wind farm consists 100 wind turbines and the total wind farm output power is 225MW (about 21.95% of total output power). The low wind speed and high wind speed are tested by RSC and PAC, respectively. Firstly, the constant low wind speed (8.5 m/s) is used in VSWT model. When 0.05 pu disturbance load

Table 6.1: Parameters of test smart power grid

Parameter	Value	Parameter	Value	Parameter	Value
T_g (s)	0.08	$m\ (pu/s)$	0.35	$J_r\ (kg \cdot m^2)$	90000
T_t (s)	0.3	K_{DDC}	10	$k_s\ (N/m)$	8×10^6
$R\ (Hzpu)$	2.5	$D_{ac}\ (kW/Hz)$	0.03	$D_s\ (s^{-1})$	8×10^4
$2H\ (pus)$	0.1667	EER	3.75	N_g	24.6
$D\ (pu/Hz)$	0.015	$k_b\ (kW/Hz)$	11.75	R_{wind} (m)	14.5
$\beta\ (pu/Hz)$	0.55	T_b (ms)	50	τ_θ (s)	0.15
$c_p\ (J/K)$	1.01	$J_g\ (kg \cdot m^2)$	10	τ_T (s)	0.1

occurs at $t = 5s$, grid frequency deviation, wind farm output active power, pitch angle and wind turbine rotor speed are compared for proposed control scheme in Figure 6.8. The wind turbine is initially operating at an over-speed point and the wind farm output is increased by reducing the rotor speed. The rotor speed is significantly reduced when the wind turbine controlled by only RSC. After combined IC, the short-term frequency is optimised. When the DSR used in the system which wind turbines participate in frequency regulation by RSC, the power system does not need more wind power energy. In Figure 6.8 (a), the fluctuation of frequency regulation is smallest and response time is fastest by the combined RSC and DSR method. However, the peak value of wind farm output power is smaller than that by RSC or RSC combined IC methods because DSR can handle controllable loads and PEVs to balance the fluctuation of grid frequency caused by the intermittent of wind power. So the rotor speed in this method changes smaller than other two control methods. Combined RSC and DSR method improves the system stability and response time under low wind speed. In this case, the PAC is invalid as shown in Figure 6.8 (c) because the rotor speed control could satisfy all the frequency support for the system.

Figure 6.9 also shows the same four physical variables when wind speed is constant high wind speed (18 m/s). When the wind speed is high, the PAC method controls the wind turbines. Similar results can be obtained from the simulations in constant low wind speed. The rotor speed is maintained the maximum value in the

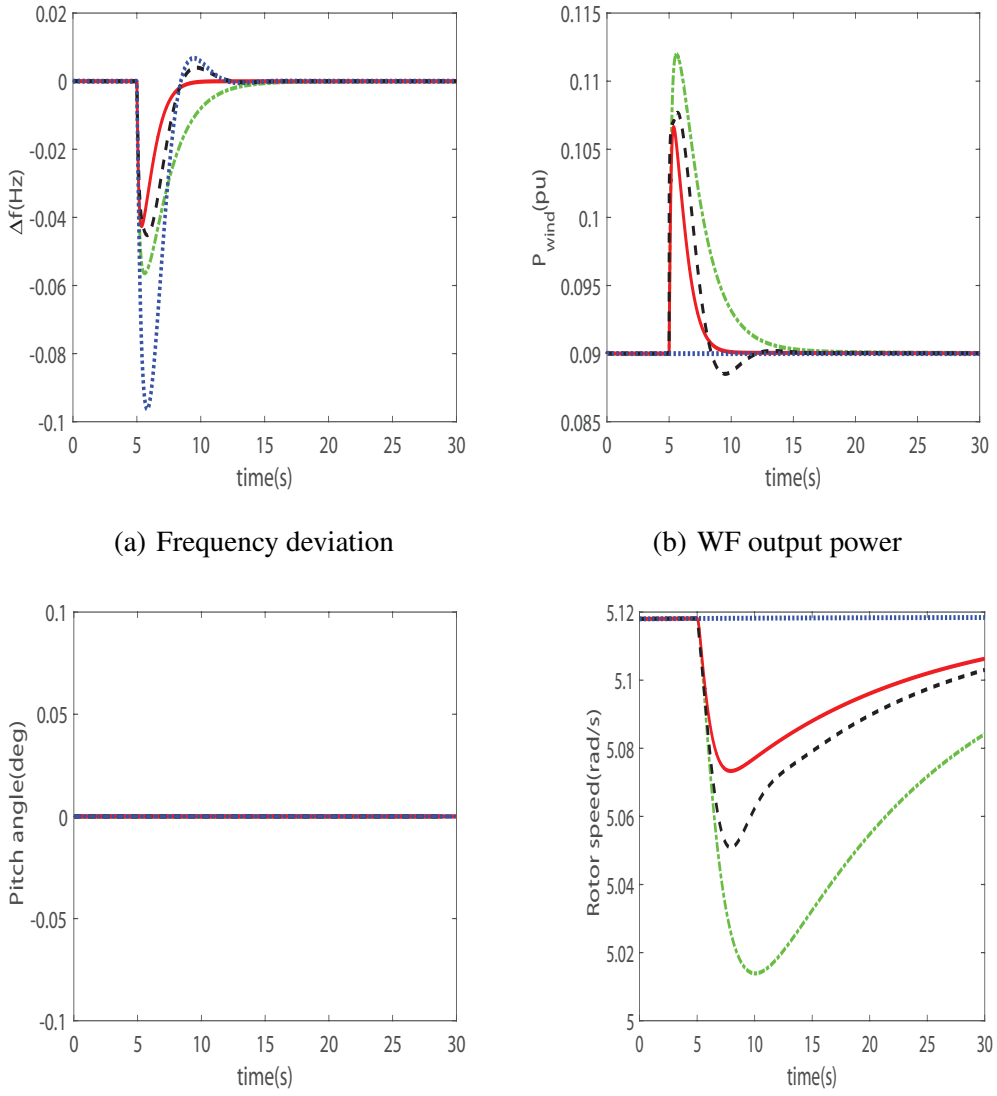

(a) Frequency deviation

(b) WF output power

(c) Pitch angle

(d) Rotor speed

Figure 6.8: Results for low wind speed (8.5 m/s): dash-dot (RSC), solid (RSC with DSR), dashed (RSC with IC), dot (no control)

stable in high wind speed. The pitch angle is presented in Figure 6.9 (c). Then the PAC can control the wind turbines produce the enough output power to keep the power system in balance. The wind turbines participating in frequency regulation by combined PAC and DSR method make the best performance than wind turbine supporting grid frequency by PAC or PAC combined IC methods.

Figure 6.10 shows frequency deviation from the power system with wind farm when the wind speed is a random variable. Figure 6.10 (a) presents frequency deviation when the wind turbines operate at wind speed in 7-10 m/s and Figure 6.10 (b) presents frequency deviation when the wind turbine operates at wind speed in 16-20 m/s. The wind turbines and DSR participating in frequency regulation can fastest recover frequency deviation in desired range with the smallest fluctuation.

In conclusion, when wind speed in 7-10 m/s, the pitch angle is kept at zero and the output power is changed by the change of rotor speed. When wind speed is higher than 12m/s, the rotor speed is constrained in the maximum values and wind power generation is controlled by pitch angle control. With IC, the kinetic energy from the wind turbine rotating mass is quickly released to the grid and therefore strong support is obtained to ensure that the grid frequency does not experience a sweeping drop. With DSR, the air conditioners and PEVs can suppress the frequency regulation to keep the power system in stable quickly. In these different control schemes, the wind turbines and DSR participating frequency regulation methods have good performances not only in low wind speed but also in high wind speed.

6.4.2 The High Penetration of Wind Power in Smart Grid

In this section, the high penetration of wind power in the power system is tested. The wind farm consists 400 wind turbines and the total wind farm output power is 900 MW (about 52.94% of total output power). The DSR and some wind turbines join in frequency regulation. There are three scenarios are tested. In these three scenarios, the percentage of wind turbines participating in frequency regulation are 10%, 50% and 90% of total wind turbines. So numbers of wind turbines supported frequency regulation are 40, 200 and 360, respective.

Scenario 1: 40 wind turbines participate in frequency regulation and 360 wind tur-

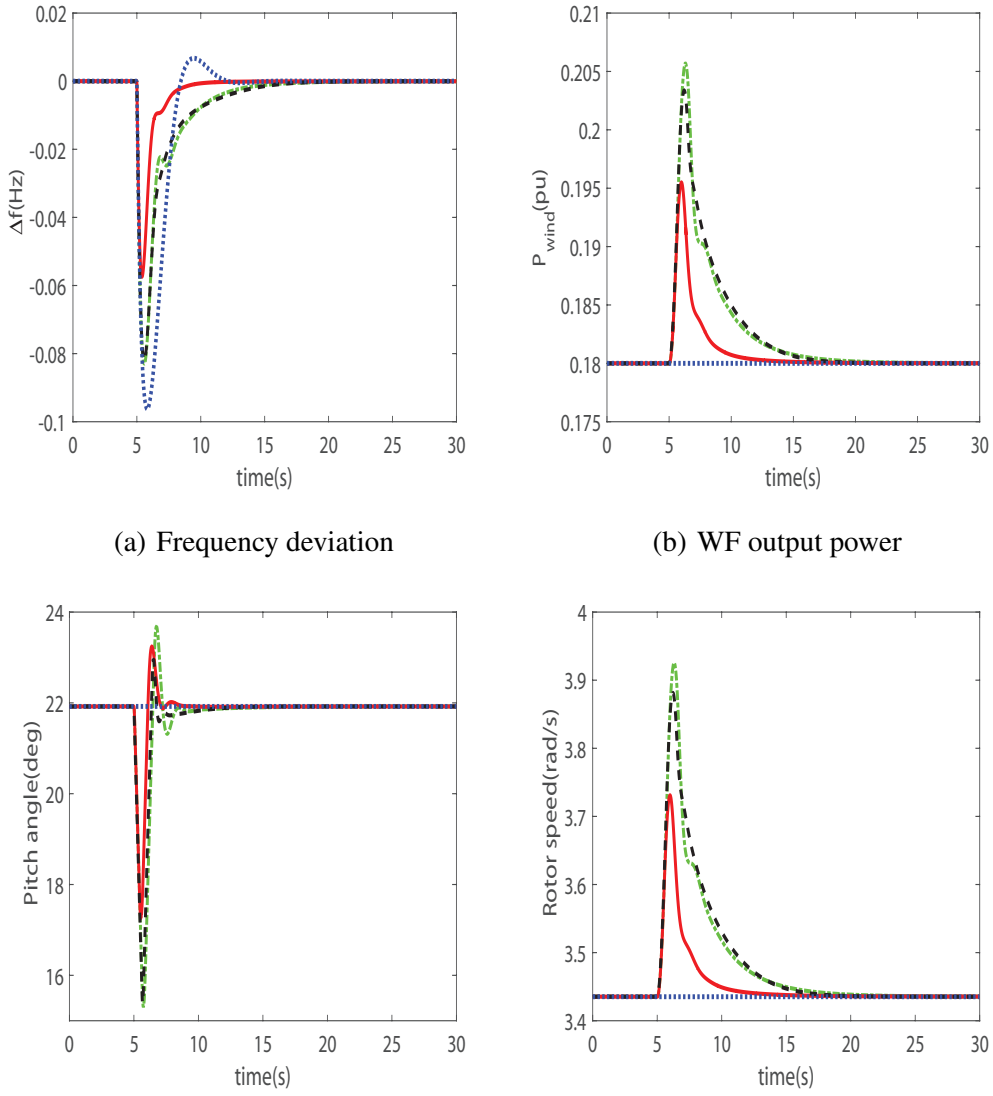

(a) Frequency deviation

(b) WF output power

(c) Pitch angle

(d) Rotor speed

Figure 6.9: Results for high wind speed (18 m/s: dash-dot (PAC), solid (PAC with DSR), dashed (PAC with IC), dot (no control)

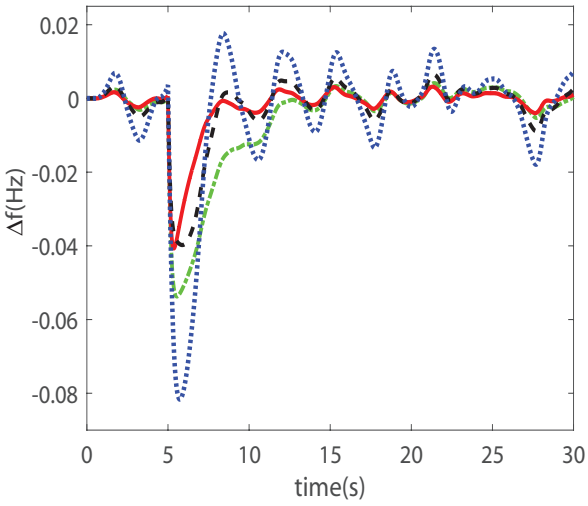

(a) Wind speed 7-10m/s

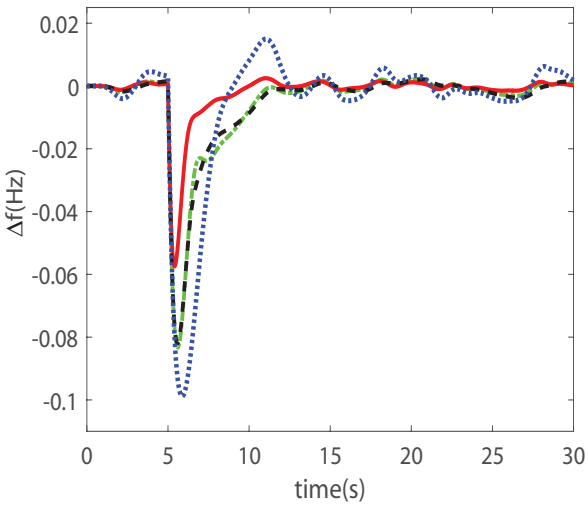

(b) Wind speed 16-20m/s

Figure 6.10: Frequency deviation for variable wind speed: dash-dot (RSC), solid (RSC with DSR), dashed (RSC with IC), dot (no control)

bines directly connect in the power system.
Scenario 2: 200 wind turbines participate in frequency regulation and 200 wind turbines directly connect in the power system.
Scenario 3: 360 wind turbines participate in frequency regulation and 40 wind turbines directly connect in the power system.

1) Wind speed is low: When the wind speed is low, the wind turbines are controlled by RSC method. The constant wind speed is 8.5 m/s and variable wind speed (VWS) is in range 7-10 m/s. Figures 6.11 and 6.12 show frequency deviation from three scenarios under constant and variable low wind speed, in which dash-dot line, dash line and solid line represent for RSC method, RSC combined IC method and combined RSC and DSR method, respectively. When wind speed is constant, frequency deviation is fastest convergent to schedule values with the smallest fluctuation by combined RSC and DSR approach. While fluctuation of frequency deviation is biggest and recover time is longest by RSC method. Compared the same method used in these three scenarios, the fluctuation of frequency deviation smallest is in Scenario 3. When wind speed is variable in 7-10 m/s, results is same as above. The combined RSC and DSR method has the best performance than RSC and RSC combined IC in these three scenarios and Scenario 3 has better performance than the same control method in Scenario 1 and Scenario 2. In conclusion, the combined RSC and DSR method can provide a better regulation transient dynamics, with the fastest settling time and smallest overshoot, compared with those provided by RSC method and RSC combined IC method in these three scenarios under low wind speed. It also found the fluctuation of frequency deviation is smaller when more wind turbines supporting in frequency regulation.

2) Wind speed is high: When the wind speed is high, the wind turbines are controlled by PAC method. The constant wind speed is in 18 m/s and variable wind speed is in range 16-20 m/s. Figures 6.13 to 6.14 show frequency deviation in three scenarios under constant and variable high wind speed, in which dash-dot line, dash line and solid line represent for PAC method, PAC combined IC method and combined PAC and DSR method, respectively. Similar results can be obtained from the simulation study. The combined PAC and DSR method is the best method

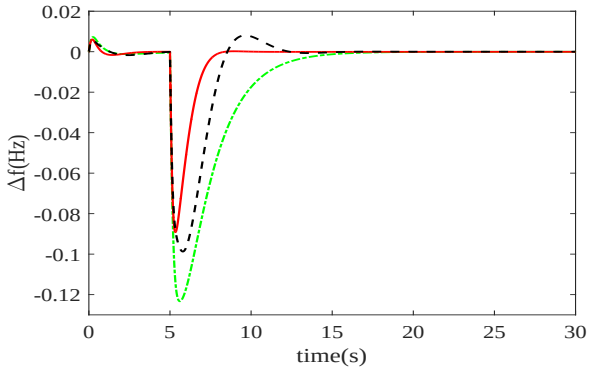

(a) Scenario 1 in constant low wind speed

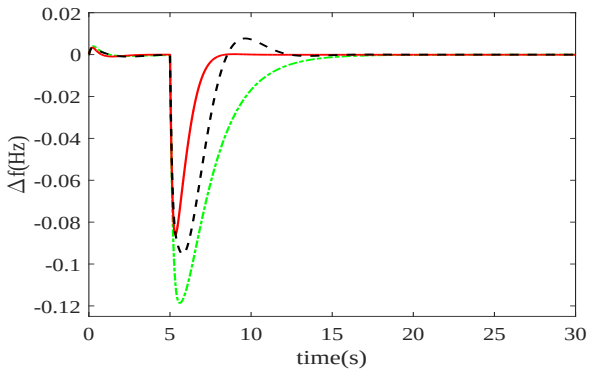

(b) Scenario 2 in constant low wind speed

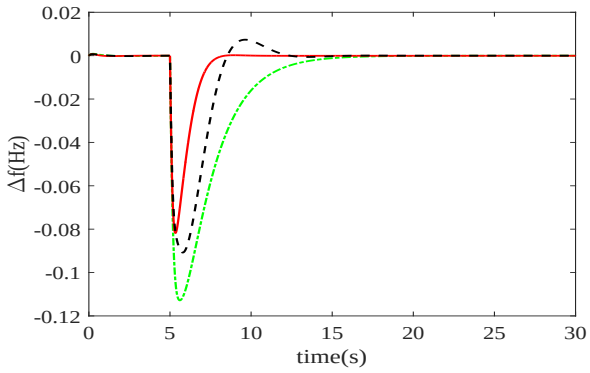

(c) Scenario 3 in constant low wind speed

Figure 6.11: Frequency deviation from different control methods in three scenarios in constant low wind speed: dash-dot (RSC), dashed (RSC with IC), solid (RSC with DSR)

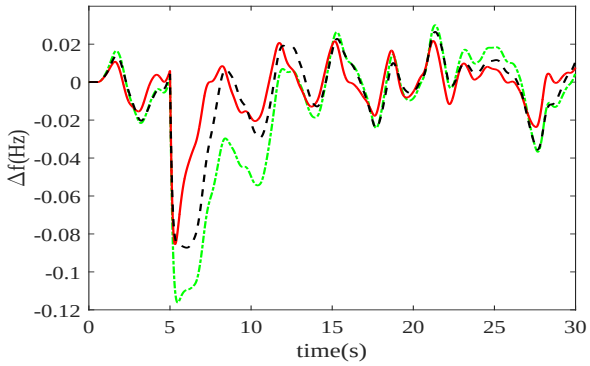

(a) Scenario 1 in variable low wind speed

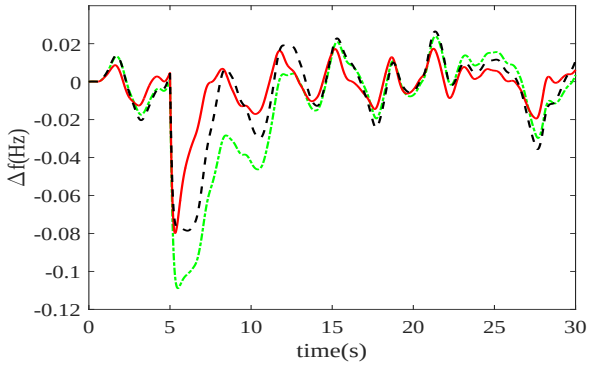

(b) Scenario 2 in variable low wind speed

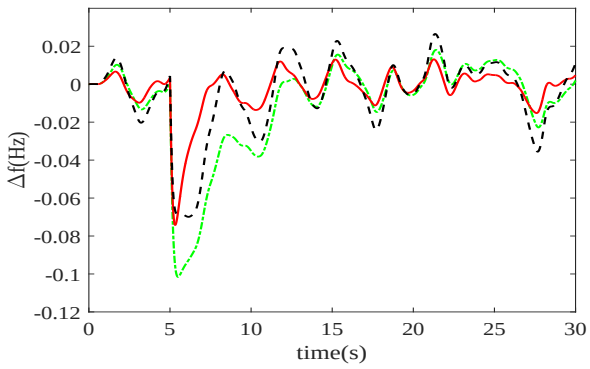

(c) Scenario 3 in variable low wind speed

Figure 6.12: Frequency deviation from different control methods in three scenarios in variable low wind speed: dash-dot (RSC), dashed (RSC with IC), solid (RSC with DSR)

to maintain frequency deviation in desired value with the smallest fluctuation and fastest response time.

In conclusion,when the power system has the high penetration of wind power energy, the combined RSC and DSR method and combined PAC and DSR method have best performances under low or high wind speed. The DSR can improve the power system stability and have a fast response time. Moreover, more wind turbines participated in frequency regulation will cause less disturbance in the power system and the fluctuation of frequency regulation is smaller.

6.4.3 The Demand Load Required Power Exceeds Produced Power

The wind farm produces wind power energy depending on the wind speed. When the high penetration of wind power connects in the power system, it will cause the generated power insufficient to demand load required. On the other hand, the demand load change suddenly becomes big sometimes in a year. Due to these two reasons, the demand side load may need more power than a total produced power in sometimes. In this section, three scenarios are introduced in the above are simulates with significant demand load change in low and high wind speed.

A step demand load change is $0.56pu$ at $t = 5s$ in the power system. When wind speed is 7-10 m/s, the RSC controls wind turbine and Figure 6.15 shows frequency dilation from 3 scenarios. In these three scenarios, the combined RSC and DSR method can recover the frequency deviation in desired range with small fluctuation and response time is fast. The fluctuation of frequency deviation from wind turbines controlled by the RSC and RSC combined IC method is bigger than RSC and DSR. When more wind turbines participate in frequency regulation, the fluctuation of frequency deviation is smaller. Figure 6.16 shows frequency deviation from three scenarios with different control methods when wind speed is in 16-20 m/s. The results are as same as above. It can conclude the DSR can improve the power system stability and can balance the power system. Meanwhile, the more wind turbines participating in the frequency regulation can reduce the fluctuation of the grid

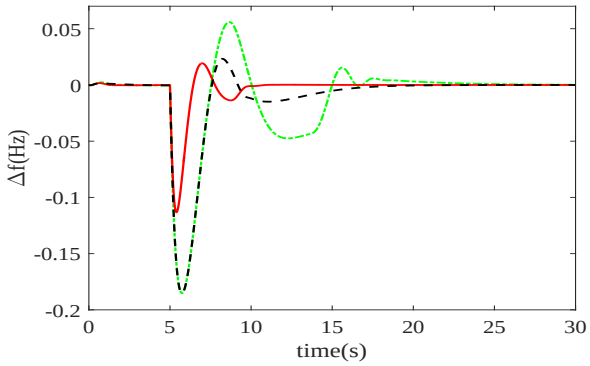

(a) Scenario 1 in constant high wind speed

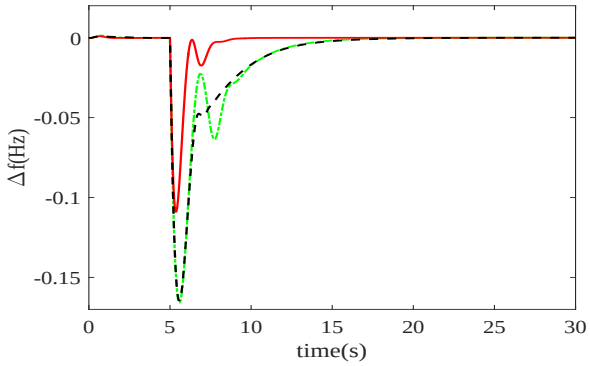

(b) Scenario 2 in constant high wind speed

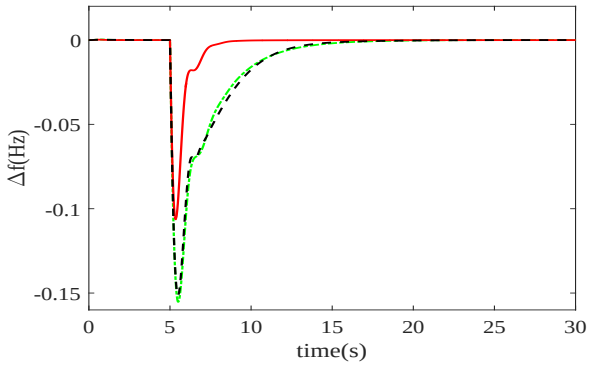

(c) Scenario 3 in constant high wind speed

Figure 6.13: Frequency deviation from different control methods in three scenarios in constant high wind speed: dash-dot (PAC), dashed (PAC with IC), solid (PAC with DSR))

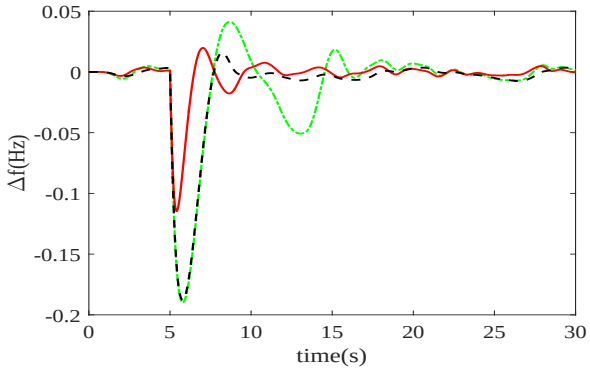

(a) Scenario 1 in variable high wind speed

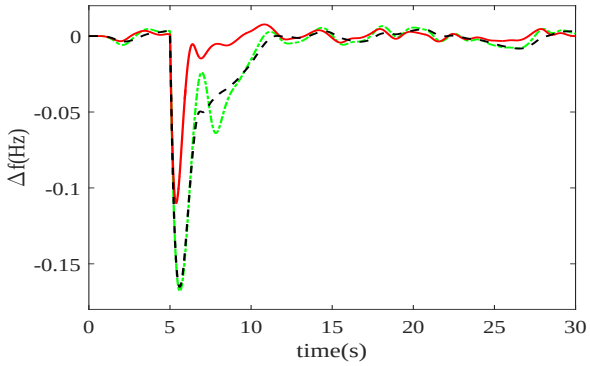

(b) Scenario 2 in variable high wind speed

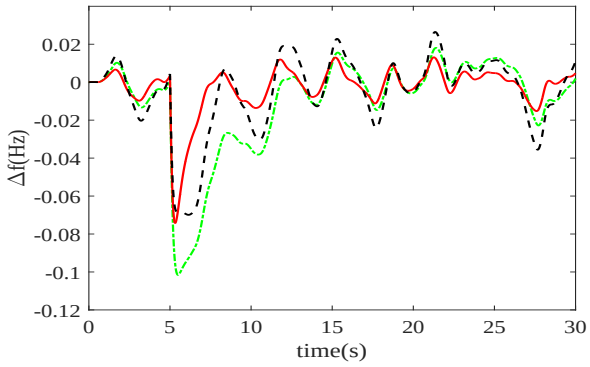

(c) Scenario 3 in variable high wind speed

Figure 6.14: Frequency deviation from different control methods in three scenarios in variable high wind speed: dash-dot (PAC), dashed (PAC with IC), solid (PAC with DSR))

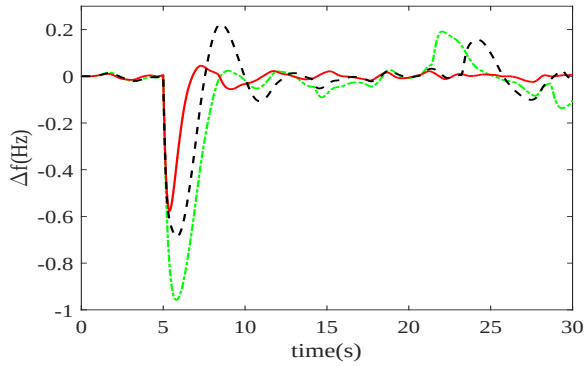

(a) Scenario 1 in variable low wind speed

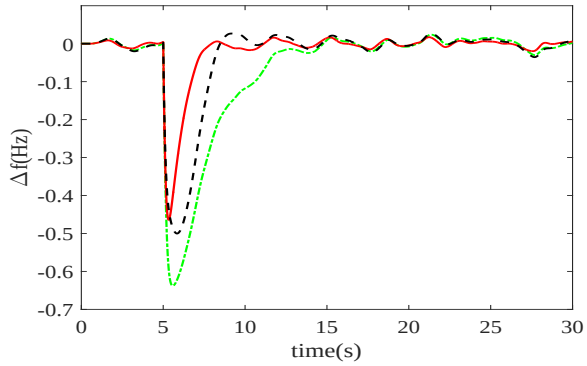

(b) Scenario 2 in variable low wind speed

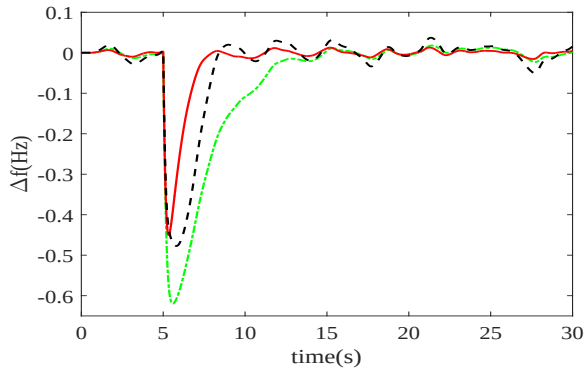

(c) Scenario 3 in variable low wind speed

Figure 6.15: Frequency deviation from different control methods in three scenarios with big load change in variable low wind speed:dash-dot (RSC), dashed (RSC with IC), solid (RSC with DSR)

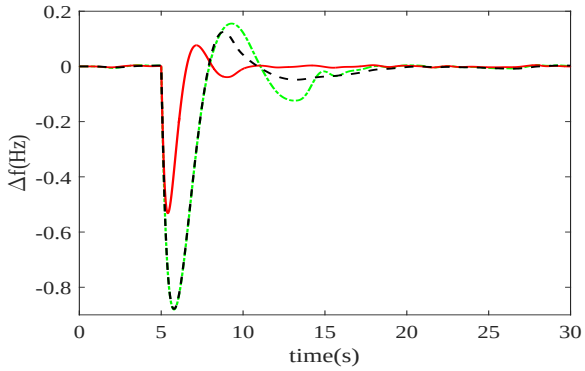

(a) Scenario 1 in variable high wind speed

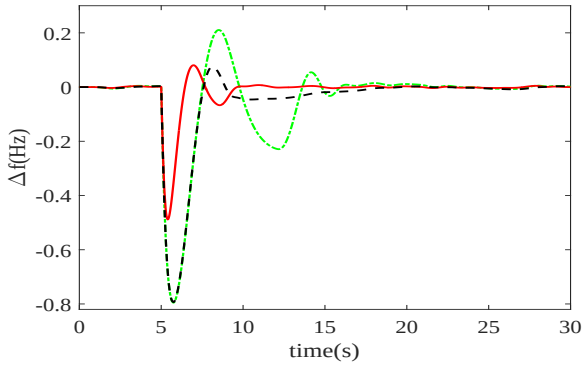

(b) Scenario 2 in variable high wind speed

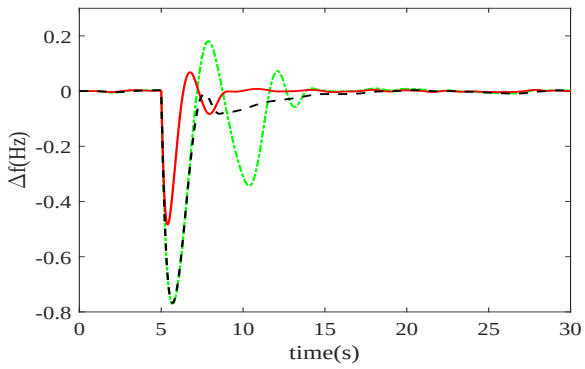

(c) Scenario 3 in variable high wind speed

Figure 6.16: Frequency deviation from different control methods in three scenarios with big load change in variable high wind speed:dash-dot (RSC), dashed (RSC with IC), solid (RSC with DSR)

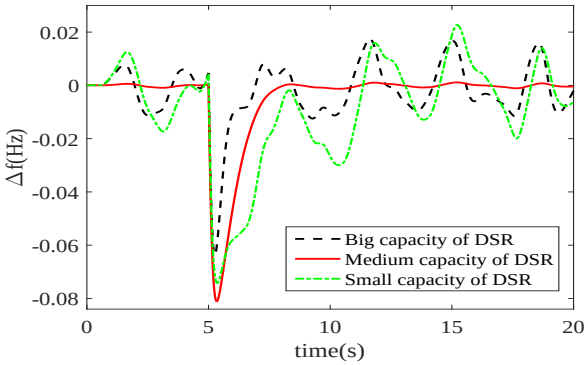

(a) Scenario 1 variable low wind speed

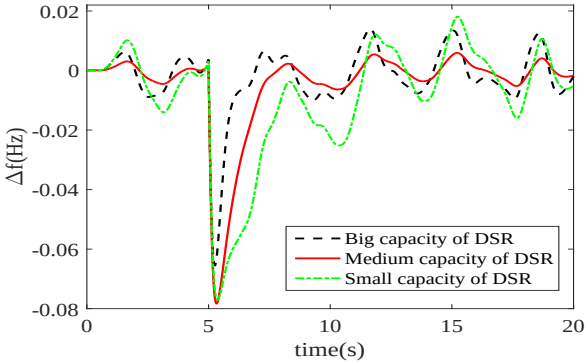

(b) Scenario 2 variable low wind speed

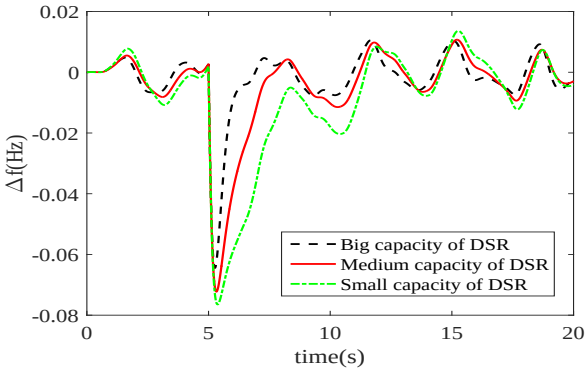

(c) Scenario 3 variable low wind speed

Figure 6.17: Frequency deviation from power system with different capacity of DSR in three scenarios in variable low wind speed

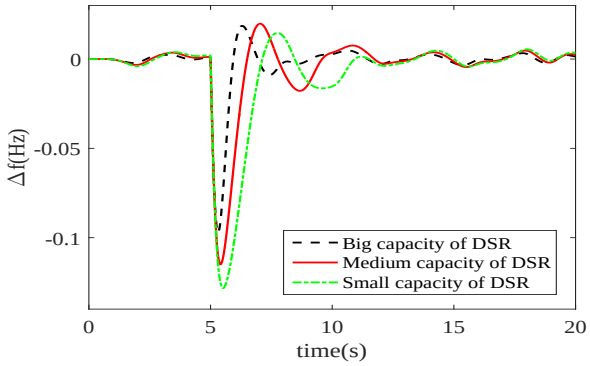

(a) Scenario 1 variable high wind speed

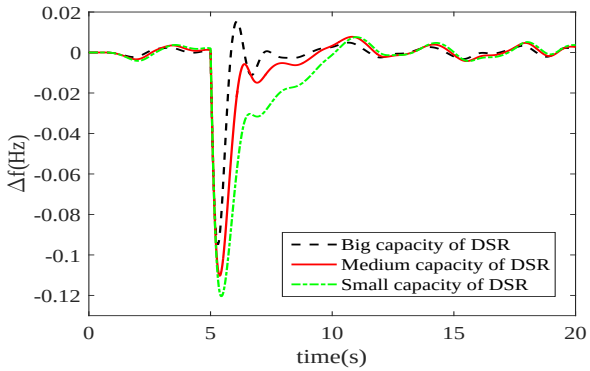

(b) Scenario 2 variable high wind speed

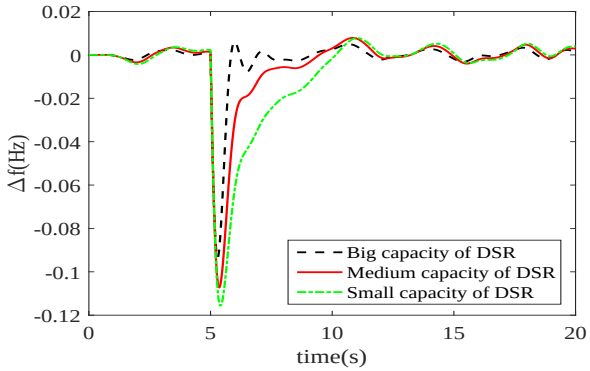

(c) Scenario 3 variable high wind speed

Figure 6.18: Frequency deviation from power system with different capacity of DSR in three scenarios in variable high wind speed

frequency.

6.4.4 Different capacity of DSR

Three scenarios in LFC with different capacity of DDC, PEVs under variable low and high wind speed are tested in the power system with high penetration of wind power. Figure 6.17 and Figure 6.18 show the frequency deviation for 3 scenarios under variable low wind speed and variable high wind speed with different capacity of DSR, respectively. The variable low wind speed is 7-10 m/s and the variable high wind speed is 16-20 m/s. From these results, it can be found that the bigger capacity of DSR which includes DDC with bigger capacity and more PEVs participating in frequency regulation can recover the frequency deviation in narrow range quicker and fluctuation smaller. In these three scenarios, the frequency deviation from the system which the wind turbines are controlled by the same control method and same capacity of DSR are still different. It can be found the capacity of DSR and the percentage of wind turbines participating in frequency regulation are all influence the grid frequency.

6.5 Conclusion

This chapter discusses coordinated supporting of grid frequency for VSWT and DSR under low or high wind speed. The VSWTs are controlled by coordinated RSC, PAC and IC at different wind speed, together with DSR for the LFC of the power system under intermittent wind power and demand load suddenly increase. Combined RSC or PAC with DSR can contribute to increase penetration of wind power and also slash peak load.

The further work will further consider different types of wind turbine, such as doubly fed induction generator (DFIG) and permanent magnet synchronous generator (PMSG). And different types of controllable loads used in DSR to help the power system to solve imbalance problem caused by intermittent wind power energy.

Chapter 7

Conclusions and Future Work

7.1 Conclusions

This thesis has investigated DSR participating in frequency regulation in the smart grid. The DSR can contribute to solve the imbalance problem caused by intermittent wind power energy when the power system with high penetration of wind power energy.

Chapter 1 is the introduction. The smart grid technology, wind power energy, DSR technology and time delays power system are introduced. The smart grids are widely used in the world and develop very fast in recent years because the smart grid can make the power system more reliable, secure and increase the efficiency of electricity production. Wind energy is renewable energy to reduce carbon emissions and DSR is an important role for balancing active power in the smart system. So the wind power energy and DSR are two important components in the smart grid. Meanwhile, motivations, objectives and main contributions of this thesis are also mentioned.

Literature reviews about DSR approaches and their applications in smart grid are introduced in Chapter 2. Two types of DSR, indirect load control (ILC) and direct load control(DLC), are introduced. The DSR can improve the stability of the power system and reduce operation cost. Then applications of DSR used in a wind power system to solve imbalance problem caused by intermittent wind power energy have

been reviewed. The DSR can balance active power between the generation side and the demand side of the power system with intermittent wind power.

In Chapter 3, DLC models based on PEV model, aggregated air conditioners model and HPWHs model are introduced, respectively. These DLC models can participate in frequency regulation. The general DLC model which can represent for different types of controllable load is introduced. The BESS model is also introduced. Time delay model of LFC system including those DLC models and BESS has been built up.

In Chapter 4, the model of LFC with DDC in a deregulated environment is investigated and the PID controller for LFC scheme is designed, considering multiple time delays in LFC scheme and DDC loop. Time delay model of the deregulated multi-area LFC with DDC based on aggregated air conditioners model is obtained at first. Then, a robust PID load frequency controller is designed for LFC via the H_∞ performance analysis and the PSO searching algorithm, in which considers the load disturbances and multiple delays in the LFC loop and the DDC loop. Simulation results demonstrate the effective of the PID controller for LFC scheme. DDC can improve performances and the stability of LFC. Moreover, several delay stable regions are revealed via simulation method.

In Chapter 5, a single area LFC system, which includes the wind farms equipped with variable-speed wind turbines, the simplified BESS, PEVs and air-conditioners, is obtained. The LFC system contains traditional primary and supplementary control loops and three additional control loops of the BESS, the PEVs, and the DDC, respectively. Then, state-space models of the closed-loop LFC scheme with communication delays in the control loops are derived and the stability of the closed-loop system with time delays is investigated via the Lyapunov functional based method. Finally, the PID-type controller for LFC scheme is designed based on the H_∞ performance analysis and the PSO searching algorithm. Case studies are carried out for the single area smart power grid by Matlab/Simulink. Both the theoretical analysis and the simulation studies demonstrate the contribution of the DSR to frequency regulation. The robustness of the designed PID-type LFC is verified, which against to the disturbances caused by the load changes and the intermittent wind power and

the delays arising in the control loops via theoretical analysis and the simulation studies. Moreover, delay margin calculated based on the developed stability analysis method and ones obtained via simulation study are very similar to each other, which shows that the proposed delay-dependent stability analysis method is effective and can be used to theoretically investigate the robustness of the controller to multiple time delays.

Chapter 6 proposes wind turbines and DSR participating in frequency regulation. The wind turbines are controlled by coordinated RSC and PAC combined IC in different wind speed. The DSR consists air conditioners and PEVs with V2G service. Case studies are carried out for single area LFC with wind farm and DSR participating frequency regulation in the power system with low or high penetration of wind power. The different proportion of wind turbines participated frequency regulation are tested and compared that with DSR. Combination wind turbines and DSR method can contribute to increase penetration of wind power and demand load suddenly increase. The DSR is useful method can help the power system with high penetration and reduce peak load.

7.2 Future Work

The future work is listed as following ideas.

I Models of DLC based on air conditioners, HPWHs and PEVs are investigated. Future work will investigate the model of DLC based on other kinds of controllable load, such as refrigerators and different kinds of EWHs.

II The ILC, which sent dynamic electricity price for consumers and encourage customers to manage their load to maintain the power balance between generation side and demand side, is not investigated in this thesis. Future work will construct the model based on ILC and use ILC to solve some problems of the power system.

III This thesis researches DLC and wind turbine together supported frequency regulation can increase penetration of wind power energy in the smart grid.

ILC which encourages customers to shifts some loads maintain the power system in balance also can be used in the power system to increase penetration of wind power in the system. Future work will consider using DLC and ILC to balance active power between the generation side and the demand side of the power system with high penetration of wind power.

IV In this thesis, VSWTs are used in Chapter 6. Future work will consider different types of wind turbine, such as DFIG and PMSG, to participate in frequency regulation; Meanwhile, different types of DSR and wind turbines also participate in frequency regulation to solve the imbalance problem caused by the high penetration of intermittent wind power.

References

[1] C. Tsai, A. Pelov, M. Chiang, C. Yang and T. Hong, "A brief introduction to classification for smart grid," in *2013 IEEE Internation Conference on System, Man and Cybernetics*, Manchester, UK, pp. 2905-2909, Oct. 2013.

[2] European Commission, *European smart grids technology platform: Vision andstrategy for Europes electricity networks of the future*, Luxembourg: Office forOfficial Publications of the European Communities, 2006.

[3] L. Gelazanskas and K. A. A. Gamage, "Demand side management in smart grid: A review and proposals for future direction," *Sustainable Cities and Society*, vol. 11, pp. 22 - 30, Feb. 2014.

[4] R. H. M. Fallon MP and D. Gray, "Smart grid vision and routemap," *Department of energy and climate change*, pp. 1-58, Feb. 2014.

[5] M. Marwan and F. Kamel, "Optimum demand side response of smart grid with reneable energy source and elctrical vehicles," in *2011 21st AUPEC*, Brisbane, Australia, pp. 1-5, Sept. 2011.

[6] M. Frerk and D. Capper, "Smart grid forum-annual report," *Department of energy and climate change*, pp. 1-6, 2015.

[7] N. B. M. Isa, T. C. Wei and A. H. M. Yatim, "Smart grid technology: communications, power electronics and control system," in *2015 ICSEEA*, Bandung, Indonesia, pp. 10-14, Oct. 2015.

[8] K. V. Rifkhatovich, E. S. Alekseyevich and N. A. Andreevich "Monitoring technical state of the power transformers is a necessary condition of the

smart-grid technology introduction within the industrial electric networks," in *2013 IEEE Internation Conference on System, Man and Cybernetics*, St. Petersburg, Russia, pp. 214-220, Feb. 2015.

[9] B. P. Esther and K. S. Kumar, "A survey on residential demand side management architecture, approaches, optimization models and methods," *European Network of Trans. Syst. Operators for Electricity*, vol. 59, pp. 342-351, Jan. 2016.

[10] 2015 in review – Wind energy, 2015. Availiable: http://www.bp.com/en/global/corporate/energy-economics/statistical-review-of-world-energy/renewable-energy/wind-energy.html 2015.

[11] R. Kyoho, T. Goya, W. Mengyan, T. Senjyu, A. Yona, T. Funabashi and C. Kim,"Thermal units communication with demand response to optimize batterry storage capacity," in *IEEE 10th PEDS Internation Conference 2013*, pp. 1-6, Apr. 2013.

[12] F. Oldewurtel, T. Borsche, M. Bucher, P. Fortenbacher, M. G. Vaya, T. Haring, J. L. Mathieu, O. Megel, E. Vrettos and G.Andersson, "A fram work for and assessment of demand response ans energy storage in power systems," in *2013 IREP Symposium Confernece*, Rethymno, Greece, pp. 1-24, Aug. 2013.

[13] C. W. Gellings, "The concept of demand-side management for electric utilities," *Proceeding of the IEEE*, vol. 73, no. 10, pp 1468-1470, 1985.

[14] US Department of Energy, *The smart grid: an introduction*, 2009.

[15] A. Vojdani, "Samrt integration," *IEEE Power Energy Mag.*, vol. 6, no. 6, pp 71-79, Nov. 2008.

[16] S. Gottwalt, W. Ketter, C. Block, J. Collins and C. Weinhardt, "Demand side management - A simulation of household behavior under variable prices," *Energy Policy*, vol. 39, no. 12, pp. 8163-8174, Oct. 2011.

[17] P. Du and N. Lu, "Appliance commitment for household load scheduling," *IEEE Trans. Samrt Grid*, vol. 2, no. 2, pp. 411-419, Jun. 2011

[18] M. Norton, H. Vanderbroucke, E. Larsen, C. Dyke, S. Banares, C. Latour and T. V. Van, "Demand side response policy paper," *Renewable and Sustainable Energy Reviews*, Sept. 2014. Available: https://www.entsoe.eu/Documents/Publications/Position.

[19] P. Palensky and D. Dietrich, "Demand side management: demand response, intelligent energy systems and smart loads," *IEEE Trans. Industrial Informatics*, vol. 7, no. 3, pp 381-388, 2008.

[20] P. Warren, "A review of demand-side management policy in the UK," *Renewable and Sustainable Energy Reviews*, vol. 29, pp. 941 - 951, Jan. 2014.

[21] US DoE, "Benefit of demand response in electricity markets and recommendations for achieving them," *Report to the US Congress*, Feb. 2006. Available: http://eetd.idi.gov.

[22] K. Ma, G. Hu and C. J. Spanos, "Distributed energy consumption control via real-time pricing feedback in smart grid," *IEEE Trans. Control Syst. Technol.*, vol. 22. no. 5, pp. 1907-1914, Sept. 2014.

[23] S. Chanana and A. Kumar, "Demand response by dynamic demand control using frequency linked real-time prices," *IEEE Trans. Power Syst.*, vol. 28, no. 2, pp. 884-892, Nov. 2013.

[24] J. M. Mauricio, A. Marano, A. G-Exposito and J. L. M. Ramos, "Frequency regulation contribution through variable-speed wind energy conversion systems," *IEEE Trans. Power Syst.*, vol. 24, no. 1, pp. 173-180, Feb. 2009.

[25] S. A. Pourmousavi and M. H. Nehrir, "Introducing dynamic demand response in the LFC model," *IEEE Trans. Power Syst.*, vol. 29, no. 4, pp. 1562-1572, Jul. 2014.

[26] W. Zhang, J. Lian, C. Chang and K. Kalsi, "Aggregated modeling and control of air conditioning loads for demand response," *IEEE Trans. Power Syst.*, vol. 28, no. 4, pp. 4655-4664, Nov. 2013.

[27] K. Kalsi, M. Elizondo, J. Fuller, S. Lu and D. Chassin, "Development and validation of aggregated models for thermostatic controlled loads with demand response," in *2012 45th HICSS*, Maui, US, pp. 1959-1966, Jan. 2012.

[28] N. Lu and Y. Zhang, "Design considerations of a centralized load controller using thermostatically controlled appliances for continuous regulation reserves," *IEEE Trans. Smart Grid*, vol. 4, no. 2, pp. 1949-3053, Jun. 2013.

[29] K. Zhou and S. Yang, "Demand side management in China: the context of China's power industry reform," *Renewable and Sustainable Energy Reviews*, vol. 47, pp. 954-965, Apr. 2015.

[30] Y. Iino, T. Hatanaka and M. Fujita, "Model predictive control for demand response aggregation management system wirh respone delay time and uncertainty model," in *SICE Annual Coference*, Sapporo, Janpan, pp 1478-1483, Sept. 2014.

[31] J. C. Fuller, S. Ciraci, J. A. Daily, A. R. Fisher and M. Hauer, "Communication simulations for power system applications," in *2013 MSCPES*, pp. 1-6, May 2013.

[32] C. Tranchita, N. Hadjsaid, M. Viziteu, B. Rozel and R. Caire, *Securing electricity supply in the cyber age*, Springer, 2009.

[33] L. Jiang, W. Yao, Q. H. Wu, J. Y. Wen, and S. J. Cheng, "Delay-dependent stability for load frequency control with constant and time-varying delays," *International Journal of Energy Sector Management*, vol. 4, no. 1, pp. 44-58, May 2010.

[34] C. K. Zhang, L. Jiang, Q. H. Wu, Y. He and M. Wu, "Delay-dependent robust load frequency control for time delay power systems," *IEEE Trans. Power Syst.*, vol. 28, no. 3, pp. 2192-2201, Aug. 2013.

[35] C. K. Zhang, L. Jiang, Q. H. Wu, Y. He and M. Wu, "Further Results on delay-dependent stability of multi-area load frequency control," *IEEE Trans. Power Syst.*, vol. 28, no. 4, pp. 4465-4474, Nov. 2013.

[36] A. Stefanov and C. Liu, "ICT modeling for integrated simulation of cyber-physical power systems," in *2012 3rd IEEE PES ISGT Europe*, Berlin, Germany, pp. 1-8, 14-17 Oct. 2012.

[37] K. Y. Yang, L. L. Zhang, and J. Zhang, "Dynamic analysis and control of three dimensional energy supply and demand system with time delay," in *2014 33rd Chinese Control Conference*, pp. 7121-7126, Nanjing, China, Jul. 2014.

[38] W. Yao, L. Jiang, Q. H. Wu, J. Y. Wen and S. J. Cheng, "Delay-dependent stability analysis of the power system with a wide-area damping controller embedded," *IEEE Trans. Power Syst.*, vol. 26, no. 1, pp. 233-240, Jan. 2011.

[39] W. Yao, L. Jiang, J. Y. Wen, Q. H. Wu and S. J. Cheng, "Wide-area damping controller of FACTS devices for inter-area oscillations considering communication time delays," *IEEE Trans. Power Syst.*, vol. 29, no. 1, pp. 318-329, Jan. 2014.

[40] W. Yao, L. Jiang, J. Y. Wen, Q. H. Wu and S. J. Cheng, "Wide-area damping controller for power system inter-area oscillations: a networked predictive control approach," *IEEE Trans. Control Syst. Technol.*, vol. 23, no. 1, pp. 27-36, Jan. 2015.

[41] H. Bevrani, *Robust power system frequency control*, Berlin, Springer, 2009.

[42] K. Ramakrishnan and G. Ray, "Improved results on delay-dependent stability of LFC systems with multiple time delays," *J. Control Autom. Electr. Syst.*, vol. 26, no. 3, pp. 235-240, Feb. 2015.

[43] J. A. Short, D. G. Infield and L. L. Freris, "Stability of grid frequency through dynamic demand control," *IEEE Trans. Power System*, vol. 22, no. 3, pp. 1284-1293, Aug. 2007.

[44] B. Wu, B. Zhang, J. Wang, J. Li, X. Zheng, Y. Liu, B. Mao and Y. Gao, "Theoretical research for the application of flow storage battery in demand side management," in *2010 Internation Conference on Power System Technology*, Hangzhou, China, pp. 1-7, Oct. 2010.

[45] P. Siano, "Demand response and smart grids - A survey," *Renewable and Sustainable Energy Reviews*, vol. 30, pp. 461 - 478, Feb. 2014.

[46] A. Conchado and P. Linares, "The economics impacted of demand response programs on power systems - A survey of the state of the art," *Handbook of networks in power systems I energy systems*, pp. 281-301, 2011.

[47] C. Triki, A. Violi, "Dynamic pricing of electricity in retail markets," *QJ Oper Res*, vol. 7, no. 1, pp.21-36, Mar. 2009.

[48] J. Berardion and C. O. Nwankpa, "Economic demand dispatch of controllable building electrical loads incorporating delayed response times," in *2013 IEEE PES ISGT*, Washington, U.S., pp. 1-6, Feb. 2013.

[49] K. Herter, "Residential implementation of critical-peak pricing of electricity," *Energy Policy*, vol. 35, no. 4, pp. 2121-2130, Apr. 2007.

[50] AH. Mohsenian-Rad and A. Leon-Garcia, "Optimal residential load control with price prediction in real-time electricity pricing environments," *IEEE Trans. Smart Grid*, vol. 1, no. 2, pp. 120-133, Sept. 2010.

[51] W. Tushar, W. Saad, H. V. Poor and D. B. Smith, "Economics of electric vehicle charging: a game theoretic approach," *IEEE Trans. Smart Grid*, vol. 3, no. 4, pp. 1767-1778, Dec. 2012.

[52] P. C. D. Granado, S. W. Wallace and Z. Pang,"The value of electricity storage in demestic homes: a smart grid perspective," *Energy Syst.*, vol. 5, no. 2, pp. 211-232, Mar. 2014.

[53] S. K. Aditya and D. Das,"Battery energy storage for load frequency control of an interconnected power system," *Electric Power Syst. Research*, vol. 5, pp. 179-185, Feb. 2001.

[54] D. Setlhaolo and X. Xia, "Combined residential demand side management strategies with coordination and economic analysis," *Electrical Power and Energy Systems*, vol. 79, pp. 150-160, Jan. 2016.

[55] Z. Wang, C. Gu, F. Li, P. Bale and H. Sun, "Active demand response using shared energy storage for household energy mangement," *IEEE Trans. on Smart Grid*, vol. 4, no.4, pp. 1888-1897, Dec. 2013.

[56] J. Zhao, F. Wen, Z. Y. Dong, Y. Xue and K. P. Wong, "Optimal dispatch of electric vechicle and wind power using enchange particle awarm optimization," *IEEE Trans. Ind. Inf.*, vol. 8, no. 4, pp. 889-899, Nov. 2012.

[57] M. Datta and T. Senjyu, "Fuzzy control of distributed PV inverters/energy storage systems/electric vehicles for frequency regulation in a large power system," *IEEE Trans. Smart Grid*, vol. 4, no. 1, pp. 479-488, Mar. 2013.

[58] Z. Ma, D. S. Callaway and I. A. Hiskens, "Decentralized charging control of large populations of plug-in electric vehicles," *IEEE Trans. Control Syst. technology*, vol. 21, no. 1, pp. 67-78, Jan. 2013.

[59] H. Ito, "Disturbance and delay robustness guarantess of gradient system based on static noncooperative games with an application to feedback control for PEV charging load allocation," *IEEE Trans. Control Syst. Trchnology*, vol. 21, no. 4, pp. 1374-1385, Jul. 2013.

[60] J. R. Pillai and B. Bak-Jensen, "Integration of vehicle-to-grid in the western Danish power system," *IEEE Trans. Sustain Energy*, vol. 2, no. 1, pp. 12-19, Jan. 2011.

[61] D. Dallinger, D. Krampe and M. Wietschel, "Vehicle-to-grid regulation reserves based on a dynamic simulation of mobility behavior," *IEEE Trans. Smart Grid*, vol. 2, no. 2, pp. 302-313, Jun. 2011.

[62] W. Kempton and T. Kubo, "Electric-drive vehicles for peak power in Japan," *Energy Policy*, vol. 28, no. 1, pp. 9-18, Jun. 2000.

[63] S. Weckx, R. D'Hulst and J. Driesen, "Primary and secondary frequency support by a multi-agent demand control system," *IEEE Trans. Power Syst.*, vol. 29, no. 6, pp. 1394-1404, May 2015.

[64] M. F. M. Arani, Y. A. I. Mohamed and E. F. EI-Saadany, "Analysis and mitigation of the impacts of asymmetrical virtual inertia," *IEEE Trans. Power Syst.*, vol. 30, no. 3, pp. 2862-2874, Nov. 2014.

[65] H. Yang, C. Y. Chung and J. Zhao, "Application of plug-in electric vehicles to frequency regulation based on distributed signal acquisition via limited communication," *IEEE Trans. Power Syst.*, vol. 28, no. 2, pp. 1017-1026, May 2013.

[66] T. N. Pham, H. Trinh and L. V. Hien, "Load frequency control of power systems with electric vehicle and diverse transmission links using distributed functional observers," *IEEE Trans. Smart Grid*, vol. 7, no. 1, pp. 238-252, Jan. 2016.

[67] K. Shimizu, T. Masuta, Y. Ota and A. Yokoyama, "Load frequency control in power system using vehicle-to-grid system considering the customer convenience of electric vehicles," in *2010 Internation conference on POWERCON*, pp. 1-8, Oct. 2010.

[68] M. A. Lopez, S. Torre, S. Martin and J. A. Aguado, "Demand-side management in smart grid operation considering electric vehicles load shifting and vehicle-to-grid support," *Electrical Power and Energy Systems*, vol. 64, pp. 689-698, Aug. 2014.

[69] Ibraheem, P. Kumar and D. P. Kothari, "Recent philosophies of automatic generation control strategies in power system," *IEEE Trans. Power Syst.*, vol. 20, no. 1, pp. 346-357, Feb. 2005.

[70] Y. Cheng, M. Tabrizi, M. Sahni, A. Povedano and D. Nichols, "Dynamic available AGC based approach for enhancing utility scale energy storage per-

formance," *IEEE Trans. on Smart Grid*, vol. 5, no. 2, pp. 1070-1078, Mar. 2014.

[71] D. Wang, S. Parkinson, W. Miao, H. Jia, C. Crawford and N. Djilali, "Online voltage security assessment considering comfort-constrained demand response control of distributed heat pump systems," *Applied Energy*, vol. 96, pp. 104-114, Jan. 2012.

[72] J. Kondoh, N. Lu and D. J. Hammerstorm, "An evaluation of the water heater load potential for providing regulation service," *IEEE Trans. Power Syst.*, vol. 26, no. 3, pp. 1309-1316, Aug. 2011.

[73] T. Masuta, A. Yokoyama, and Y. Tada, "System frequency control by Heat Pump Water Heaters (HPWHs) on customer side based on statistical HPWH model in power system with a large penetration of renewable energy sources," in *Proc. Int. Conf. on PST*, pp. 1-7, Oct. 2010.

[74] Y. Kim, L. K. Norford and J. L. Kirtley, "Modelling and analysis of a variable speed heat pump for frequency regulation through direct load control," *IEEE Trans. Power Syst.*, vol. 30, no. 1, pp. 397-408, Jan. 2015.

[75] Y. Kim, L. E. Fuentes and L. K. Norford, "Experimental study of grid frequency regulaiton ancillary service of a variable speed heat pump," *IEEE Trans. Power Syst.*, vol. 31, no. 4, pp. 3090-3099, Jul. 2016.

[76] D. Angeli and P. A. Kountouriotis, "A stochastic approach to dynamic-demand refrigerator control," *IEEE Trans. Control Syst. Technol.*, vol. 20, no. 3, pp. 581-592, Jun. 2012.

[77] Z. Baharlouei, M. Hashemi, H. Narimani and H. M. Rad, "Achieving optimality and fairness in autonomous demand response: benchmarks and billing mechanisms," *IEEE Trans. Smart Grid*, vol. 4, no. 2, pp. 968-975, Jun. 2013.

[78] D. Angeli and P. A. Kountouriotis, "A stochastic approach to dynamic-demand refrigerator control," *IEEE Trans. Control Syst. Technol.*, vol. 20, no. 3, pp. 581-592, Jun. 2012.

[79] D. Jay and K. S. Swarup, "Frequency restoration using dynamic demand control under smart grid environment," in *IEEE PES ISGT*, Kollam, India, pp. 311-315, Dec. 2011.

[80] Q. Zhu, W. Yao, L. Jiang, C. Luo and Q. H. Wu, "Load frequency control with dynamic demand control for deregulated power system," in *2014 IEEE PES General Meeting*, Washington, U.S., pp. 1-5, Jul. 2014.

[81] C. Ninagawa, S. Kondo, S. Isozumi and H. Yoshida, "Fine-time-granularity fast demand control of building HVAC facilities for future smart grid," in *2012 3rd IEEE PES ISGT Europe*, Berlin, Germany, pp. 1-6, Oct. 2012.

[82] N. Lu, "An envalution of the HVAC load potential for providing load balancing service," *IEEE Trans. Smart Grid*, vol. 3, no. 3, pp. 1263-1270, Sept. 2012.

[83] E. Vrettos, S. Koch and G. Andersson, "Load frequency control by aggregations of thermally stratified electric water heaters," in *2012 3rd IEEE PES ISGT Europe*, Berlin, Germany, pp. 1-8, Oct. 2012.

[84] G. C. Heffner, C. A. Goldman and M. M. Moezzi, "Innovative approaches to verifying demand response of water heater load control," *IEEE Trans. Power Delivery*, vol. 21, no. 1, pp. 388-397, Jan. 2006.

[85] N. Lu, P. Du and Y. V. Makarov, "The potential of thermostatically controlled appliances for intra-hour energy storage applications," in *2012 IEEE PES General Meeting*, San Diego, U.S., pp. 1-6, Jul. 2012.

[86] S. A. Pourmousavi and M. H. Nehrir, "Real-time central demand response for primary frequency regulation in mircogrids," *IEEE Trans. Smart Grid*, vol. 3, no. 4, pp. 1988-1996, Dec. 2012.

[87] N. Lu, D. P. Chassin and S. E. Widergren, "Modeling uncertainties in aggregated thermostatically controlled loads using a state queueing model," *IEEE Trans. Power Syst.*, vol. 20, no. 2, pp. 725-733, May 2005.

[88] C. Chang, W. Zhang, J. Lian and K. Kalsi, "Modeling and control of aggregated air conditioning loads under realistic condotions," in *2013 IEEE PES ISGT Conference*, Washington, US, pp. 1-6, Feb. 2013.

[89] W. Zhang, K. Kalsi, J. Fuller, M. Elizondo and D. Chassin, "Aggregate model for heterogeneous thermostatically controller loads with demand response," in *2012 IEEE PES General Meeting*, San Diego, US, pp. 1-8, Jul. 2012.

[90] W. Zhang, J. Lian, C. Chang, K. Kalsi and Y. Sun, "Reduced-order modelling of aggregated thermostatic loads with demand response," in *51st IEEE Conference on Decision and Control*, Maui, Hawaii, U.S., pp. 5592-5597, Dec. 2012.

[91] S. S. Oren, "A historical perpective and business model for load response aggregation based on priority service," in *46th Hawaii International Conference on System Sciences*, Hawaii, U.S., pp. 2206-2214, Jan. 2013.

[92] K. Kalsi, F. Chassin and D. Chassin, "Aggregated modeling of thermostatic loads in demand response: A systems and control persoective," in *2011 50th IEEE CDC-ECC*, Orlando, US, pp. 15-20, Dec. 2011.

[93] S. Koch, J. L. Mathieu and D. S. Callaway, "Modeling and control of aggregated heterogeneous thermostically controlled loads for ancillary services," in *17th Power System Conference*, Orlando, US, pp. 15-20, Aug. 2011.

[94] M. Erol-Kantarci and H. T. Mouftah, "The Impact of Smart Grid Residential Energy Management Schemes on the Carbon Footprint of the Household Electricity Consumption," in *2010 IEEE Confernece on EPEC*, pp. 1-6, Aug. 2010.

[95] A. Safdarian, M. Fotuhi-Firuzabad and M. Lehtonen, "Integration of price-bansed demand response in DisCos' short-term decision model," *IEEE Trans. Smart Grid*, vol. 5, no. 5, pp. 2235-2245, Sept. 2014.

[96] K. Samarakoon, J. Ekanayake and N.Jenkins, "Investigation of domestic load control to provide primary frequency response using smart meters," *IEEE Trans. Smart Grid*, vol. 3, no. 1, pp. 282-292, Mar. 2012.

[97] A. Barbato, A. Capone, L. Chen, F, Martignon and S. Paris, "A distributed demand-side management framework for the smart grid," *Computer Communications*, vol. 57, pp. 13-24, Nov. 2014.

[98] H. Bae, J. Yoon, Y. Lee, J. Lee, T. Kim, J. Yu and S. Cho, "User-freidendly demand side management for smart grid networks," in *2014 conference on ICOIN*, Phuket, Thailand, pp. 481-485, Feb. 2014.

[99] J. Kwac, J. Flora and R. Rajagopal, "Household energy consumption segmentation using hourly data," *IEEE Trans. Smart Grid*, vol. 4, no. 1, pp. 606-616, Mar. 2013.

[100] P. Samadi, A. H. M. Rad, R. Schober, V. W. S. Wong and J. Jatskevich, "Optimal real-time pricing algorithm based on utlity maximization for smart grid," in *2010 1st IEEE Int. Conf. Smart Grid Commun.*, Gaithersburg, U.S., pp. 415-420, Oct. 2010.

[101] N. Gatsis and G. B. Giannakis, "Residential load control: distributed scheduling and convergence with load AMI messages," *IEEE Trans. Smart Grid*, vol. 3, no. 2, pp. 770-786, Jun. 2012.

[102] N. Li, L. Chen and S. H. Low, "Optimal demand response bassed on utility maximization in power networks," in *IEEE Power and Energy Society General Meeting*, Detroit, U.S., pp. 1-8, Jul. 2011.

[103] C. Bergaentale, C. Clastres and H. Khalfallah, "Demand-side management and european environment and energy goals: an optimal complementary approach," *Energy Policy*, vol. 67, pp. 858-869, Jan. 2014.

[104] P. Faria, J. Soare, Z. Vale, H. Morais and T. Sousa, "Modified particle swarm optimization applied to integrated demand response and DG resources scheduling," *IEEE Trans. Smart Grid*, vol. 4, no. 1, pp. 606-616, Mar. 2013.

[105] Z. Zhu, J. Tang, S. Lambotharan, W. H. Chin and Z. Fan, "An integer linear programming based optimization for home demand-side management in smart grid," in *2012 IEEE PES ISGT*, Washington, U.S., pp. 1-5, Jan. 2012.

[106] A. Sepulveda, L. Paull, W. G. Morsi, H. Li, C. P. Diduch and L. Chang, "A novel demand side management program using water heater and particle swarm optimization," in *2010 IEEE EPEC*, Nova Scotia, Canada, pp. 1-5, Aug. 2010.

[107] K. Diereich, J. M. Latorre, L. Olmos and A. Ramos, "Demand response in an isolated sustem with high wind intefration," *IEEE Trans. Power System*, vol. 27, no. 1, pp. 20-29, 2012.

[108] G. Hug-Glanzmann, "Coordination of intermittent generation with storage, demand control and conventional energy sources," in *2010 IREP Symposium-Bulk Power System Dynamics and Control - VIII (IREP)*, Buzios, Brazil, pp. 1-7, Aug. 2010.

[109] D. L. Yao, S. S. Choi, K. L. Tseng and T. T. Lie, "Determination of short-term power dispatch schedule for a wind farm incorporated with dual-battery energy storage scheme," *IEEE Trans. Sustainable Energy*, vol. 3, no. 1, pp. 74-84, Jan. 2012.

[110] I. Stadler, "Power grid balancing of energy systems with high renewable energy penetration by demand response," *Utilities Policy*, vol. 16, no. 2, pp. 90-98, Jun. 2008.

[111] T. Masuta and A. Yokoyama, "Supplementary load frequency control by use of a number of both electric vehicles and heat pump water heaters," *IEEE Trans. Smart Grid*, vol. 3, no. 3, pp. 1253-1262, Sept. 2012.

[112] S. Huang, D. Infield, A. Cruden, D. Frame and D. Densley, "Plug-in electric vehicles as demand response to absorb local wind generation in power distribution network," in *2010 IREP Symposium- Bulk Power System Dynamics and Control - VIII (IREP)*, Barcelona, Spain, pp. 1-5, Nov. 2013.

[113] A. Molina-Garcia, I. Munoz-Benavente, A. D. Hansen and E. Gomez-Lazaro, "Demand-side contribution to primary frequency control with wind farm auxiliary control," *IEEE Trans. Power Syst*, vol. 29, no. 5, Sept. 2014.

[114] A. S. Kowli and S. P. Meyn, "Supporting wind generation deployment with demand response," in *2011 IEEE PES General Meeting*, San Diego, Canada, pp. 1-8, Jul. 2010.

[115] S. D. Rijcke, K. D. Vos, and J. Drisen, "Balancing wind power with demand-side response," Katholieke University Leuven, Feb. 2010.

[116] A. J. Roscoe and G. Ault, "Supporting high penetrations of renewable generation via implementation of real-time electricity pricing and demand response," *IET Renew. Power Gener.*, vol. 4, no. 4, pp. 369-382, Feb. 2010.

[117] H. P. Khomami and M. H. Javidi, "Energy management of smart microgrid in presence of renewable energy sources based on real-time pricing," in *2014 Smart Grid Conference*, pp. 1-6, 9-10 Dec. 2014.

[118] K. Tomiyama, Y. Kawano, T. Hashimoto and T. Ohtsuka, "Real-time price optimization for load frequency control on electric power systems with wind farms," in *2016 ISCS Conference*, pp. 71-76, 7-10 Mar. 2016.

[119] D. Neves, M. C. Brito and C. A. Silva, "Impact of solar and wind forecast uncertainties on demand response of isolated microgrid," *Renewable Energy*, vol. 87, pp. 1003-1015, Sept. 2015.

[120] E. O'Toole and S. Clarke, "Dynamic forecasting and adaptation for demand optimization in smart grid," in *Software Engineering for the Smart Grid (SE4SG)*, Zurich, Switzerland, pp. 30-33, Jun. 2012.

[121] J. Pascual, J. Barricate, P. Sanchis and L. Marroyo, "Energy management stratrgy for a renwable-based residential microgrid with generation and demand forecasting," *Applied Energy*, vol. 158, pp. 12-25, Nov. 2015.

[122] C. Sahin, M. Shahidehpour and I. Erkmen, "Allocation of hourly reserve versus demand response for security-constrained scheduling of stochastic wind energy," *IEEE Trans. Sustainable Energy*, vol. 4, no. 1, pp. 219-228, Jan. 2013.

[123] A. H. M. Rad, V. W. S. Wong, J. Jatskevich, R. Schober and A. L. Garcia, "Autonomous demand-side management based on game-theoretic energy consumption scheduling for the future smart grid," *IEEE Trans. Smart Grid*, vol. 1, no. 3, pp. 320-331, Dec. 2010.

[124] Q. Zhu, L. Jiang, W. Yao, CK. Zhang and C. Luo, "Robust load frequency control with dynamic demand response for deregulated power systems with communication delays," Accepted by *Electric Power Components and Systems*, Sept. 2016.

[125] Q. Zhu, W. Yao, CK. Zhang and L. Jiang, "Chapter 8: Frequency regulation of smart grid via dynamic demand control and battery energy storage system," *Smarter Energy : form Smart Metering to the Smart Grid*, IET Press, 2016.

[126] P. Kundur, *Power system stability and control*, McGraw-Hill, New York, 1994, 1st edu.

[127] P. Kundur, J. Paserba, V. Ajjarapu, G. Andersson, A. Bose, C. Canizares, N. Hatziargyriou, D. Hill, A. Stankovic, C. Taylor, T. V. Cutsem and V. Vittal, "Definition and classification of power system stability," *IEEE Trans. Power Syst.*, vol. 9, no. 3, pp. 1387-1401, Aug. 2004.

[128] C. P. Steinmetz, "Power control and stability of electric generating stations," *AIEE Trans. Power Syst.*, vol. XXXIX, no. 2, pp. 1215-1287, Jul. 1920.

[129] J. H. Eto, J. Nelson-Hoffman, C. Torres, S. Hirth, B. Yinger, J. Kueck, B. Kirby, C. Bernier, R. Wright, A. Barat and D. S. Watson, "Demamd respinse spinning reserve demonstration," *Energy Analysis Dept. Ernest Orlando Lawrence Berkeley Nat. Lab.*, Berkeley, CA, US, LBNL62761, 2007.

[130] M. H. Albadi and E. F. El-Saadany, "A summary of demand response in electricity markets," *Electron. Power Syst. Res.*, vol. 78, no. 11, pp. 1989-1996, Nov. 2008.

[131] J. W. Black and M. Ilic, "Demand-based frequency control for distributed generation," in *IEEE PES Summer Meeting*, pp. 427-432, Jul. 2002.

[132] Members of National Grid, "Frequency sensitive electric vehicle and heat pump power comsumption final report," *National Grid*, pp. 1-68, Jul. 2015.

[133] Y. Ma, T. Houghton, A. Cruden and D. Infield, "Modeling the benefits of Vehicle-to-Grid technology to a power system," *IEEE Trans. Power Syst.*, vol. 27, no. 2, pp. 1012-1020, May 2012.

[134] A. Hajizadeh and M. A. Golkar, "Intelligent power management strategy of hybrid distributed generation system," *Int. J. Elect.Power Energy Syst.*, vol. 29, no. 10, pp. 783-795, Dec. 2007.

[135] Y. Ota, H. Taniguchi, T, Nakajima, K. M. Liyanage, J. Baba and A. Yokoyama, "Autonomous distributed V2G (vehicle-to-grid) satisfying scheduled charging," *IEEE Trans. Smart Grid*, vol. 3, no. 1, pp. 559-564, Mar. 2012.

[136] R. C. Dorf and R. H. Bishop, *Modern control system*, 7th ed. New York, NY, U.S.: Addison-Weslay, 1995.

[137] G. H. Golub and C. F. Van Loan, *Matrix Computations*, 3rd ed. Baltimore, MD, USA: Johns Hopkins University, 1996.

[138] R. K. Sahu, S. Panda and P. C. Pradhan, "Design and analysis of hybrid firefly algorithm-pattern search based fuzzy PID controller for LFC of multi area power systems," *Int. J. Electr. Power Energy Syst.*, vol. 69, pp. 200-212, Jul. 2015.

[139] I. P. Kumar, and D. P. Kothari, "Recent philosophies of automatic generation control strategies in power system," *IEEE Trans. Power Syst.*, vol. 20, no. 1, pp. 346-357, Feb. 2005.

[140] S. K. Panday, S. R. Mohanty and N. Kishor, "A literature survey on load-frequency control for conventional and distribution generation power systems," *Renew. Sust. Energ. Rev.*, vol. 25, pp. 318-334, Sept. 2013.

[141] B. H. Bakken and O. S. Grande, "Automatic generation control in a deregulated power system," *IEEE Trans. Power Syst.*, vol. 13, no. 4, pp. 1401-1406, Nov. 1998.

[142] Y. Arya and N. Kumar, "AGC of a multi-area multi-source hydrothermal power system interconnected via AC/DC parallel links under deregulated environment," *Int. J. Electr. Power Energy Syst.*, vol. 75, pp. 127-138, Feb. 2016.

[143] A. R. Abhyankar and S. A. Khaparde, "Introduction to deregulation in power industry," *Indian institute of technology bombay*, pp. 1-28, 2003.

[144] H. Shayeghi, H. A. Shaynfar and A. Jalili, "Multi-stage fuzzy PID power system automatic generation controller in deregulated environment," *Energy Convers. Manage.*, vol. 47, no. 18-19, pp. 2829-2845, Nov. 2006.

[145] C. Goldman, M. Reid, R. Levy and A. Silverstein, "Coordination of energy efficiency and demand response," *Ernest Orlando Lawrence Berkelay National Laboratory*, Jan. 2010.

[146] H. Fan, L. Jiang. C.K. Zhang and C. Mao, "Frequency regulation of multi-area power system with plug-in electric vehicles considering communication delays," *IET GTD*, vol. 10, no. 14, pp. 3481-3491, Nov. 2010.

[147] W. Yao, K. Y. Lee and W. Texas, "A wind farm configuration for load-following control and its application to primary frequency support," in *North American Power Symposium*, Boston, U.S., pp. 1-6, Aug. 2011.

[148] R. Dhanalakshmi and S. Palaniswami, "Application of multi stage fuzzy logic control for load frequency control of an isolated wind diesel hybrid power system," in *Int. Conf. on GTEC*, Chennai, India, pp. 309-315, Dec. 2011.

[149] H. Bevrani and P. R. Daneshmand, "Fuzzy logic based load frequency control concerning high penetration of wind turbines," *IEEE Syst. J.*, vol. 6, no. 1, pp. 173-180, Mar. 2012.

[150] R. Dhanalakshmi and S. Palaniswami, "Application of multi stage fuzzy logic control for load frequency control of an isolated wind diesel hybrid power system," in *Proc. Int. Conf. on GTEC*, pp. 309-315, Chennai, India, 15-17 Dec. 2011.

[151] S. W. Mohod and M. V. Aware, "Micro wind power generator with battery energy storage for citical load," *IEEE Syst. J.*, vol. 6, no. 1, pp. 118-125, Mar. 2012.

[152] M. Datta and T. Senjyu, "Fuzzy control of distributed PV inverters/energy storage systems/electric vehicles for frequency regulation in a large power system," *IEEE Trans. Smart Grid*, vol. 4, no. 1, pp. 479-488, Mar. 2013.

[153] X. Luo, S. Xia and K. W. Chan, "A decentralized charging control strategy for plug-in electric vehicles to mitigate wind farm intermittency and enhance frequency regulation," *J. Power Sources*, vol. 248, pp. 604-614, Feb. 2014.

[154] S. Bhowmik, K. Tomsovic and A. Bose, "Communication models for third party load frequency control," *IEEE Trans. Power Syst.*, vol. 19, no. 1, pp. 543-548, Feb. 2004.

[155] H. Bevrani, and T. Hiyama, "On load-frequency regulation with time delays: design and real-time implementation," *IEEE Trans. Energy Convers.*, vol. 24, no. 1, pp. 292-300, Mar. 2009.

[156] H. Bevrani and T. Hiyama, "Robust decentralised PI based LFC design for time delay power systems," *Energy Convers. Manage.*, vol. 49, no. 2, Feb. 2008.

[157] A. N. Brooks, "Vehicle-to-grid demonstration project: Grid regulation ancillary service with a battery electric vehicle," *California Air Resources Board*

and the California Environmental Protection Agency, Research Division, Dec. 2002.

[158] Y. Tang, J. Yang, J. Yan, H. He, "Intelligent load frequency controller using GrADP for island smart grid with electrical vehicles and renewable resources," *Neurocomputing*, vol. 170, pp. 406-416, Dec. 2015.

[159] S. C. Thomsen and N. K. Poulsen, "A disturbance decoupling nonlinear control law for variable speed wind turbines," in *15th Meditereanean Confernece*, Athens, Greece, pp. 1-6, Jun. 2007.

[160] B. Boukhezzar and H. Siguerdidjane, "Nonlinear control of a variable-speed wind turbine using a two mass model," *IEEE Trans. Energy Convers.*, vol. 26, no. 1, pp. 149-162, Mar. 2011.

[161] L. Chang-Chien, C. Sun and Y. Yeh, "Modeling of wind farm participation in AGC," *IEEE Trans. Power Syst.*, vol. 29, no. 3, pp. 1204-1211, May 2014.

[162] A. Seuret and F. Gouaisbaut, "Wirtinger-based integral inequality: application to time-delay systems," *Automatica*, vol. 49, no. 9, pp. 2860-2866, Sept. 2013.

[163] T. Ting, M. Rao, and C. Loo, "A novel approach for unit commitment problem via an effective hybrid particle swarm optimization," *IEEE Trans. Power Syst.*, vol. 21, no. 1, pp. 411-418, Feb. 2006.

[164] J. Zhao, F. Wen, Z. Y. Dong, Y. Xue and K. P. Wong, "Optimal dispatch of electric vechicle and wind power using enchange particle awarm optimization", *IEEE Trans. Ind. Inf., 2012*, vol. 8, no. 4, pp. 889-899, Nov. 2012.

[165] Z. S. Zhang, Y. Z. Sun, G. J. Li, "Coordinated frequency regulation by doubly fed induction generator-based wind power plants," *IET Renewable Power Generation*, vol. 6, no. 1, pp. 38-47, Jan. 2011.

[166] H. T. Ma and B. H. Chowdhury, "Working towards frequency regulation with wind plants: combined control approaches," *IET Renewable Power Generation*, vol. 4, no. 4, pp. 308-316, 2010.

[167] J. Morel, H. Bevrani, T. Ishii and T. Hiyama, "A robust control approach for primary frequency regulation through variable speed wind turbines," *IEEJ Trans. Power and Energy*, vol. 130, no. 11, pp. 1002-1009, Jan. 2010.

[168] L. Chang-Chien, W. Lin and Y. Yin, "Enhancing frequency response control by DFIGs in the high wind penetrated power system," *IEEE Trans. Power Syst.*, vol. 26, no. 2, pp. 710-718, May 2011.

[169] I. D. Margaris, S. A. Papathanassious, N. D. Hatziargyriou, A. D. Hansen and P. Sorensen, "Frequency control in autonomous power systems with high wind power penetration," *IEEE Trans. Sustainable Energy*, vol. 3, no. 2, pp. 189-199, Apr. 2012.

[170] P. Moutis, E. Loukarakis, S. Papathanasiou and N. D. Hatziargyriou, "Primary load-frequency control from pitch controlled wind turbine," in *2009 IEEE Bucharest Power Tech Conference*, Bucharest, Romania, pp. 1-7, Jul. 2009.

[171] K. H. S. V. S. Nunna and S. Doolla, "Responsive end-user-based demand side management in multimicrogrid environment," *IEEE Trans. Industrial Information*, vol. 10, no. 2, pp. 1262-1272, May 2014.

[172] Balas G., Chiang R., Packard A., Safonov, "Robust control toolbox user's guide," Natick, MA: MathWorks, 2010.